ENFOQUE

UTE

REVISTA

Facultad Ciencias de la Ingeniería e Industrias
elSSN:13906542

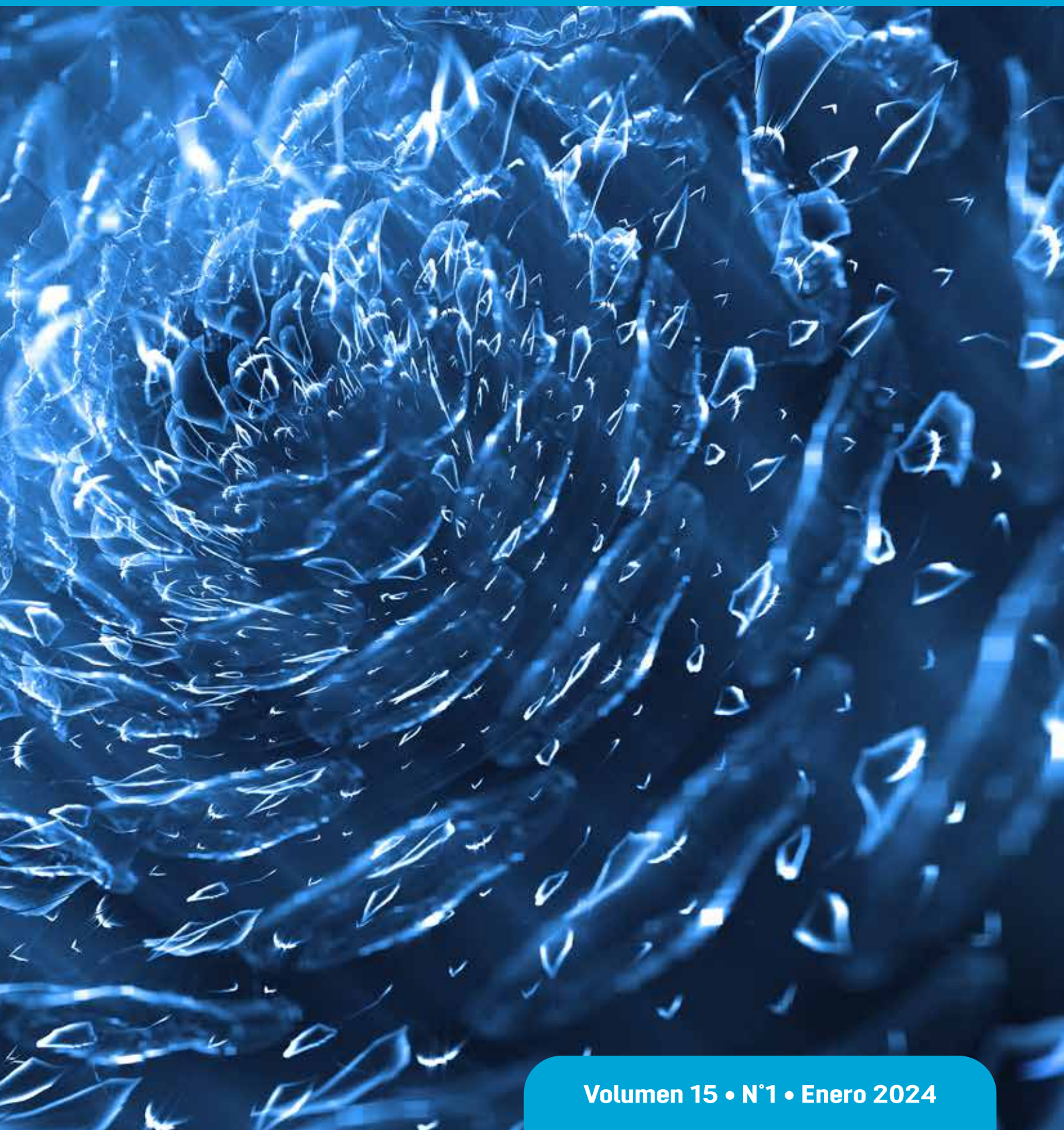

Volumen 15 • N°1 • Enero 2024

Sumario

Analysis Of the Effect of Vegetal and Coking Coals on the Surface Hardness of Carburized AISI 8620 Steel

Leonidas Ramírez[1], Nicolás Rodríguez[2], Isaac Simbaña[3], David Saquinga[4]

***Abstract* — In this investigation was developed a comparative study of the superficial hardness of AISI 8620 steel thermally treated by carburizing, by the use of vegetable and coking coals. The objective was to propose an alternative to the element used to generate the carburizing atmosphere. The previous stages have been described, such as the preparation of the material and its verification, as well as the dimensions and characteristics, defined by the ASTM E-18 standard. By considering four variables, each one with two levels, an orthogonal array matrix of 16 experiments was generated. The surface hardness measurements were processed through an analysis of variance (ANOVA), where the significance of each variable considered as a factor was obtained. Coking coal can be used as an element for the generation of carburizing atmosphere since a maximum relative error of 3.86% was obtained between the experimental values and the values in the literature. In contrast, the vegetable coal did not improve the mechanical properties of the steel, reaching an average hardness of 25.95 HRC after heat treatments.**

***Keywords* – AISI 8620; Heat treatments; Carburizing; Surface Hardness.**

***Resumen* — En esta investigación, se desarrolló el estudio comparativo de la dureza superficial del acero AISI 8620 tratado térmicamente con cementación, utilizando carbón vegetal y coque. El objetivo fue proponer una alternativa al elemento utilizado para generar la atmósfera de cementado. Se describen las etapas previas, tales como la preparación del material y la verificación del mismo, también se analizaron las dimensiones y características que define la norma ASTM E-18. Al considerar cuatro variables, cada una con dos niveles, se generó una matriz de arreglo ortogonal de 16 experimentos. Las mediciones de dureza superficial fueron procesadas mediante un análisis de varianza (ANOVA), se obtuvo la significancia de cada variable considerada como factor. El carbón coque puede utilizarse como elemento para la generación de atmósfera de cementado, ya que se obtuvo un error relativo máximo de 3.86% entre los valores experimentales y los valores presentes en la literatura. Por otra parte, el carbón vegetal no mejoró las propiedades mecánicas del acero, alcanzando una dureza en promedio de 25.95 HRC luego de los tratamientos térmicos.**

***Palabras clave* – AISI 8620; Tratamientos térmicos; Cementado; Dureza superficial.**

I. INTRODUCTION

THE constant technological development seeks to satisfy the basic needs of people, in addition to improving their lifestyle [1]. Therefore, it is required that the research fields prioritize the development of new technologies, which are important in the analysis of the materials used in manufacturing or as machine elements. Carbon steel encompasses steel alloys that contain carbon. Generally, the prices of carbon steels are low, compared to other alloy steels, for this reason, they are frequently utilized in industrial of manufacturing environments [2]. They are resistant to heat, which makes them ideal for manufacturing, hence, carbon steels are recommended for most applications [3]. AISI 8620 steel is a low alloy steel, its main components are nickel, chromium, and molybdenum, being easy to weld by common procedures. It is a steel for carburizing, increasing its hardness on the surface, although it continues to have good core toughness. It is recommended to carburize at temperatures between 900 to 930 °C and then perform oil quenching to harden [4]. The importance of heat treatment is that it allows for obtaining specific mechanical properties through the use and control of temperatures and times, to heat and cool the steel [5].

Feldiorean and Tiernan [6] studied the hardening process of AISI 8620 steel obtained by Metal Injection Model (MIM). Carburizing was done under a methane-nitrogen-methanol atmosphere for 135 minutes, followed by austenitizing heating at 830 °C to quench in oil. The hardness was controlled by tempering at temperatures of 130 and 170 °C for 60 minutes. After the heat treatments, the carbon content increased from 17% to 76% with a maximum layer depth of 0.51 mm. The hardness of the cemented and tempered steel reached 63.8 HRC, decreasing to 45.6 HRC with the maximum values of time and temperature for tempering.

The wear and mechanical properties of case-hardened AISI 8620 steel produced by powder metallurgy were analyzed by Erden and Aydun [7]. The specimens were carburized at 925 °C for 4 hours, reaching an increase in the ultimate stress

[1] Engineering, Productivity and Industrial Simulation Research Group (GIIPSI), Universidad Politécnica Salesiana, Quito, Ecuador. (e-mail: lramirezg@ups.edu.ec). ORCID number 0000-0003-2569-2974

[2] Mechanical Engineering, Universidad Politécnica Salesiana, Quito, Ecuador. (e-mail: nrodriguezp2@est.ups.edu.ec). ORCID number 0009-0005-7774-8396

[3] Electromechanical Career's Mechanical Engineering and Pedagogy Research Group (GIIMPCEM), Instituto Superior Universitario Sucre, Quito, Ecuador. (e-mail: isimbana@tecnologicosucre.edu.ec). ORCID number 0000-0002-3324-3071

[4] Electromechanical Career's Mechanical Engineering and Pedagogy Research Group (GIIMPCEM), Instituto Superior Universitario Sucre, Quito, Ecuador. (e-mail: dsaquinga@tecnologicosucre.edu.ec). ORCID number 0000-0001-8353-1621

Manuscript Received: Sep 06, 2023
Revised: Nov 13, 2023
Accepted: Nov 23, 2023
DOI: https://doi.org/10.29019/enfoqueute.997

of 138.1%, but the elongation decreased by 64.7%. The maximum thickness of the carburized coating was 42.99 µm, a layer that increases hardness and resistance. In addition, this case-hardened steel presents greater resistance to wear and abrasion.

Kumar et al. [8] analyzed the thermal and metallurgical characteristics of the surface modification of AISI 8620 steel produced due to the TIG arc process. Through a thermal process, an average hardness of 50 HRC was obtained, starting from 15 HRC of the material in its base state. The elastic modulus reached a maximum of 205 GPa and the Poisson's radius was 0.29. The obtained characteristic and dominant microstructures were martensite and bainite, as well as a slight presence of ferrite.

Studies of the degradation in the sliding wear behavior of case-hardened AISI 8620 steel at 100 °C in non-lubricated conditions were presented by Thirugnanasambantham and Ganesh [9]. Using a scanning electron microscope, delamination and debris generation were observed as the dominant wear mechanisms of carburized AISI 8620. However, for steel without heat treatment, bow formation and adhesive fragments occurred in the form of loose fine wear particles. When applying a load of 150 N, the deformation area was greater in the untreated steel, with an increase of 0.1 mm.

A review of the case-hardening temperature and mechanical qualities of low-carbon content steels was presented by Wani and Kumar [10]. For AISI 8620 steel it was shown that, with a longer carburizing time, the thickness of the hardened layer also increases. The wear resistance, as well as the ultimate tensile stress, are higher when carburizing, followed by water quenching. Carburizing is a heat treatment in a hermetic controlled-atmosphere box that is responsible for introducing carbon into a solid ferrous alloy. This process is carried out by heating the metal in a carbonaceous atmosphere, with a temperature higher than the transformation temperature, and for a certain period. After carburizing, the elements are cooled to harden the carburizing layer on the surface and the nucleus does not undergo any change [11]. Therefore, the purpose of this investigation is to comparatively study the surface hardness of AISI 8620 steel heat-treated by carburizing using vegetable and coking coals.

II. MATERIALS AND METHODS

Minitab is a specialized software for the Design of Experiments, for obtaining the combinations of factors and levels, and determining the number of experiments to be developed. It has been considered to heat treat the AISI 8620 steel according to the indications of the supplier's technical sheet [4]. The experimental design responds to a 4^2 factorial design, with four factors and two levels, which are indicated in Table I.

AISI 8620 steel was selected since it is a steel that requires carburizing because it is a material that has a lower percentage of carbon and low hardness. According to ASTM E-18 standard [12], the material to be experimented with must have a diameter of no more than 55 mm and a thickness of 10 to 16 mm.

TABLE I
EXPERIMENTAL PARAMETERS

Factor	Levels	
Carburizing environment	**Vegetable coal**	**Coking coal**
Carburizing temperature	900 °C	950 °C
Quenching temperature	800 °C	830 °C
Hardening temperature	150 °C	210 °C

Therefore, the dimension available in the local market, closest to the requirement is 50.4 mm (2"), a shaft that is going to be cut and machined to reach the established thickness. AISI 8620 steel was machined on a lathe to carry out processes, such as facing, to obtain a good surface quality and avoid possible reading errors in hardness tests. Figure 1 presents the result of the machined specimens and the measurement of surface roughness, following the indications of the ASTM E-18 standard, with which the standard thickness of 15 mm was established for all the specimens. Is recommended a surface finish with quality N5 equivalent to a roughness of approximately 0.4 µm.

Fig. 1. Machined specimens and experimental measurement of surface roughness

The first step to develop the carburizing process is to put specimens inside the hermetic box, and then fill it with coal. Consequently, this box needs to be covered to introduce it into the furnace for heat treatments to increase its temperature until it reaches the austenitization phase of the AISI 8620 material, as indicated in figure 2. In this manner, the material absorbs the gases emanated by the coal (CO_2), and it can increase the perlite area.

Fig. 2. Hermetic box for carburizing

The carburizing experiments carried out were four, which had variations in temperature (880 and 950 °C), as well as in the carburizing time (6 and 8 hours). An inlet temperature of 200 °C and a holding time of 8 hours were established for all carburizing processes. The hermetic box with vegetable coal was entered into the heat treatment furnace with test specimens 1, 2, 3 and 4, until reaching the austenitization temperature of 900 °C. The procedure was repeated with the same carburizing environment for specimens 5, 6, 7 and 8, modifying the carburizing temperature to 950 °C.

The same methodology was repeated for the carburizing procedure with the hermetic box with coking coal. Test specimens 9, 10, 11 and 12 were treated until reaching a temperature of 900 °C. An austenitizing temperature of 950 °C was used for test specimens 13, 14, 15 and 16. Additionally, fiberglass wool was placed on the borders of the box to seal and retain the carburizing atmosphere.

The tempering process is required on steel to increase the surface hardness, which is obtained by heating the steel to the austenitization temperature, which is detailed in the material technical data sheet, and then it is cooled abruptly by making a temperature change. For this temperature change was utilized Durixol W25 oil, which is an oil specially manufactured for carrying out heat treatments. It has a rapid cooling characteristic since it has a property that supports high temperatures before proceeding to evaporate [13].

Was applied the direct cooling methodology, from the hermetic box, since the CO_2 formed must be quickly separated from the surface, otherwise, it would act as a decarbonizer. In the case of carburizing with vegetable coal, it was difficult to control the carburizing atmosphere, more CO_2 than CO is being formed [14]. Tempering is a thermal procedure implemented for steels to improve their mechanical characteristics by increasing their temperature below the melting temperature. The objective of this thermal procedure is to reduce the weakness of the material by decreasing internal stresses [15]. To finish the experimental stage, the measurement of surface hardness was carried out after the heat treatments, according to the ASTM E-18 standard. Figure 3 shows the specimens marked with the points where these measurements were made.

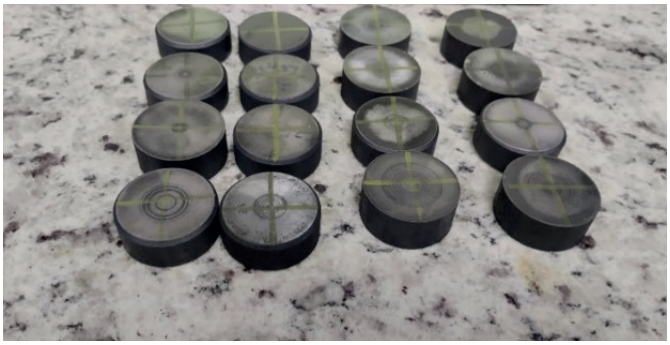

Fig. 3. Specimens after heat treatments, before measurement of surface hardness.

Figure 4 also shows the evidence of the values corresponding to the surface hardness of test specimens 3 and 13, which were thermochemically treated with vegetable and coking coal, respectively. A value of 58.3 and 24.5 HRC is observed for each of these specimens, which are close to the tabulated average values of 59.31 and 25.95 HRC for the carburizing with coking and vegetable coal, respectively.

Fig. 4. Surface hardness measurements with carburizing in coking coal and charcoal

III. RESULTS AND DISCUSSION

The Analysis of Variance (ANOVA) is implemented to verify the variability of each value by computing its variance. It is proposed to identify the measures that are involved in the experimental process and to determine greater surface hardness [16]. Table II presents the defined levels and factors in the experiments, in addition to the obtained average hardness, based on the five measurements that the ASTM E-18 standard indicates.

TABLE II
EXPERIMENTAL HARDNESS MEASUREMENTS

Experiment	Carburizing environment	Carburizing temperature [°C]	Quenching temperature [°C]	Hardening temperature [°C]	Average Hardness [HRC]
1	Coking	900	800	150	58.56
2	Coking	900	800	210	57.10
3	Coking	900	830	150	58.42
4	Coking	900	830	210	57.16
5	Coking	950	800	150	61.46
6	Coking	950	800	210	59.70
7	Coking	950	830	150	61.92
8	Coking	950	830	210	60.13
9	Vegetable	900	800	150	24.60
10	Vegetable	900	800	210	22.48
11	Vegetable	900	830	150	25.02
12	Vegetable	900	830	210	23.66
13	Vegetable	950	800	150	28.94
14	Vegetable	950	800	210	26.79
15	Vegetable	950	830	150	29.40
16	Vegetable	950	830	210	26.80

After carrying out the experiments with the heat treatments and the thermochemical carburizing treatment, the external hardness calculations were made for all the specimens, which was important to carry out the validation of these obtained values. A normality test is then required by using specialized software. Figure 5a analyzes the coherence of the distribution of carburized coal coking hardness values focused on a normal distribution curve, guaranteeing that the obtained values are correct and measured adequately. For the normality study of the obtained hardness values, it considered a confidence interval of 95 %, obtaining a high probability that the real values found follow a normal distribution. Figure 5b presents the same normality test for the surface hardness by vegetable coking carburizing.

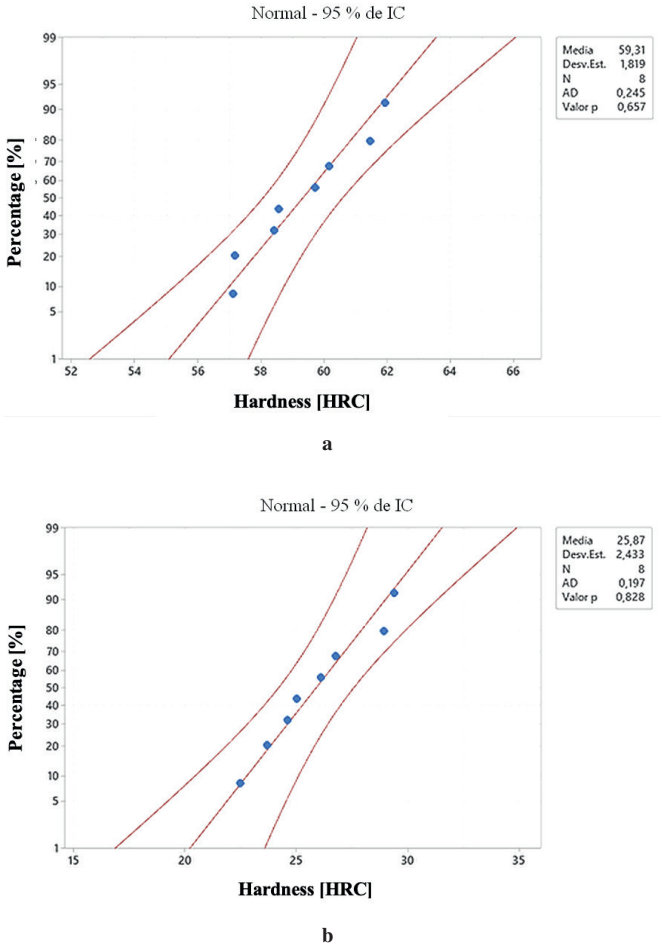

Fig. 5. Normality test of hardness measurements a) coal coking carburizing, b) vegetable coal carburizing.

Figure 6 graphically presents the main effects to identify the differences between the means. Therefore, a great significance is observed for the mean carburizing factor, considering this as the main effect. In contrast, the carburizing and tempering temperatures have a slight difference, and they come to present a significance, but with less influence. Finally, the quenching temperature between the analyzed levels does not present significance, being practically a straight line.

Figure 7 shows how each factor interacts with the others. It is confirmed that the carburizing environment is the most significant and is influenced by the carburizing and tempering temperature. Visually, a slope generated by the modification of these factors is evident.

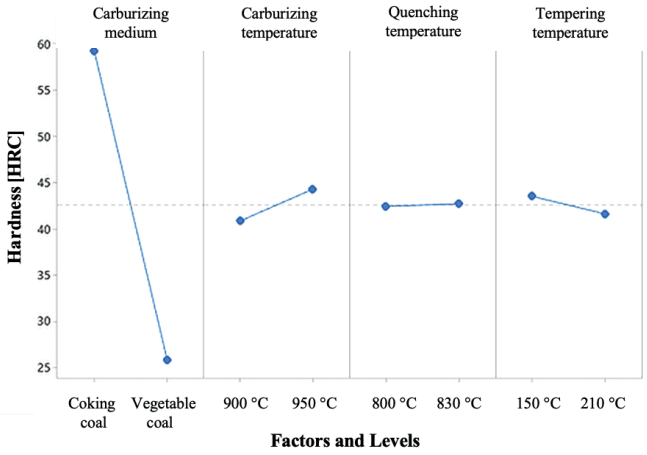

Fig. 6. Main effects for surface hardness.

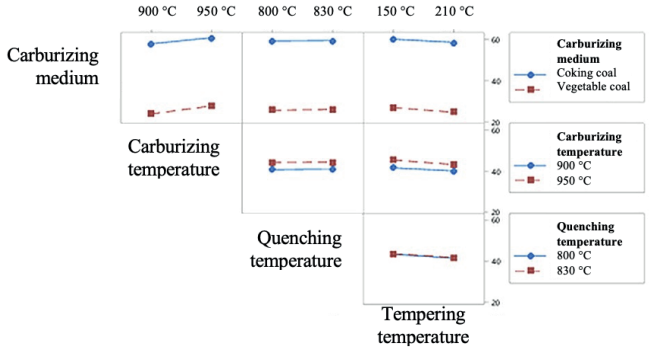

Fig. 7. Interaction between factors and levels.

The distribution diagram indicates the influence of the discontinuities found on the response variable. The mean value data of 2.2 was taken as a reference to verify the level of significance, hence, any factor that exceeds this limit has an influence. Figure 8 allows to observe that the carburizing environment is statistically the most significant. The carburizing and tempering temperature factors are also over the limit, therefore, they are going to be significant. Finally, the quenching temperature has not reached the limit, allowing to affirm that it does not influence surface hardness after heat treatments and thermochemical treatment.

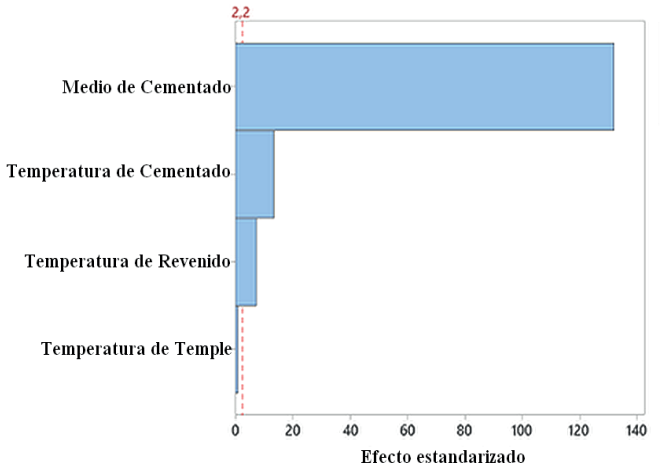

Fig. 8. Pareto diagram of standardized effects.

IV. CONCLUSIONS

The application of thermochemical carburizing treatment is required before its use, to improve its mechanical properties and prolong the useful life of the elements manufactured with this steel. A thermochemical carburizing treatment has been carried out, using different elements, such as vegetable and coking coal, to generate different carburizing atmospheres and identify which of them obtains the best results. These carburizing processes were carried out for two hours at the limit values indicated by the manufacturer, from 900 to 950 °C. It is required to perform a one-stage carburizing, that is (after the carburizing time) the specimens must be immediately cooled in oil, to be quenched. Minitab was used as specialized software for the elaboration of an orthogonal arrangement matrix, considering as factors the temperatures for carburizing, quenching, and tempering, each factor with two levels. The experimental design responds to a 4^2 factorial design with 16 experiments. In addition, the indications of the ASTM E-18 standard for the measurement of surface hardness were considered, requiring the preparation of the material according to the established dimensions.

After the experimental measurement of hardness, the data was statistically analyzed by using an analysis of variance (ANOVA). It was defined that the quenching temperature does not influence the surface hardness, while the carburizing and tempering temperatures do have significance, with a value of 1.34% and 0.032%, respectively. The factor that most influenced this experimental study was the material used in a carburizing environment, with a value of 98.62%. From this analysis, it can be stated that vegetable coal requires control for the generation of the carburizing atmosphere, otherwise, as was the case, it acts as a decarburizer.

Therefore, coking coal can be used as an element for the generation of carburizing atmosphere since a maximum relative error of 3.86% was obtained between the experimental values and data presented by the manufacturer. Conversely, vegetable coal does not have a positive effect on the improvement of the mechanical properties of the steel, since the obtained hardness values after the heat treatments were, 25.95 HRC, on average. The manufacturer indicates that, for 150 and 210 °C, the hardness to be obtained must be between 62.5 and 60 HRC, values that do not resemble those obtained using vegetable coal as a carburizing environment.

REFERENCES

[1] S. Mishra and R. Dalai. "Effect of Quenching and Partitioning Treatment on Low Carbon Medium Manganese Alloyed Steels-A Short Review," *Materials Today: Proceedings,* vol. 43, pp. 593-596, 2021. Available: HYPERLINK "https://doi.org/10.1016/j.matpr.2020.12.107" 10.1016/j.matpr.2020.12.107

[2] Y. Martínez and R. Collazo. "Revisión bibliográfica de los efectos de los parámetros de soldadura en las tensiones residuales del proceso," *Investigaciones en Ingeniería,* vol. 16, pp. 85-98, 2018. Available: HYPERLINK "https://dialnet.unirioja.es/servlet/articulo?codigo=6996989" https://dialnet.unirioja.es/servlet/articulo?codigo=6996989

[3] Y. González and J. Rengel. "Comportamiento termo fluidodinámico del acero en un molde de colada continua: una revisión," *TecnoLógicas,* vol. 24, no. 51, pp. 230-262, 2021. Available: HYPERLINK "https://doi.org/10.22430/22565337.1856" 10.22430/22565337.1856

[4] Böhler. "Steels for Carburizing: AISI 8620 / 5115," 2022. [Online]. Available: HYPERLINK "https://www.bohlerperu.com/app/uploads/sites/138/2019/09/ECL.pdf" https://www.bohlerperu.com/app/uploads/sites/138/2019/09/ECL.pdf. [Accessed 08 May 2022].

[5] S. Akande, O. Ajaiyeoba, T. Azeez, O. Ikumapayi, S. Akinlabi and E. Akinlabi. "Investigating the Precipitation Hardening of 2024 Aluminium Alloy Under Different Quenching Media," *Materials Today: Proceedings,* vol. 2214, pp. 1-4, 2022. Available: HYPERLINK "https://doi.org/10.1016/j.matpr.2022.04.775" 10.1016/j.matpr.2022.04.775

[6] D. Feldiorean and M. Tierean. "Studies on the Carburizing Process of AISI 8620 Steel Obtained by MIM Technology," *Recent,* vol. 19, no. 2, pp. 70-77, 2018. Available: HYPERLINK "http://dx.doi.org/10.31926/RECENT.2018.55.070" 10.31926/RECENT.2018.55.070

[7] M. Erden and F. Aydun. " Wear and Mechanical Properties of Carburized AISI 8620 Steel Produced by Powder Metallurgy," *International Journal of Minerals, Metallurgy and Materials,* vol. 28, no. 3, pp. 430-440, 2021. Available: HYPERLINK "https://doi.org/10.1007/s12613-020-2046-8" 10.1007/s12613-020-2046-8

[8] R. Kumar, P. Gosh and S. Kumar, "Thermal and Metallurgical Characteristics of Surface Modification of AISI8620 Steel Produced by TIG Arcing Process," *Journal of Materials Processing Technology,* vol. 240, p. 420–431, 2017. Available: HYPERLINK "https://doi.org/10.1016/j.jmatprotec.2016.10.020" 10.1016/j.jmatprotec.2016.10.020

[9] K. Thirugnanasambantham and A. Ganesh. "Mechanistic Studies on Degradation in Sliding Wear Behavior of carburized AISI 8620 Steel at 100°C Under Unlubricated Conditions," *Materials Today: Proceedings,* vol. 5, p. 6258–6267, 2017. Available: HYPERLINK "https://doi.org/10.1016/j.matpr.2017.12.235" 10.1016/j.matpr.2017.12.235

[10] Z. Wani and N. Kumar. "A Review on Carburizing Temperature and the Mechanical Behaviour of Mild Steel," *Dogo Rangsang Research Journal,* vol. 10, no. 9, pp. 115-128, 2020. Available: HYPERLINK "https://www.researchgate.net/publication/351711511" https://www.researchgate.net/publication/351711511

[11] J. Mathews, H. Farahani, J. Sietsma, J. Petrov, M. Mecozzi and M. Santofimia. "Microstructures in a Carburized Steel After Isothermal Pearlitic Treatment," *Journal of Materials Science & Technology,* vol. 160, no. 10, pp. 66-75, 2023. Available: HYPERLINK "https://doi.org/10.1016/j.jmst.2023.03.017" 10.1016/j.jmst.2023.03.017

[12] ASTM International. "ASTM E18 - Standard Test Methods for Rockwell Hardness of Metallic Materials," 2022. [Online]. Available: HYPERLINK "https://www.astm.org/Standards/E18.htm" https://www.astm.org/Standards/E18.htm. [Accessed 24 July 2022].

[13] BonGROUP. "High-Performance DURIXOL Quenching Oils With a Very Fast Cooling Effect," 2023. [Online]. Available: HYPERLINK "https://www.bongroup.de/produkte/abschreckoele/" https://www.bongroup.de/produkte/abschreckoele/. [Accessed 30 February 2023].

[14] X. Pham, A. Hoang, D. Nguyen and V. Le. "Effect of Factors on the Hydrogen Composition in the Carburizing Process," *Interna-*

tional Journal of Applied Engineering Research, vol. 12, no. 9, pp. 8238-8244, 2017. Available: HYPERLINK "https://www.ripublication.com/ijaer17/ijaerv12n19_33.pdf" https://www.ripublication.com/ijaer17/ijaerv12n19_33.pdf

[15] M. Groover. *Fundamentos de Manufactura Moderna - Materiales, procesos y sistemas*, Naucalpan: Pearson Pretice Hall, 1997.

[16] I. Simbaña, W. Quitiaquez, J. Estupiñán, F. Toapanta-Ramos and L. Ramírez. "Evaluación del rendimiento de una bomba de calor de expansión directa asistida por energía solar mediante simulación numérica del proceso de estrangulamiento en el dispositivo de expansión," *Revista Técnica Energía,* vol. 19, no. 1, pp. 110-119, 2022. Available: HYPERLINK "https://doi.org/10.37116/revistaenergia.v19.n1.2022.524" 10.37116/revistaenergia.v19.n1.2022.524

Developing Fuel Efficiency and CO_2 Emission Maps of a Vehicle Engine Based on the On-Board Diagnostic (OBD) Approach

Fredy Rosero[1], Xavier Rosero[2], Zamir Mera[3]

***Abstract* — In real traffic conditions vehicle interacts with the road, other vehicles, and traffic control devices. The level of traffic influences driving patterns and, consequently, this can affect the vehicle's fuel efficiency and emissions. This study aims to develop engine maps of fuel consumption and carbon dioxide (CO_2) emissions for a light vehicle operating under real traffic conditions. A representative passenger vehicle powered by gasoline of the ecuadorian vehicle fleet was selected for the experimental campaign that was developed on a test route designed according to real driving emission (RDE) regulation. An on-board diagnostic (OBD) device was used for recording in real-time engine and vehicle operating parameters. Moreover, CO_2 emissions were estimated using the fuel rate registered from the OBD system of the vehicle This study proposed a novel methodology for developing two-dimensional contour engine maps based on OBD data. The result showed that the vehicle engine operated in real traffic conditions with a brake thermal efficiency (BTE) of 27 %, a brake-specific fuel consumption (BSFC) of 275 g/kWh, and a CO_2 energy-emission factor of 716 g/kWh. In terms of distance, the CO_2 emission factor for the tested vehicle was approximately 190 g/km. Overall, this study demonstrates that the OBD approach is a potential method to be used to assess the fuel consumption and CO_2 emissions of a vehicle operating under real-world traffic conditions, especially in Latin American countries, where portable emission measurement systems (PEMS) are not readily available.**

***Keywords* — Fuel Consumption; *CO2* Emissions; Engine Maps; On-Board Diagnostic (OBD).**

***Resumen* — En condiciones reales de circulación un vehículo interactúa con la carretera, con otros vehículos y con los dispositivos de control del tráfico. El nivel de tráfico influye en los patrones de conducción y, en consecuencia, esto puede afectar a la eficiencia del combustible y las emisiones del vehículo. El objetivo de este estudio es desarrollar mapas motorizados de consumo de combustible y emisiones de dióxido de carbono (CO_2) para un vehículo ligero que circule en condiciones reales de tráfico. Un vehículo de pasajeros propulsado a gasolina y representativo del parque automotor ecuatoriano fue seleccionado para la campaña experimental que se desarrolló en una ruta de prueba diseñada de acuerdo a la normativa de emisiones en conducción real (RDE). Se utilizó un dispositivo de diagnóstico a bordo (DAB) para registrar en tiempo real los parámetros de funcionamiento del motor y del vehículo. Además, las emisiones de CO_2 se estimaron utilizando la tasa de combustible registrada desde el sistema OBD del vehículo. Este estudio propuso una metodología novedosa para desarrollar mapas de motor de contorno bidimensional basados en datos OBD.**

El resultado mostró que el motor del vehículo funcionaba en condiciones reales de tráfico con una eficiencia térmica de frenado (ETF) del 27 %, un consumo de combustible específico de frenado (CCFE) de 275 g/kWh y un factor de emisión de energía de CO_2 de 716 g/kWh. En términos de distancia, el factor de emisión de CO_2 del vehículo probado fue de aproximadamente 190 g/km. En general, este estudio demuestra que el enfoque OBD es un método potencial para ser utilizado para evaluar el consumo de combustible y las emisiones de CO2 de un vehículo que opera en condiciones de tráfico del mundo real, especialmente en los países de América Latina, países en los que los sistemas portátiles de medición de emisiones (PEMS) no están fácilmente disponibles.

***Palabras clave* — Consumo de combustible; Emisiones de CO_2; Mapas de motor; Diagnóstico a bordo (OBD).**

I. INTRODUCTION

In cities around the world, road transport is a major source of greenhouse gas (GHG) emissions and air pollution, affecting the environment and human health, respectively. From 2022 to 2050, global energy consumption for road transport is projected to increase by 28 % [1]. In Ecuador, the energy balance calculated for 2021 by the Ministry of Energy and Mines estimates that transport with approximately 49 % is the sector that showed the highest energy consumption. In fact, diesel and gasoline were the energy sources with the highest demand, with annual growth rates of up to 25 % [2]. As a result, the sector with the highest GHG emissions in Ecuador in 2021 was transport with 50.7 %. Hence, the energy and environmental problems produced by road transport cannot be ignored.

Fuel consumption and emissions of vehicles under real traffic conditions are the result of the interaction of several factors and conditions [3]. In general, these conditions can be categorized into: (I) vehicle design (for example, vehicle type, powertrain configuration and technology, fuel type and aftertreatment system technology). (II) driver characteristics. (III) travel conditions (for example, passenger load and use of auxiliary systems). (IV) traffic flow conditions (for example, congestion). (V) road conditions (for example, slope level and road type). (VI) environmental conditions (for example, temperatu-

[1] Corresponfing author: Fredy Rosero Ph.D. of the Faculty of Applied Sciences, Universidad Técnica del Norte, 100105 Ibarra, Ecuador (e-mail: farosero@utn.edu.ec). ORCID number 0000-0003-0971-1944.

[2] Xavier Rosero Ph.D. of the Faculty of Applied Sciences, Universidad Técnica del Norte, 100105 Ibarra, Ecuador (e-mail: cxrosero@utn.edu.ec). ORCID number 0000-0002-5396-6621.

[3] Zamir Mera Ph.D. of the Faculty of Applied Sciences, Universidad Técnica del Norte, 100105 Ibarra, Ecuador (e-mail: zamera@utn.edu.ec). ORCID number 0000-0003-2897-8847.

Manuscript Received: Sep 21, 2023
Revised: Nov 08, 2023
Accepted: Nov 27, 2023
DOI: https://doi.org/10.29019/enfoqueute.1002

re). And (VII) geographical conditions (for example, altitude). Hence, unlike laboratory testing with controlled conditions, evaluation under real traffic conditions is a strategy that the scientific community is currently applying to obtain real-world vehicle performance.

In recent times, several studies have reported that vehicles show significant differences between the emission levels measured experimentally in real traffic conditions and the levels obtained in vehicle type-approval processes with controlled operating conditions. This has led to additional and rapid changes in enforcement in the United States [4], China and the European Union [5]. In fact, Europe already requires the use of portable emission measurement systems (PEMS) and on-board diagnostic (OBD) systems to verify vehicle emissions, both for type-approval and real-traffic testing [6]. In Latin America, Brazil has adopted OBD requirements like the Euro V standard. In the case of OBD systems, they have been designed to monitor the performance of the engine and aftertreatment system components of the vehicles. Consequently, OBD systems have become a key component of vehicle inspection and maintenance programs, as well as for verifying that a vehicle meets regulatory compliance limits [7]. In general, PEMS measurements and OBD data collection are the two strategies commonly applied worldwide to assess the performance of vehicles and engines in real-traffic conditions. However, in Latin America PEMS equipment is not widely available. Hence, the OBD approach becomes a valid strategy to be applied in studies developed in countries such as Ecuador.

In parallel, to minimize discrepancies between type-approval emission levels and those in real traffic, the European Union has introduced the Regulation (EU) 2016/427 [8], which includes a testing procedure called 'Real Driving Emissions' (RDE) as a complement to the globally harmonized light-duty vehicle test cycles (WLTC) [9]. RDE test method is based on the use of PEMS to monitor on-road emission levels of light-duty vehicles. In addition, the routes defined in the RDE tests need to meet certain characteristics: environmental, dynamic, driving behaviour and equipment accuracy, among others described in the Regulation (EU) 2017/115 [10]. Therefore, the design of a test route according to the RDE regulation would be a strategy to improve the reliability of the data obtained in a study.

Previous work has focused on assessing the fuel efficiency and emission levels of vehicles using four approaches: (a) emission modelling and vehicle simulators, (b) vehicle specific power (VSP) based assessments, (c) real traffic testing with PEMS, and (d) engine map development. Some relevant work for each approach can be mentioned below. In the case of emission modelling, Wen et al. [11] recently used a random forest model to map real-time vehicle emissions on a motorway in Chengdu (China). Regarding the VSP approach, this was used by He et al. [12] to develop and statistically compare VSP distributions as a function of speed and vehicle typology in Beijing. In the case of experimental PEMS data, Bishop et al. [13] used it to identify discrepancies in fuel efficiency and nitrogen oxide (NO_x) emissions between homologation processes and real traffic for various diesel and gasoline vehicle models. Regarding engine maps, Mera et al. [14] combined engine operation data and the VSP approach to reduce emission estimation error. It can also be mentioned that Castresana et al. [15] recently investigated the robustness of artificial neural networks to predict multiple performance and emission parameters using information from a diesel engine map for marine applications. In general, the engine mapping approach characterizes the fuel consumption and emission performance of a vehicle's engine for different engine speed and torque ranges [16]. In addition, this resulting information is very useful as input data for emission models and vehicle simulators.

Based on the literature review, three gaps were identified concerning engine maps: (I) maps have not been developed using only data from the vehicle's OBD system. (II) transient maps have not been constructed from a vehicle operating under a test route designed according to RDE regulations. (III) in Latin America, the engine map approach has not been applied to assess vehicle performance. Hence, this study focuses on the development of engine maps of fuel consumption and carbon dioxide (CO_2) emissions for a vehicle operating under real traffic conditions on an RDE test route in the city of Ibarra, Ecuador.

There are three research questions posed for this study:

- Is it possible to develop contour engine maps using information from the OBD system of a light-duty vehicle operating in real traffic?
- What are the most used torque and RPM ranges in engine maps of a vehicle operating on an RDE test route?
- How do fuel efficiency and CO_2 emission levels vary for different engine map zones?
- What are the average fuel consumption and CO_2 emission factors of a light-duty vehicle for the motorway, suburban and urban sections of the RDE route?

II. METHODOLOGY

A. Test vehicle

A representative passenger vehicle powered by gasoline of the ecuadorian vehicle fleet was selected to analyze the performance of an engine in real traffic conditions. In fact, in the last decade, this vehicle has been one of the most used models for the taxi service in several cities of Ecuador [17]. The tested vehicle was a Chevrolet Aveo Emotion, equipped with an engine of 1.6 liters. In general, the characteristics of the test vehicle are representative of passenger capacity, weight, engine torque and power and gearbox type for the automotive segment of the country. Table I provides additional information of the tested vehicle. Moreover, it is important to note that the tested vehicle underwent an exhaustive preventive and corrective maintenance program to guarantee the results of this study. In fact, this maintenance ensured that the vehicle successfully passed the mandatory annual technical inspection required by ecuadorian regulations. Consequently, the evaluated vehicle was in optimal technical condition before the execution of the experimental campaign.

TABLE I
TECHNICAL SPECIFICATIONS OF THE TESTED VEHICLE

Vehicle parameter	Value
Fuel type	Gasoline
Model name	Chevrolet Aveo Emotion
Model year	2011
Gross vehicle weight (t)	1.592
Weight (t)	1.203
Length /Width/ Height (m)	4.04/1.67/1.16
Max passengers	5
Axle configuration	4×2
Gearbox	Manual (5)
Number of engine cylinders	4 in-line
Engine total displacement (cm^3)	1598
Engine maximum power (kW@rev/min)	76@5800
Engine peak torque (N.m@rev/min)	145@3600
Fuel injection type	Indirect injection
Compression ratio	9.5:1

B. Test route

In this study, an experimental campaign was conducted along a test route designed in the city of Ibarra, Ecuador. This city is the capital of the province of Imbabura and has a population of approximately 200 000 inhabitants. In terms of vehicle fleet, Ibarra has experienced a significant growth of approximately 6 % per year in recent years [18], which has generated challenges in terms of traffic and mobility. In this study, the test route was designed under the regulation (EU) 2017/1151 [10], which establishes different kinematic parameters, such as distance by route section, vehicle speeds, cumulative altitudes, and total trip duration. Hence, this study was carried out on an RDE test route (with approximately 53 km) including urban (0-60 km/h), suburban (60-90 km/h), and motorway (>90 km/h) sections, as shown in Fig. 1. However, it is important to mention that this study is not intended to represent an RDE homologation process to evaluate the fuel consumption and CO_2 emissions of the vehicle. In addition, details of the test route are provided in Table II.

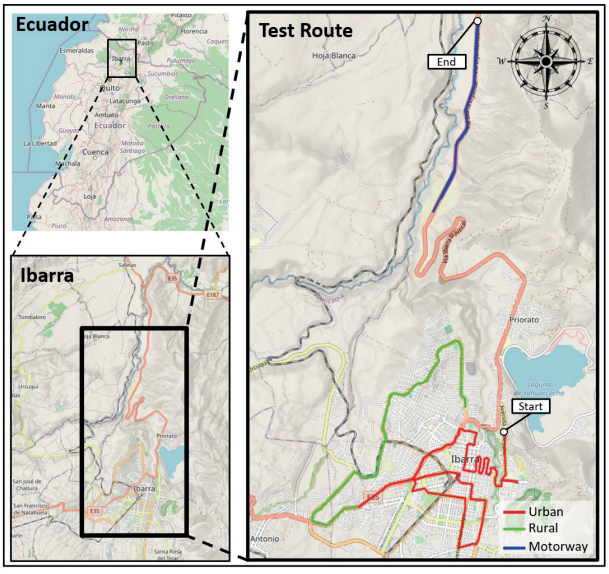

Fig. 1. Selected experimental route for field data collection.

TABLE II
INFORMATION OF TEST ROUTE

Start position	Avenue 17 de Julio
Final position	Panamericana Norte E-35
Altitude at origin/destination position (m)	2219/1853
Total trip distance (km)	52.8
Urban trip distance (km)	19.1
Suburban trip distance (km)	12.3
Motorway trip distance(km)	21.4
Altitude difference (m)	366

C. Instrumentation

In general, the study required instruments for measuring the following three types of information: (I) vehicle kinematics (for example, position and speed), (II) vehicle and engine operating parameters (for example, torque and speed engine values), and (III) instantaneous fuel consumption data. A global positioning system (GPS) logger device, called 'GL-770', was installed in the test vehicle to record latitude, longitude, altitude, and vehicle speed with a frequency of 1Hz. It is important to note that this device is non-intrusive, resulting in the collection of vehicle kinematic information without affecting the regular operation of the tested vehicle operation. To record engine operating parameters and the vehicle fuel consumption data, an OBD interface device (called ELM Electronics 327) was connected to a mobile phone application (called Torque Pro). The ELM 327 was connected to the OBD2 diagnostic port to read the engine operating parameters in real time from the engine control unit (ECU). At the same time, these parameters were sent via Bluetooth from the ELM 327 to the Torque Pro mobile application to be recorded. In this study, the paid version of Torque Pro was used to set the 1 Hz sampling time of the data. The three instruments used for field data collection are shown in figure 2.

Fig. 2. Tested vehicle equipped on board with GPS logger, OBD interface, and OBD data recording application for field data collection.

D. Experimental campaign

As mentioned above, a Chevrolet Aveo vehicle equipped with GPS and OBD interface devices was evaluated on a test route in the city of Ibarra. The experimental campaign of this study was conducted in February 2023. The campaign for the tested vehicle included both peak (7:00 and 13:00) and non-peak (10:00 and 15:00) periods. The vehicle was driven normally on the test route, respecting the traffic signals and speed limits established in the city. During the experimental campaign, the vehicle was powered by a commercially available type of gasoline called 'Extra' in Ecuador. This gasoline is characterised by an octane number of 85. The air conditioning of the vehicle was turned off to avoid additional loads on the engine operation during the experimental campaign. Before the start of each test, the vehicle was warmed up for 15 minutes until the engine reached normal operating temperature. To ensure the repeatability of the tests, the same driver drove the vehicle during all tests. Regarding the passenger load, the campaign was conducted with two people: a driver and a staff technician. The experimental campaign included six entire trips on the RDE route. These tests were conducted during peak periods (7:00 and 13:00) and off-peak periods (10:00 and 15:00). This strategy was designed to ensure that the results obtained accurately reflected vehicle performance at different levels of congestion. The average duration of each entire trip (urban, suburban and motorway road sections) on the test route was approximately 1.7 hours, and the average trip speed of the vehicle was approximately 35 km/h. Table III shows an overview of the operating conditions for the tested vehicle by road section in the experimental campaign.

TABLE III
OVERVIEW OF THE OPERATING CONDITIONS FOR THE TESTED VEHICLE IN TERMS OF THE ROAD SECTION IN THE EXPERIMENTAL CAMPAIGN

Operating condition	Road section			All sections
	Urban	Suburban	Motorway	
Tests	6	6	6	6
Average trip time (s)	5 040	820	846	6 084
Average trip speed (km/h)	18.35	53.39	92.77	35.01
Average moving speed (km/h)	25.42	58.35	93.73	44.24
Maximum trip speed (km/h)	55.64	85.52	115.16	115.16
Average positive accel (m/s^2)	0.45	0.44	0.28	0.41
Total idle period (%)	28.06	8.49	1.01	21.04
Total accel period (%)	32.4	39.51	31.33	33.24
Total decele period (%)	27.29	33.85	29.93	28.63
Total cruise period (%)	12.24	18.13	37.7	17.08

E. Pre-processing real-world vehicle data

In this study, the applied preprocessing method was developed using R Studio software [19]. As the measurements of the experimental campaign were recorded using two devices with different initial recording times, a preprocessing step was developed to synchronise the different signals from the two devices through the vehicle speed. This speed was recorded second-by-second using both the GPS position data and through the OBD system of the vehicle. It is important to mention that the speed profiles were smoothed using a moving window filter [20]. Overall, the data pre-processing stage ensures to guarantee of the results presented in this study.

F. Method for developing engine maps based on OBD data

Three variables are necessary in order to develop an engine map graph. Typically, torque and speed are used as the primary factors for the horizontal and vertical axes of the maps. Meanwhile, the third variable (Brake Thermal Efficiency (BTE), fuel consumption, brake-specific fuel consumption (BSFC) and emission rates) served as the parameter defining the theme of the map. In this study, the method applied to develop the engine maps included the following two stages: (1) generate grid engine maps by engine speed and torque ranges with averaged values of the third variable, and (2) develop two-dimensional contour engine maps based on grid data. These two stages were performed using R Studio [19].

Initially, the grid engine maps were developed following the methodology proposed by Rosero et al. [21]. Initially, grids were generated based on torque and speed engine intervals, and the remaining engine operating data (referred to as the third variable) were assigned to their corresponding grid. Subsequently, the grouped data were averaged to obtain a single value by grid (speed-torque). Outliers were filtered by examining the relative frequency and standard deviation of each data group. Finally, the averaged values were discretized and assigned specific colours for each data interval when plotted on the engine maps.

Subsequently, to plot the two-dimensional contour engine maps, this study utilized the RStudio software [19] with an R package called 'ggplot2' R [22]. This package includes a function named 'geom_contour_filled()', which generates contour plots using z variable observations (for example, fuel consumption, and emission rates) that should be previously grouped into interval combinations of two variables, x (engine speed) and y (torque). Based on this requirement, the data matrices resulting from the grid engine were used as input data to generate the contour engine maps. Finally, to develop the Contour-plot engine maps, a divergent colour scale was applied for each defined interval of the third variable. As a result of these two processing stages, this study obtained contour maps of BTE, BSFC, brake-specific CO_2 emissions, fuel consumption rates and CO_2 rates.

III. CALCULATION METHODS

A. Effective power and torque of the engine

The OBD system provided engine load values $(L_{e_{obd}})$ as a percentage relative to the maximum effective power $(P_{e_{max}})$that the engine could produce. Based on the technical specifications of the tested vehicle manufacturer, the $P_{e_{max}}$ assumed for this study was 76 kW. To determine the actual effective engine power (P_e) in kW at any given moment, equation 1 was utilized.

Equation 1

$$P_e = L_{e_{obd}} \cdot P_{e_{max}} \quad (1)$$

The instantaneous engine torque values (τ) expressed in N.m, were calculated by multiplying the effective power and the engine speed.

B. Fuel energy efficiency and CO_2 emission factors

The grid engine map generation process involved the calculation of the second-by-second BTE and BSFC values expressed in $(\%)$ and (g/kWh), respectively, for the tested engine. These calculations were performed using equation 2 and 3, as follows:

Equation 2

$$BTE = \frac{P_e}{P_{th}} = \frac{P_e}{FC \cdot CV_{fuel}} \quad (2)$$

Equation 3

$$BSFC = \frac{3600 \cdot FC}{P_{-}} \quad (3)$$

Here, FC is the instantaneous fuel consumption expressed in (g/s), P_{th} represents the instantaneous thermal power (kW) resulting from the fuel being injected, while CV_{fuel} is the calorific value of the gasoline used $(46.3\ MJ/kg)$ [23].

In this study, based on the stoichiometry of gasoline combustion, the CO_2 emission rate (ER_{CO_2}) was calculated using equation 4 as follows:

Equation 4

$$ER_{CO_2} = FC \cdot \frac{44}{12+\left(\frac{H}{C}\right)} \quad (4)$$

Here, since the fuel utilized is gasoline (C_8H1_8), the assumed values were 18 for hydrogen (H) and 8 for carbon (C) [24].

To assess the performances of the tested engine for different road sections (i), the average values of BTE (%), BSFC (g/kWh), energy-specific CO_2 emission factor (g/kWh), as well as fuel consumption and CO_2 emission rates (g/s), were estimated using equations 5-9, as follows:

Equation 5

$$\overline{BTE_i} = \frac{\sum_{t=1}^{T_i}(BTE_i)}{T_i} \quad (5)$$

Equation 6

$$\overline{BSFC_i} = \frac{\sum_{t=1}^{T_i}(BSFC_i)}{T_i} \quad (6)$$

Equation 7

$$\overline{EF_{CO_2\,i}}^{e} = \frac{\sum_{t=1}^{T_{i,w}}\left(EF_{CO_{2\,i,}}\right)}{T_i} \quad (7)$$

Equation 8

$$\overline{FC_i} = \frac{\sum_{t=1}^{T_i}(FC_i)}{T_i} \quad (8)$$

Equation 9

$$\overline{ER_{CO_2\,i}} = \frac{\sum_{t=1}^{T_{i,w}}\left(ER_{CO_{2\,i,}}\right)}{T_i} \quad (9)$$

Here, T is the number of second-by-second test data.

Moreover, to evaluate the vehicle performance for different road sections, the average distance-specific fuel consumption $(\overline{FC}^d)$ and CO_2 emission $(\overline{EF_{CO_2}}^d)$ factors, expressed in (g/km), were estimated using equations 10 and 11, as follows:

Equation 10

$$\overline{FC_i}^d = \frac{\sum_{t=1}^{T_i}(FC_{i,t})}{\sum_{t=1}^{T_i}(d_t)} \quad (10)$$

Equation 11

$$\overline{EF_{CO_2\,i}}^d = \frac{\sum_{t=1}^{T_i}\left(ER_{CO_{2\,i,t}}\right)}{\sum_{t=1}^{T_i}(d_t)} \quad (11)$$

IV. RESULTS AND DISCUSSION

The results provided in this section address the research questions and are organized into three topics: (a) typical engine operation patterns by torque and speed for different road sections, (b) contour engine maps of BTE, fuel efficiency, and CO_2 emissions, and (c) the overall fuel consumption and emission factors.

A. Typical engine operation patterns by torque and speed

Figure 3 presents the patterns of engine operation by torque and speed for motorway, suburban, and urban roads. Grey circles represent the cumulative relative frequency (CRF) of engine operation points calculated for each torque and speed interval, while yellow shaded areas identify the highest engine operation patterns. In the case of the motorway section, the engine operated approximately 85 % of the time in a speed range of 2 500-3 500 rev/min, which are half-load intervals considering that the maximum engine power is reached at 5 800 rev/min. On the suburban section, engine performance was heterogeneous, operating approximately 95 % between low and high (75–100 N·m) torque ranges and low and medium (3 000-3 500 rev/min) speed ranges. In the case of the urban section, approximately 50 % of engine operation was between the lowest torque and lowest speed ranges. Based on Table II, these low-load operation results for urban roads are related to the fact that the vehicle operated with approximately 30 % at idle conditions and an average travel speed of less than 20 km/h. Overall, these results demonstrate that the type of road section significantly influences the torque and speed

ranges that a vehicle engine can operate in real traffic conditions. This is consistent with that reported by Bishop et al. [25], who also found that the engine load patterns can vary with the type of road section, especially due to large changes in vehicle kinematics. In fact, Bishop et al. found that a light passenger vehicle engine ran approximately 35 % in low (90-110 N·m) torque ranges and low (1 000-1 500 rev/min) speed ranges. This value of 35 % operation at low load conditions is slightly higher than the 30 % found in the present study. Moreover, Tsiakmakis et al. [26] reported that the average travel speed and $v*a$ factors for light passenger vehicles (LDVs) vary significantly with the type of road section. In fact, Tsiakmakis et al. found that between motorway and urban sections, the average trip speed was reduced approximately 3.5 times (from 67 to 19 km/h). Whereas, in the present study, this speed was strongly reduced by 5 times (from 92 to 18 km/h).

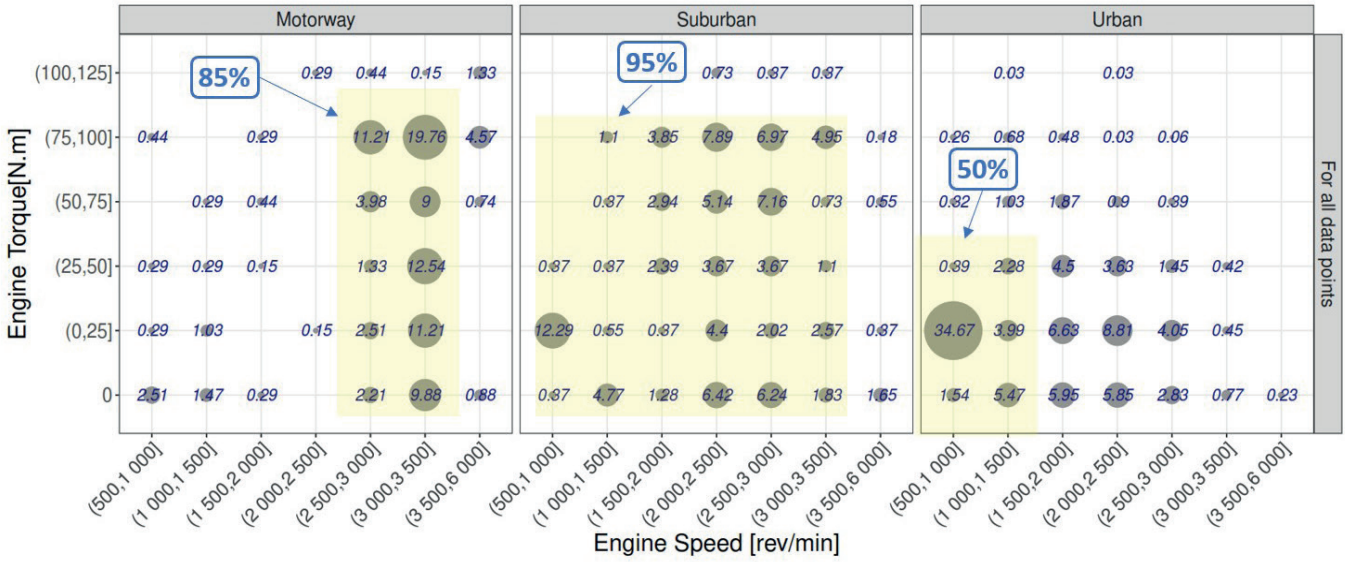

Fig. 3. Typical engine operation patterns by type of road section for all data points

B. Contour engine maps based on OBD data

1. Fuel energy efficiency and brake-specific CO_2 emission maps

Figure 4 illustrates the contour engine maps for BTE (a), BSFC (b), and brake-specific CO_2 emissions (c). In figure 4. a) the areas with the highest BTE (light green) values correspond to operating ranges with medium torque and engine speed, while those with the lowest efficiency (blue) are in areas of low torque demand. Additionally, at high torque and speed ranges, the engine shows values above 25 %. In figure 4.b) and 4.c) it can be seen that the contours with the lowest fuel efficiency and brake-specific CO_2 emissions (respectively) are in low torque ranges, which are common for an engine running in idle mode. Figure 4. b) shows that the largest contour corresponds to a range of BSFC with values between 175 and 250 g/kWh. This range is typical for engines mounted on light vehicles [27]. Figure 4.c) shows that the lowest CO_2 emissions (light green) areas with values below 600 g CO_2/kWh are in the mid-range of torque and speeds. Overall, these results indicate that the lowest fuel consumption and CO_2 emissions correspond to medium torque and engine speed ranges. Similar patterns were found by previous studies that evaluated engine performance of engines based on the engine mapping approach [13], [25]. In fact, Bishop et al. [13] found that between medium and high load conditions, the brake-specific CO_2 emissions of an engine were reduced by approximately 2.5 times (from 500 to 200 g CO_2/kWh). Moreover, these three figures show that in idle mode, which is typical of urban operation conditions, the engine has a lower fuel efficiency in terms of energy.

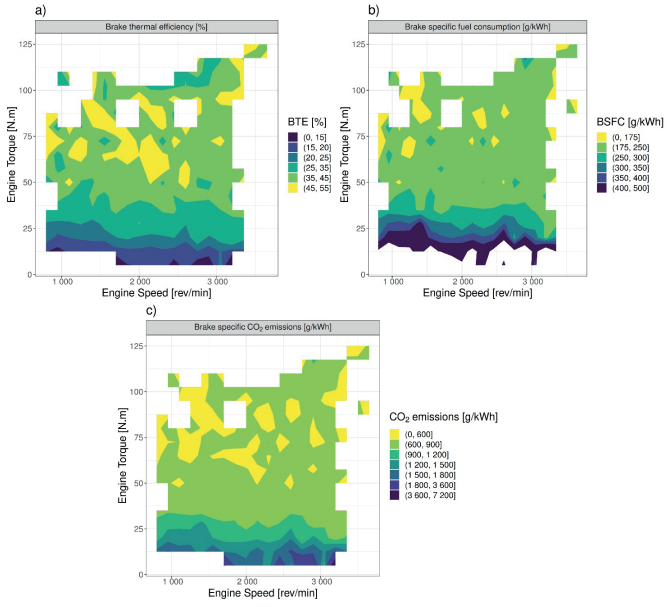

Fig. 4. Engine maps for (a) brake thermal efficiency, (b) brake-specific fuel consumption, and (c) brake-specific CO_2 emissions.

2. Fuel consumption and emission rates maps

Figure 5.a) and 5.b) present contour engine maps for fuel consumption and CO_2 emissions rates, respectively. Overall, these figures have similar sharply increasing trends (from light green to blue areas) of strong increase. In fact, Figure 5.a) and 5.b) show that the engine under maximum power operating conditions with an increase in torque and speed, fuel consumption and CO_2 emissions rates reached the highest values (blue) of 3.5 and 10.0 g/s, respectively. In contrast, as expected, when there is a lower demand for engine power, the fuel consumption and emission rates have the lowest values (light green). Although these green areas show lower fuel consumption expressed in terms of rates, based on Figure 6, it can be stated that these same areas are the least efficient in energy terms. The resultant increasing trends are consistent with previous works for LDV's [13], [14], [28] and heavy-duty vehicles (HDV's) [21], [29], and emissions models [30]. For instance, Mera et al. [13] found that between low and high load conditions, the CO_2 emissions rates of an LDV engine increased approximately 20 times (from 0.32 to 7.2 g CO_2/s). Similarly, in the present study, the CO_2 emissions rates were increased by about 14 times (from 0.69 to 10 g CO_2/s). It is important to note that the information contained in figure 5, expressed in terms of (g/s), can be used as input data to develop an empirical emission model. Previously, the information from the maps must be arranged in the form of a matrix by torque and engine speed intervals [21], [31]. The model can predict second-by-second fuel consumption and CO_2 emission values of the vehicle for any given operating scenario. Hence, future work will focus on using the engine map matrix resulting from this study for predicting fuel consumption and emissions of a vehicle by using torque and speed signals from engine operation as input data.

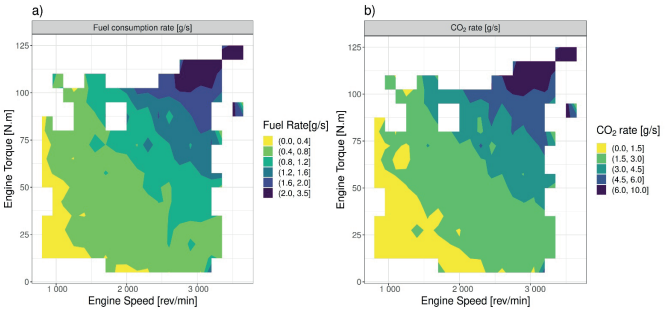

Fig. 5. Engine maps for (a) fuel consumption, and (c) CO_2 rates.

C. Overview of vehicle engine performance

Table IV shows the overall engine performance of the tested vehicle for motorway, suburban, and urban road sections. The performance of the vehicle is expressed in terms of energy-emission factors, average emission rates and distance-emission factors. In the case of BTE, the average value was 27 % for all sections, although in urban a BTE of approximately 25 % was found. This result is consistent with figure 3 and 4, which showed that in urban conditions, the engine frequently ran in low torque and speed ranges, where there was lower fuel efficiency. In the case of energy-emission factors, this study found an average value of BSFC and CO_2 of approximately 275 and 716 g/kWh, respectively. The minimum BSFC was for the motorway section with 250.18 g/kWh. In the case of the CO_2 emission factor in terms of distance, the average value was approximately 190 g/km. Comparing urban and motorway road sections, CO_2 emission factors of the vehicle increase by up to 50 %. The average value of 190 g CO_2/km found in the present study is higher than the range of 140-150 g CO_2/km reported by Zurita et al. [32], who used standardized driving cycles (for example, New European Driving Cycle (NEDC) and Federal Test Procedure (FTP) 75) to evaluate the performance of a Chevrolet Aveo under controlled laboratory conditions. This demonstrates the importance of a vehicle being evaluated with driving cycles that reflect the actual kinematic conditions of the spatial domain in which the vehicle operates [33]. Otherwise, there may be a discrepancy between the values obtained in type-approval processes and those obtained in real traffic conditions. Overall, these results demonstrate that the vehicle and its engine performed better in highway conditions. Hence, to improve engine performance, especially in urban conditions, the use of start-stop technologies in engines is a valid strategy [28]. This leads to reduced engine running times in low load ranges (idle conditions), which are characterized by low fuel efficiency as this study has shown.

TABLE IV
OVERALL ENGINE PERFORMANCE OF FUEL EFFICIENCY, ENERGY EMISSIONS, EMISSION RATES, AND DISTANCE EMISSIONS (FROM VEHICLE) BY ROAD SECTION

Road section	Average value (%)	Energy-emission factors (g/kWh)		Average emission rates (g/s)		Distance-emission factors (g/km)	
	BTE	BSFC	CO_2	FC	CO_2	FC	CO_2
Urban	0.25	287.01	765.28	0.39	1.23	78.21	241.50
Suburban	0.27	244.81	654.74	0.76	2.35	51.49	159.01
Motorway	0.31	250.18	692.06	1.34	4.14	52.11	160.91
All sections	0.27	275.26	716.72	0.59	1.84	61.58	190.14

V. Conclusion

Under real traffic conditions a vehicle interacts with the road, other vehicles, and traffic control devices. The level of traffic influences driving patterns and, consequently, this could affect travel times, fuel consumption and emission levels of vehicles. In this context, this study aimed to create contour engine maps of fuel consumption and CO_2 emissions from a vehicle operating under real-world traffic conditions. A typical gasoline-powered light vehicle from the ecuadorian car fleet was chosen for the experimental campaign developed on an RDE route. This study presents a novel methodology for constructing two-dimensional engine contour maps using real-time recording of engine and vehicle parameters from the OBD system.

The results showed that the engine of the tested vehicle operated with a BTE of 27 %, a BSFC of 275 g/kWh, and a CO_2 energy-emission factor of 716 g/kWh under real traffic conditions. Furthermore, in terms of distance, the CO_2 emission factor for the tested vehicle was approximately 190 g/km. Overall, these results demonstrate two aspects: (I) the tested vehicle and its engine had lower fuel efficiency for urban conditions, which were characterized by frequent engine operation at low-load conditions; and (II) it was demonstrated that the OBD approach is a valid method to evaluate the performance of a vehicle in real traffic conditions. Hence, the OBD approach is a valid alternative for Latin American countries, where PEMS equipment is not readily available. Finally, it is important to note that the resulting engine maps of this study include valuable information that can be used as input data for vehicle simulators, as well as for developing emission inventories in cities.

ACKNOWLEDGEMENT

The authors would like to thank Andrés Espinosa and Luis Cuzco, those who contributed to the experimental campaign carried out as part of this study.

REFERENCES

[1] H. C. Frey. “Trends in Onroad Transportation Energy and Emissions,” *Journal of the Air & Waste Management Association.*, vol. 68, no. 6, pp. 514-563, 2018, doi: 10.1080/10962247.2018.1454357.

[2] Instituto de Investigación Geológico y Energético del Ecuador, “Balance Energético Nacional del Ecuador 2021,” Quito, Ecuador, 2022. [Online]. Available: https://www.recursosyenergia.gob.ec/wp-content/uploads/2022/08/Balance_Energético_Nacional_2021-VF_opt.pdf.

[3] F. Rosero, N. Fonseca, J.M. López, and J. Casanova. “Effects of Passenger Load, Road Grade, and Congestion Level on Real-World Fuel Consumption and Emissions from Compressed Natural Gas and Diesel Urban Buses,” *Applied Energy*, vol. 282, no. November 2020, p. 116195, Jan. 2021, doi: 10.1016/j.apenergy.2020.116195.

[4] EPA, NHTSA, and DOT. *Greenhouse Gas Emissions and Fuel Efficiency Standards for Medium- Heavy-Duty Engines and Vehicles-Phase 2*, vol. 81, no. 206. 2016, pp. 73478-74274.

[5] EU. “Commission Regulation (EU) No 582/2011 Of 25 May 2011 Implementing and Amending Regulation (EC) No 595/2009 of the European Parliament and of the Council With Respect to Emissions From Heavy Duty Vehicles (Euro VI) and Amending Annexes I And III to Direct,” *Official Journal of the European Union*, 2011. https://eur-lex.europa.eu/eli/reg/2011/582/oj.

[6] F. Posada and A. Bandivadekar. “Global Overview of On-Board Diagnostic (OBD) Systems for Heavy-Duty Vehicles,” *ICCT*, no. January, 2015.

[7] Á. Ramos, R. García-Contreras, and O. Armas. “Performance, Combustion Timing and Emissions from a Light Duty Vehicle at Different Altitudes Fueled with Animal Fat Biodiesel, GTL and Diesel Fuels,” vol. 182, pp. 507-517, 2016, doi: 10.1016/j.apenergy.2016.08.159.

[8] European Commission and Council of the European Union. “Commission Regulation (EU) 2016/427 Amending Regulation (EC) No 692/2008 as Regards Emissions from Light Passenger and Commercial Vehicles (Euro 6) (Text With EEA Relevance),” *Official Journal of the European Union*, vol. 82, no. 31/03/2016, pp. 1-98, 2016, [Online]. Available: http://data.europa.eu/eli/reg/2016/427/oj.

[9] J. M. Luján, V. Bermúdez, V. Dolz, and J. Monsalve-Serrano. “An Assessment of the Real-World Driving Gaseous Emissions from a Euro 6 Light-Duty Diesel Vehicle Using a Portable Emissions Measurement System (PEMS),” *Atmospheric Environment,* vol. 174, no. July 2017, pp. 112-121, 2018, doi: 10.1016/j.atmosenv.2017.11.056.

[10] European Commission. “Commission Regulation (EU) 2017/1151 of 1 June 2017 Supplementing Regulation (EC) No 715/2007 of the European Parliament and of the Council on Type-Approval of Motor Vehicles with Respect to Emissions from Light Passenger and Commercial Vehicles (Euro 5 a)” *Official Journal of the European Union,* no. 692, pp. 1–643, 2017.

[11] Y. Wen, et al. “A Data-Driven Method of Traffic Emissions Mapping with Land use Random Forest Models,” *Applied Energy*, vol. 305, no. July 2021, 2022, doi: 10.1016/j.apenergy.2021.117916.

[12] W. He, L. Duan, Z. Zhang, X. Zhao, and Y. Cheng. “Analysis of the Characteristics of Real-World Emission Factors and VSP Distributions. A Case Study in Beijing,” *Sustainability*, vol. 14, no. 18, p. 11512, Sep. 2022, doi: 10.3390/su141811512.

[13] J. D. K. Bishop, N. Molden, and A. M. Boies. “Using Portable Emissions Measurement Systems (PEMS) to Derive More Accurate Estimates of Fuel Use and Nitrogen Oxides Emissions from Modern Euro 6 Passenger Cars Under Real-World Driving Conditions,” *Applied Energy*, vol. 242, no. February, pp. 942-973, 2019, doi: 10.1016/j.apenergy.2019.03.047.

[14] Z. Mera, R. Varella, P. Baptista, G. Duarte, and F. Rosero.“Including Engine Data for Energy and Pollutants Assessment into the Vehicle Specific Power Methodology,” *Applied Energy*, vol. 311, no. February, p. 118690, Apr. 2022, doi: 10.1016/j.apenergy.2022.118690.

[15] J. Castresana, G. Gabiña, L. Martin, A. Basterretxea, and Z. Uriondo. “Marine Diesel Engine ANN Modelling with Multiple Output for Complete Engine Performance Map,” *Fuel*, vol. 319, no. March, 2022, doi: 10.1016/j.fuel.2022.123873.

[16] Z. Gao, J. C. Conklin, C. S. Daw, and V. K. Chakravarthy. “A Proposed Methodology for Estimating Transient Engine-Out Temperature and Emissions from Steady-State Maps,” *International Journal of Engine Research*, vol. 11, no. 2, pp. 137-151, 2010, doi: 10.1243/14680874JER05609.

[17] AEADE. “Anuario 2020 AEADE,” Quito, 2020. [Online]. Available: https://abimapi.com.br/anuario/pdf/anuario_2020-3.pdf.

[18] Instituto Nacional de Estadística y Censos (INEC). “Ecuador-Estadísticas de Transportes 2020,” Quito, 2021. [Online]. Available: https://anda.inec.gob.ec/anda/index.php/catalog/894/related_materials.

[19] RStudio. “RStudio: Integrated Development Environment for R.” Boston, MA, 2018.

[20] J. Wang, H. Rakha, L. C. Marr, P. Murray-Tuite, and I. El-Shawarby. “Multi-Modal Energy Consumption Modeling and Eco-routing System Development,” 2017, [Online]. Available: https://vtechworks.lib.vt.edu/bitstream/handle/10919/78624/Wang_J_D_2017.pdf?sequence=1&isAllowed=y.

[21] F. Rosero, N. Fonseca, J.-M. López, and J. Casanova. “Real-World Fuel Efficiency and Emissions from an Urban Diesel Bus Engine Under Transient Operating Conditions,” *Applied. Energy*, vol. 261, no. December 2019, p. 114442, Mar. 2020, doi: 10.1016/j.apenergy.2019.114442.

[22] H. Wickham. *Ggplot2: Elegant Graphics for Data Analysis*. Springer-Verlag New York, 2016.

[23] A. Quimbita and E. Guallichico. “Determinación del potencial energético y mecánico del motor Mazda F2 al utilizar los tipos de gasolina comercial empleados en el Ecuador,” Universidad de las Fuerzas Armadas - ESPE, 2017.

[24] J. B. Heywood. *Internal Combustion Engine Fundamentals*. New York: McGraw-Hill, 1988.

[25] J. D. K. Bishop, M. E. J. Stettler, N. Molden, and A. M. Boies. “Engine Maps of Fuel Use and Emissions From Transient Driving Cycles,” *Applied Energy*, vol. 183, pp. 202-217, 2016, doi: 10.1016/j.apenergy.2016.08.175.

[26] S. Tsiakmakis, et al. “From Lab-to-Road & Vice-Versa : Using a Simulation-Based Approach for Predicting Real-World CO_2 Emissions” *Energy*, vol. 169, pp. 1153–1165, 2019, doi: 10.1016/j.energy.2018.12.063.

[27] J. Gao, et al. “Fuel Consumption and Exhaust Emissions of Diesel Vehicles in Worldwide Harmonized Light Vehicles Test Cycles and Their Sensitivities to Eco-Driving Factors,” *Energy Conversion and Management*, vol. 196, no. May, pp. 605–613, 2019, doi: 10.1016/j.enconman.2019.06.038.

[28] G. Triantafyllopoulos, A. Dimaratos, L. Ntziachristos, Y. Bernard, J. Dornoff, and Z. Samaras. “A Study on the CO_2 and NO X Emissions Performance of Euro 6 Diesel Vehicles Under Various Chassis Dynamometer and On-Road Conditions Including Latest Regulatory Provi-

sions," *Science of the Total Environmen.*, vol. 66, no. x, pp. 337–346, 2019, doi: 10.1016/j.scitotenv.2019.02.144.

[29] E. G. Giakoumis and A. I. Alafouzos. "Study of Diesel Engine Performance and Emissions During a Transient Cycle Applying an Engine Mapping-Based Methodology," *Appied. Energy*, vol. 87, no. 4, pp. 1358–1365, 2010, doi: 10.1016/j.apenergy.2009.09.003.

[30] H. Steven and H. Steven. "VECTO Tool Development : Completion of Methodology to Simulate Heavy Duty Vehicles Fuel Consumption and CO_2 Emissions Upgrades to the Existing Version of VECTO and Completion of Certification Methodology to be Incorporated into a Commission legislative," no. I, 2017.

[31] F. Rosero, L. Garzón, and C. León. "Los patrones de viaje en taxi como herramienta de gestión de la movilidad urba," in *Tecnologías aplicadas a la Ingeniería*, Ibarra: Editorial UTN, 2017.

[32] B. J. Zurita and E. Llanes. "Comparativa de los factores de emisión entre el ciclo europeo y el FTP75 para un vehículo de ciclo otto categoría M1," Universidad Internacional SEK, 2022.

[33] J. Pavlovic, B. Ciuffo, G. Fontaras, V. Valverde, and A. Marotta. "How Much Difference in Type-Approval CO_2 Emissions from Passenger Cars in Europe Can be Expected from Changing to the New Test Procedure (NEDC Vs. WLTP)?," *Transportation Research,* vol. 111, no. October 2017, pp. 136–147, 2018, doi: 10.1016/j.tra.2018.02.002.

Assessing the Efficacy of *Metarhizium anisopliae* (Metschnikoff) Sorokin as a Biological Control Agent against Rose Sawfly Larvae

Nahdia Perveen[1], Eman Rashid[2], Huda Aitzaz[3], Malaika Shaheen[4], Haroon Gul[5], Muhammad Arshad[6], and Muhammad I. Ullah[7]

Abstract — **Increasing concerns over the environmental impact of chemical pesticides have prompted the exploration of alternative, and eco-friendly solutions for controlling insect pests. The use of entomopathogenic fungus (EPF) as a biological control agent is of paramount importance. We aimed to investigate the effect of different concentrations of *Metarhizium anisopliae* (Metschnikoff) Sorokin on larval mortality and pupal formation, of sawfly larvae, a major pest of rose plants. Our study revealed a concentration-dependent effect of *M. anisopliae* on sawfly larvae. At 7 days after EPF exposure, the highest concentration (1×10^9 conidia/ml) led to a mortality rate of 65.0% and at the 11th day, the larval mortality was reached up to 82.5%. The highest EPF concentration resulted in a minimal pupal formation (7.5%). This study demonstrates the potential of *M. anisopliae* as a valuable biological control agent against sawfly larvae infestations in rose plants.**

***Keywords* – sawfly; rose plants; integrated pest management; Microbial control.**

***Resumen* — La creciente preocupación por el impacto ambiental de los pesticidas químicos ha impulsado la exploración de soluciones alternativas y ecológicas para controlar las plagas de insectos. El uso de hongos entomopatógenos (FPE) como agente de control biológico es de suma importancia. Nuestro objetivo fue investigar el efecto de diferentes concentraciones de *Metarhizium anisopliae* (Metschnikoff) Sorokin sobre la mortalidad larvaria y la formación de pupas de larvas de mosca sierra, una plaga importante de las plantas de rosas. Nuestro estudio reveló un efecto dependiente de la concentración de *Metarhizium anisopliae* sobre las larvas de mosca sierra. A los 7 días después de la exposición al EPF, la concentración más alta (1×10^9 conidios/ml) condujo a una tasa de mortalidad del 65.0 % y al día 11 la mortalidad larvaria alcanzó hasta el 82.5 %. La concentración más alta de EPF resultó en una formación de pupas mínima (7.5 %). Este estudio demuestra el potencial de *Metarhizium anisopliae* como un valioso agente de control biológico contra las infestaciones de larvas de mosca sierra en plantas de rosas.**

***Palabras Clave* — Mosca sierra; Plantas de rosas; Manejo integrado de plagas; Control microbiano.**

I. INTRODUCTION

ROSES, (genus Rosa L.), are enduring woody perennial flowering plants of the Rosaceae family. This genus of roses has an extensive diversity, comprising approximately 200 distinct species and a wide range of 18,000 varieties [1]. These plants hold significant importance as ornamental additions, widely cultivated and cherished in parks and gardens across the globe. Beyond their aesthetic value for landscaping, certain species, such as *Rosa gallica* L., *R. centifolia* L., and *R. damascena* Mill., have been used for the extraction of rose oil and water [2].

A great number of insect pests attack rose plants at almost every stage and sometimes they cause severe damage to plants [3]. The rose sawfly belonging to the family Argidae is a pest that primarily feeds on rose plants and infests different species of roses, including *R. bourboniana, R. multiflora, R. moschata, R. centifolia, R. damascena*, and *R. indica* [4]. However, it has been reported on many other host plants such as birch (*Betula spp*.) including silver birch (*Betula pendula*) and downy birch (*Betula pubescens*) [5], Hazel plant (*Corylus avellana*), Common alder (*Alnus glutinosa*), Grey alder (*Alnus incana*), Goat willow (*Salix caprea*), Grey willow (*Salix cinerea*) [6], Hawthorn (*Crataegus spp*.) [7].

The rose sawfly, *Arge ochropus* (Argidae: Hymenoptera) is a major pest of rose plants and is widely distributed in Asia and Europe [4]. *Arge pagana* larvae mainly feed on rose foliage causing complete defoliation of plants [8]. The female rose sawfly lays eggs in newly emerging shoots causing long scratches on the twigs. Rose twigs are often dried out by these scars and the plants ultimately shed their leaves, resulting in reduced yield and quality of roses [9], [10].

No funding was available for this research work. The authors are thankful to the Department of Plant Pathology, University of Sargodha, for providing research facilities. All the authors contributed equally.

[1] *Corresponding author:* Nahdia Perveen is with the Department of Entomology, University of Sargodha, 40100, Sargodha, Pakistan (e-mail: nasirnhdi@gmail.com). ORCID number 0009-0002-8429-7683

[2] Eman Rashid is with the Department of Entomology, University of Sargodha, 40100, Sargodha, Pakistan (e-mail: emanrashidchrashid@gmail.com). ORCID number 0009-0007-3048-9635

[3] Huda Aitzaz is with the Department of Entomology, University of Sargodha, 40100, Sargodha, Pakistan (e-mail: hudaaitzaz016@gmail.com). ORCID number 0009-0003-3945-8481

[4] Malaika Shaheen is with the Department of Entomology, University of Sargodha, 40100, Sargodha, Pakistan (e-mail: malaikaawan52@gmail.com). ORCID number 0009-0009-0072-6315

[5] Haroon Gul is with the Department of Entomology, University of Sargodha, 40100, Sargodha, Pakistan (e-mail: haroongulquraishi3811@gmail.com). ORCID number 0009-0003-6317-3283

[6] Muhammad Arshad is with the Department of Entomology, University of Sargodha, 40100, Sargodha, Pakistan (e-mail: makuaf@gmail.com). ORCID number 0000-0002-5442-0380

[7] *Corresponding author:* Muhammad Irfan Ullah is with the Department of Entomology, University of Sargodha, 40100, Sargodha, Pakistan (e-mail: muhammad.irfanullah@uos.edu.pk). ORCID number 0000-0002-2463-2665

Manuscript Received: Sep 21, 2023
Revised: Oct 17, 2023
Accepted: Nov 27, 2023
DOI: https://doi.org/10.29019/enfoqueute.1004

Currently, insect pest management primarily relies on the utilization of synthetic insecticides. However, in recent years, these pesticides have not achieved the desired levels of control, possibly due to the development of resistance within the pest populations [11], [12]. Moreover, many of the commonly employed pesticides, notably pyrethroids, and organophosphates, pose a high level of toxicity to the natural enemies of insect pests found in the field [13].

Consequently, as a more environmentally sustainable approach to pest control, biological control is frequently explored as an alternative method. Therefore, the utilization of environmentally friendly methods, such as microbial control, holds a significant promise in Integrated Pest Management [14]. *Metarhizium anisopliae* (Metschnikoff) Sorokin —commonly known as the muscadine fungus— holds a significant position in the realm of entomopathogenic fungi (EPF). It has served as a well-established model for the study of biological pest control using fungi [15]. Notably, it holds the distinction of being the first fungus to achieve global-scale mass production and deployment for the purpose of insect pest control [16]. *Metarhizium anisopliae*, being a soil-borne entomopathogenic fungus, offers an environmentally sustainable alternative to chemical pesticides [17]. Numerous studies have explored the impact of *Metarhizium anisopliae* isolates on various insect pests [18], [19], [20]. This approach, utilizing bioinsecticides, is not only effective but also safe for both environmental and agricultural applications [21], [22].

To date, the existing scientific studies addressing sawfly control have predominantly centered around pesticide application and the timing of such applications during egg hatch stages [23], [24]. However, as far as our knowledge extends, no study is available on the use of formulated products of EPF to control sawfly larvae.

II. MATERIAL AND METHODS

A. Insect Rearing

The adults of rose sawfly were collected from the infested rose plants (*Rosa indica L.*) at the College of Agriculture in the University of Sargodha, and reared in the biocontrol laboratory. The confined pairs of adults were placed in glass cages with nylon nets (45cm$_X$45cm$_X$45cm). Eight small pots with medium-sized rose plants, *R. indica* (30 cm long) were placed in a rearing cage to provide an innate environment for the female to oviposit. As the female inserted eggs into the tissues of rose twigs, they were moved to separate petri dish. After egg hatching the first instar larvae were placed in clean petri plates. Fresh rose foliage was used as feed for larvae along with sanitation on a daily basis. The culture was maintained in a growth chamber (BIOBASE, BJPX-A400) under controlled conditions of 25± 2°C temperature, 60-70 % RH, and 12:12h (L:D) photoperiod. Pupal cocoons were placed in large glass jars until adult emergence. Cotton soaked with honey solution (30 %) was given to adults as feed. Insects were reared for up to three consecutive generations for further studies.

B. Fungal isolates

The EPF, *Metarhizium anisopliae* strain Met F52, (Earth Bio-Sciences in New Haven, CT), was tested against third instar larvae of sawflies. In a controlled laboratory environment, the EPF was cultured on Potato Dextrose Agar (PDA) at conditions of 25 ± 2°C temperature, 70 % relative humidity (RH), and a 12:12h light-to-dark (L:D) photoperiod. The quality of conidia was assessed using a Neubauer chamber hemocytometer. In the subsequent bioassay, a suspension containing 90 % conidial germination was employed, with adjustments made to achieve various concentrations, including 1_X10^6, 1_X10^7, 1_X10^8 and 1_X10^9 conidia/ml in distilled water, supplemented with 0.05 % tween 80.

C. Pathogenicity of EPF isolates against A. ochropus

Different concentrations of *Metarhizium anisopliae* were tested against 3rd instar larvae of sawflies taken from the insect culture reared in the laboratory. The treatments were replicated four times and, in each replication, 10 larvae were tested. Forty individuals were released on the fresh rose leaves, kept in petri plates (9mm in diameter) separately, and treated against each concentration. All larvae were treated with different suspensions (1_X10^6, 1_X10^7, 1_X10^8 and 1_X10^9 conidia ml^{-1} suspension) on the thorax of larvae by using a micro-pipette. The control groups were treated with sterile distilled water with tween 80. After treatment, all petri plates were incubated at 25± 2°C temperature and 60±5 % R.H. Mortality data was recorded on the 7 and 11 days after EPF exposure [25]. The effect of each concentration was also recorded on pupal formation.

D. Data analysis

The data were first tested for normality using Shapiro-Wilk test and normalized using log transformation where needed. However, back-transformed means were presented in the results. Data were analyzed by using one-way ANOVA to check the significance of *Metarhizium anisopliae* concentrations on larval mortality and pupal formation. Means were separated with the least significant difference (LSD) test at a 5 % level of significance. The analyses were performed using Minitab 18.0 software.

III. RESULTS

There was a notable effect of different concentrations of *Metarhizium anisopliae* on sawfly larval mortality at 7 days ($F = 11.4$, $P < 0.001$) and 11 days ($F = 14.5$, $P < 0.001$) of application. The data clearly showed that the mortality of sawfly larvae increased with increasing concentrations of *Metarhizium anisopliae*, both after 7 days and 11 days. The highest concentration (1_X10^9 conidia/ml) of EPF resulted in the highest larval mortality 82.5 % on the 11 day and 65.0 % on the 7 day, indicating the most effective control of sawfly larvae. With the application of 1_X10^8 concentration, the mortality rate was also 65.0 % at 11 days after exposure. Using the lowest concentration (1_X10^6 conidia/ml), the larval mortality, was 17.5 % at 7 days and 37.5 % at 11 days of application. In the control group,

the mortality rates were much lower at both time points (7.5 % at 7 day and 12.5 % at 11 day) (figure 1).

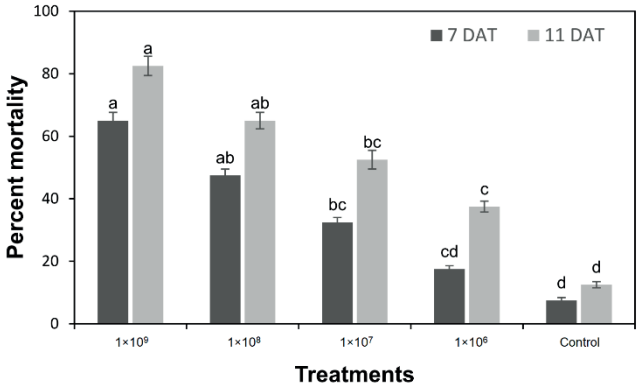

Fig. 1. Percent mortality (means±SE) of sawfly larvae after application of different concentrations of *Metarhizium anisopliae* at 7 and 11 days of applications, means sharing similar letters are not significantly different at P > 0.05.

A significant effect (F = 21.0, P < 0.001) of different concentrations of *Metarhizium anisopliae* was found on pupal formation. The control group, without any EPF treatment, had a high pupal formation rate of 85.0 %, indicating that most larvae in the control group were pupated. In contrast, as the concentration of *Metarhizium anisopliae* increased, the pupal formation rates decreased. The highest EPF concentration (1_X10^9 conidia/ml) resulted in the lowest pupal formation rate at 7.5 %, suggesting that this concentration had the most significant impact on preventing pupation. The pupal formation rate was 37.5 % after the application of a lower concentration (1_X10^6 conidia/ml) of EPF. *Metarhizium anisopliae* at any concentration inhibited pupation compared to the control (figure 2).

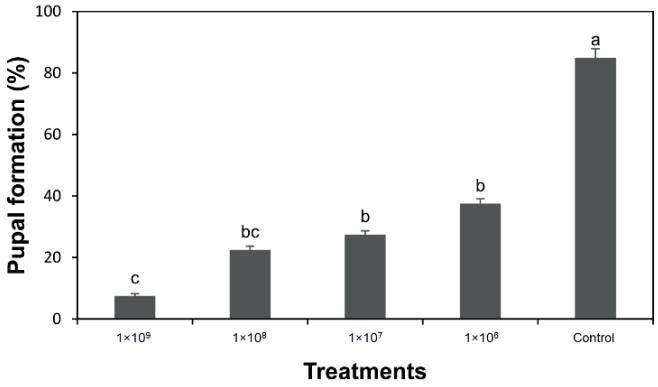

Fig. 2. Percent pupal formation (means±SE) of sawfly after application of different concentrations of *Metarhizium anisopliae*, means sharing the same letters are not significantly different at P > 0.05.

IV. DISCUSSION

Entomopathogenic fungi play a vital role in natural insect population regulation. A wide array of EPF isolates has been extensively examined for their capacity to manage insect pests [26]. In this study, we checked the efficacy of different concentrations of *Metarhizium anisopliae* in controlling sawfly larvae infesting rose plants. Our results demonstrated a concentration-dependent effect of *Metarhizium anisopliae* on sawfly larval mortality.

The highest concentration tested (1_X10^9 conidia/ml) yielded a significant mortality rate, showing the rapid action of the fungus against the larvae. Even the lowest concentration tested had an apparent impact on larval mortality compared to the control group, affirming the potential of *Metarhizium anisopliae* as a sawfly larvae biocontrol agent. Our findings are similar to previous studies related to the successful use of EPFs against rose sawfly. Khosravi et al. [27] evaluated four *B. bassiana* isolates (IR-K-40, IRAN403C, SP566, and SPT22) using five distinct conidial concentrations when targeting fourth-instar *A. rosae* larvae. Notably, the IRAN403C isolate emerged as the most promising candidate for pest biological control at a concentration of 2_X10^8 conidia/mL. Swiergiel et al. [28] reported the potential use of two EPF, a commercial product containing *B. bassiana* strain GHA and an indigenous isolate (KVL 14–90) of *M. brunneum* Petch, for controlling the apple sawfly (*Hoplocampa testudinea* Klug). Our findings are also similar to Baki et al. [29] who studied the pathogenicity of 17 entomopathogenic fungal (EPF) isolates, encompassing three distinct species: *Beauveria bassiana* with 14 isolates, *Clonostachys rosea* (Link) with 2 isolates, and *Isaria farinosa* (Holmsk) with 1 isolate. The assay results demonstrated a notable and significant enhancement in the bio-efficacy of the tested isolates as time passed, particularly up to 9 days following inoculation.

In addition to larval mortality, we assessed the impact of *Metarhizium anisopliae* on pupal formation. Our results showed a clear inverse relationship between EPF concentration and pupal formation. The control group, compared to EPF treatment, exhibited a high pupal formation, indicating that untreated larvae primarily progressed to the pupal stage under normal conditions. Conversely, the highest EPF concentration (1_X109 conidia/ml) led to a low pupal formation rate, emphasizing the potency of the fungus in inhibiting pupation. The trend continued with lower concentrations, demonstrating that even minimal exposure to the fungus can disrupt the normal pupation process. The current study demonstrates that *Metarhizium anisopliae* exhibits pupicidal activity against sawflies. This EPF is capable of breaking down the cuticle layer of pupae, ultimately resulting in their death. Wakil et al. [30] previously documented a reduced pupation rate in *Rhynchophorus ferrugineus* (Olivier) after the application of EPFs. Our findings align with those of Yehia et al. [31], who observed that *B. bassiana* and *Metarhizium anisopliae* also reduce the pupation percentage of the house fly, *Musca domestica*. Similarly, Ibrahim et al. [32] reported significant pupal mortality percentages when using EPFs such as *B. assiana*, *Metarhizium anisopliae,* and *Paecilomyces fumosoroseus*.

The method of infection of *Metarhizium anisopliae* on susceptible hosts involves the direct penetration of their cuticle [33]. To simplify the explanation of this intricate process, it can be dissected into six distinct stages, as reported by Gao et al. [34]:

1. These stages encompass the attachment of conidia to the host's cuticle.
2. The germination and development of conidia.

3. The formation of specialized structures called *appressoria*.
4. The penetration of the host's cuticle.
5. The establishment and colonization within the host's hemolymph.
6. The subsequent extrusion and sporulation of the fungus.

Applying the minimal effective dose to control sawflies in rose crops is likely to diminish the infection risk in larvae. However, it's essential to recognize that the ecological susceptibility in a field setting [35] might vary due to factors like abiotic conditions and local habitat variations. Surviving a fungal infection could have consequences on fitness, such as a potential decrease in lifetime fecundity. Consequently, it is imperative to investigate these potential effects on sawflies.

V. CONCLUSION

The results of this research provide encouraging information regarding the potential application of *Metarhizium anisopliae* as a biological control to combat sawfly larvae infestations in rose plants. Our results highlight the importance of EPF concentration in achieving effective control, with higher concentrations demonstrating superior performance in terms of larval mortality and inhibition of pupal formation. Further research is warranted to explore the practicality and ecological implications of employing *Metarhizium anisopliae* in field conditions.

REFERENCES

[1] K. S. Sastry, B. Mandal, J. Hammond, S. W. Scott, R. W. Briddon. "Rosa Spp. (Rose)". In: *Encyclopedia of Plant Viruses and Viroids*, Springer, New Delhi, 2019. Available: https://doi.org/10.1007/978-0-387-95919-1_50

[2] H. Özçelik. "General Appearances of Turkish Roses. Suleyman Demirel University," *Journal of Natural and Applied Sciences,* vol. 17, pp. 29-42, 2013.

[3] P. Duraimurugan, A. Jagadish. "Preliminary Studies on the Biology of '*Scirtothrips dorsalis'* Hood (Thysanoptera: Thripidae) as a Pest of Rose in India," *Archives of Phytopathology and Plant Protection*, vol. 44, pp. 37–45. 2011. Available: https://doi.org/10.1080/03235400902831141

[4] Y. G. Zhao, B. Z. Hua. "Morphology of the Immature Stages of 'Arge Pagana' (Panzer, 1798) (Hymenoptera: Argidae) with Notes on its Biology," *Journal of Asia-Pacific Entomology*, vol. 19, pp. 903-909, 2016. Available: https://doi.org/10.1016/j.aspen.2016.08.010

[5] K. Beneš. "Sawflies (Hymenoptera, Symphyta) of the 'Bohemian Forest' and its Foothills," *Silva Gabreta*, vol. 20, pp. 131-147, 2014.

[6] A. Haris. "Sawflies of Belső-Somogy (Hymenoptera: Symphyta)," *Natura Somogyiensis*, vol. 22, pp. 141-162, 2012. Available: https://doi:10.24394/NatSom.2012.22.141

[7] G. Japoshvili, A. Haris. "Sawflies (Hymenoptera: Symphyta) from North Western Georgia (Sakartvelo) (Part II.)," *Natura Somogyiensis*, vol. 39, pp. 35-46, 2022. Available: https://doi.org/10.24394/NatSom.2022.39.35?

[8] J. L. Boevé. "Behavior and Body Size Modulate the Defense of Toxin-Containing Sawfly Larvae Against Ants," *Scientific Reports*, vol. 11, 13610, 2021. Available: https://doi.org/10.1038/s41598-021-93074-2

[9] R. Khosravi, J. J. Sendi, A. Zibaee, A.M. Shokrgozar. "Virulence of Four '*Beauveria Bassiana'* (Balsamo) (Asc., Hypocreales) Isolates on Rose Sawfly, '*Arge rosae'* (Hymenoptera: Argidae) Under Laboratory Condition," *Journal of King Saud University-Science*, vol. 27, pp. 49-53, 2015. Available: doi: 10.1016/j.jksus.2014.04.003

[10] H. Bolu, M. Aslan, H. Maral. "Life History and Biology of Rose Sawfly, '*Arge rosae'* Linnaeus (Hymenoptera: Argidae)," *Munis Entomology and Zoology*, vol. 16, pp. 484-493, 2021.

[11] M. L. Pappas, F. Migkou, G. D. Broufas. "Incidence of Resistance to Neonicotinoid Insecticides in Greenhouse Populations of the Whitefly, '*Trialeurodes vaporariorum'* (Hemiptera: Aleyrodidae) from Greece," *Journal Applied Entomology and Zoology*, vol. 48, pp. 373–378, 2013. Available: https://doi:10.1007/s13355-013-0197-z

[12] M. C. Reid, F. E. McKenzie. "The Contribution of Agricultural Insecticide Use to Increasing Insecticide Resistance in African Malaria Vectors," *Malaria Journal*, vol. 15, pp. 1–8, 2016. Available: https://doi:10.1186/s12936-016-1162-4

[13] A. G. S. Cuthbertson. "Unnecessary Pesticide Applications in Northern Ireland Apple Orchards Due to Miss-Identification of a Beneficial Mite Species," *Research Journal of Chemistry and Environment*, vol. 8, pp. 77–78, 2004.

[14] M. S. Goettel, J. Eilenberg, T. Glare., "Entomopathogenic Fungi and Their Role in the Regulation of Insect Populations" In: *Comprehensive Molecular Insect Science*, L. I. Gilbert, K. Iatrou S. Gill, Eds., Academic Press, London, UK, 2005, pp. 361-406.

[15] G. Zimmermann. "The Entomopathogenic Fungus '*Metarhizium anisopliae*' and its Potential as a Biocontrol Agent," *Journal of Pesticide Science*vol. 37, pp. 375–379, 1993.

[16] D. W. Roberts, R. J. St Leger. "*Metarhizium Spp*., Cosmopolitan Insect-Pathogenic Fungi: Mycological Aspects," *Advances in Applied Microbiology,* vol. 54, pp. 1–70, 2004. Available: doi: 10.1016/S0065-2164(04)54001-7.

[17] G. Zimmermann. "Review on Safety of the Entomopathogenic fungus '*Metarhizium anisopliae'*," *Biocontrol Science and Technology*, vol. 17, pp. 879–920, 2007. Available: https://doi.org/10.1080/09583150701593963

[18] S. B. Alves, L. S. Rossi, R. B. Lopes, M. A. Tamai, R. M. Pereira. "'B*eauveria Bassiana'* Yeast Phase on Agar Medium and its Pathogenicity Against '*Diatraea Saccharalis'* (Lepidoptera: Crambidae) and '*Tetranychus urticae'* (Acari: Tetranychidade)," *Journal of Invertebrate Pathology*, vol. 81, pp. 70-77, 2002. Available: doi:10.1016/s0022-2011(02)00147-7.

[19] M. V. Garcia, A. C. Montero, M. J. P. Szabo, N. Prette, G. H. Bechara. "Mechanism of Infection and Colonization of '*Rhipicephalus sanguineus'* Eggs by '*Metarhizium anisopliae'* as Revealed by Scanning Electron Microscopy and Histopathology," *Brazilian Journal of Microbiology*, vol. 36, pp. 368-372, 2005. Available: https://doi.org/10.1016/j.jip.2021.107648

[20] N. Mubeen, A. Khalid, M. I. Ullah, N. Altaf, M. Arshad, L. Amin, A. Sadaf. "Effect of '*Metarhizium anisopliae'* on the Nutritional Physiology of the Fall Armyworm, '*Spodoptera frugiperda'* (JE Smith)(Lepidoptera: 'Noctuidae')," *Egyptian Journal of Biological Pest Control,* vol. 32, pp. 1-5, 2022. Available: https://doi.org/10.1186/s41938-022-00573-z

[21] A. Egbuna, B. Sawicka, H. Tijjani, L. T. Kryeziu, J. C. Ifemeje, D. Skiba, C. B. Lukong. "Biopesticides, Safety Issues and Market Trends," In: Egbuna, C. and Sawicka, B. (eds.), *Natural Remedies For Pest, Disease and Weed Control*," Academic Press, San Diego, pp. 43-53, 2020. Available: https://doi.org/10.1016/B978-0-12-819304-4.00004-X

[22] M. C. Camara, R. A. Monteiro, L. B. Carvalho, J. L. Oliveira, L. F. Fraceto. "Enzyme Stimuli-Responsive Nanoparticles for Bioinsecticides an Emerging Approach for Uses in Crop Protection," *ACS Sustainable Chemistry & Engineering*, vol. 9, pp. 106-112, 2021. Available: https://doi.org/10.1021/acssuschemeng.0c08054

[23] J. Kienzle, J. Zimmer, P. Maxin, H. Rank, H. Bathon, C. P. W. Zebitz. "Control of the Apple Sawfly '*Hoplocampa testudinea'* Klug in Organic Fruit Growing Ecofruit," at the *12th International Conference on Cultivation Technique and Phytopathological Problems in organic Fruit-Growing*. Proceedings of the conference. M. Booss (ed-), Traubenplatz 5, D-74189 Weinsberg, Germany, pp. 25-29, 2006.

[24] V. Psota, J. Ouředníčková, V. Falta. "Control of *Hoplocampa testudinea* Using the Extract from Quassia Amara in Organic Apple Growing," *Journal of Horticultural Sciences,* vol. 37, pp. 139−144, 2010. Available: doi: 10.17221/76/2009-HORTSCI

[25] S. Opisa, H. du Plessis, K. S. Akutse, K. K. M. Fiaboe, S. Ekesi. "Effects of Entomopathogenic Fungi and '*Bacillus thuringiensis'* Based Biopesticides on '*Spoladea recurvalis'* (Lepidoptera: Crambidae)," *Journal of Applied Entomology*, vol. 142, pp. 617–626, 2018. Available: https://doi.org/10.1111/jen.12512

[26] M. G. Feng, B. Chen, S. H. Ying. "Trials of '*Beauveria bassiana'*, '*Paecilomyces fumosoroseus'* and Imidacloprid for Management of '*Trialeurodes vaporariorum'* (Homoptera: Aleyrodidae) on Green-

house-Grown Lettuce," *Biocontrol Science and Technology*, vol. 14, pp. 531-544, 2004. Available: https://doi.org/10.1080/09583150410001682269

[27] R. Khosravi, J. J. Sendi, A. Zibaee, A. M. Shokrgozar. "Virulence of Four '*Beauveria bassiana'* (Balsamo) (Asc., Hypocreales) Isolates on Rose Sawfly, 'Arge Rosae' (Hymenoptera: Argidae) Under Laboratory Condition," *Journal of King Saud University*, vol. 27, pp. 49-53, 2015. Available: doi:10.1016/j.jksus.2014.04.003

[28] W. Swiergiel, N. V. Meyling, M. Porcel, B. Ramert. "Soil Application of '*Beauveria bassiana'* GHA Against Apple Sawfly, '*Hoplocampa testudinea'* (Hymenoptera: Tenthredinidae): Field Mortality and Fungal Persistence," *Insect Science*, vol. 23, pp. 854-868, 2016. Available: doi: 10.1111/1744-7917.12233

[29] D. Baki, H. S. Tosun, F. Erler. "Indigenous Entomopathogenic Fungi as Potential Biological Control Agents of Rose Sawfly, '*Arge rosae*' L. (Hymenoptera: Argidae)," J*ournal of Zoology*, vol. 45, pp. 517-525, 2021.

[30] W. Wakil, M. Yasin, D. Shapiro-Ilan. "Effects of Single and Combined Applications of Entomopathogenic Fungi and Nematodes Against '*Rhynchophorus ferrugineus'* (Olivier)," *Scientific Reports*, vol. 7, 5971, 2017. Available: https://doi.org/10.1038/s41598-017-05615-3

[31] R. S. Yehia, E. A. Shaalan, H. M. Al-Sheikh. "Efficacy of Two Entomopathogenic Fungi, '*Beauveria Bassiana'* and '*Metarhizium anisopliae',* Isolated from Eastern Saudi Arabia Against the House Fly, 'Musca Domestica'," *Journal of Zoology*, vol. 54, pp. 1405-1411, 2022.

[32] A. Ibrahim, M. I. Hassan, A. I. Hasaballah, M. A. Fouda, G. M. Omar. "Evaluation of Some Entomopathogenic Fungi Against Larvae, Pupae and Adults of House Fly*, 'Musca domestica'* L," *Journal of Nuclear Science and Technology,* vol. 4, pp. 103-112, 2016.

[33] F. M. Freimoser, G. Hu, R. J. S. Leger. "Variation in Gene Expression Patterns as the Insect Pathogen '*Metarhizium anisopliae*' Adapts to Different Host Cuticles or Nutrient Deprivation in Vitro," *Microbiology*, vol. 151, 2005. Available: doi:10.1099/mic.0.27560-0.

[34] Q. Gao, K. Jin, S. H. Ying, Y. Zhang, G. Xiao, Y. Shang. "Genome Sequencing and Comparative Transcriptomics of the Model Entomopathogenic Fungi '*Metarhizium anisopliae'* and '*M. acridum*'," *PLOS Genetics*, vol. 7, 2011. Available: doi:10.1371/journal.pgen.1001264.

[35] H. E. Roy, J. K. PELL. "Interactions Between Entomopathogenic Fungi and other Natural Enemies: Implications for Biological Control," *Biocontrol Science and Technology*, vol. 10, pp. 737 – 752, 2000. Available: doi: 10.4236/ae.2020.83010.

Flow Patterns in Two Nanorefrigerants R600a/CuO and R410A/CuO During the Boiling Process

Fernando Toapanta-Ramos[1], Elizabeth Suquillo[2] and Carlos Cornejo[3]

Abstract — **The present study aims to know the flow patterns in two nanorefrigerants R600a / CuO and R410A / CuO throughout the forced boiling process in horizontal square pipes. Those are obtained using the thermophysical properties of the refrigerants R600a and R410A in state liquid and vapor, as well as the properties of the CuO nanoparticles. The analysis was carried out using two methods: analytical and numerical. The analytical method was established by formulas and correlations through scientific articles and books to find an improvement in the two-phase heat transfer, under the conditions at an inlet temperature of 8 ° C and with a quality range of 0 to 1. This allowed to verify that by adding nanoparticles to the refrigerant, the transition between the flow regimes increases progressively, while the quality of the vapor decreases. For the numerical method, the different transition limits are specified in a simulation process in the Ansys Fluent CFD Software, under established design conditions, which consequently increases the general efficiency of any refrigeration system.**

Keywords — **Ansys Fluent; Boiling; Nanoparticles; Nano refrigerants; Simulation.**

Resumen — **El presente estudio tiene como propósito identificar los patrones de flujo en los nanorefrigerantes R600a/CuO y R410a/CuO durante el proceso de ebullición forzada en tuberías cuadradas horizontales. Dichos patrones se obtienen empleando las propiedades termofísicas de los refrigerantes R600a y R410A en estado líquido y de vapor, así como, también las propiedades de las nanopartículas de CuO. El análisis se lo realizó mediante dos métodos: analítico y numérico. El método analítico se estableció mediante fórmulas y correlaciones a través de artículos científicos y libros para encontrar una mejora en la transferencia de calor de dos fases. El trabajo se llevo a cabo bajo las condiciones a una temperatura de entrada de 8 °C y con un rango de calidad de 0 a 1, comprobando que al añadir nanopartículas al refrigerante la transición entre los regímenes de flujo aumenta de manera progresiva, mientras que, la calidad de vapor reduce. Para el método numérico se procedió a especificar los diferentes límites de transición en un proceso de simulación en el Software CFD Ansys Fluent, bajo condiciones establecidas de diseño, lo que en consecuencia aumenta la eficiencia general de cualquier sistema de refrigeración.**

[1] Fernando Toapanta-Ramos works at the Salesian Polytechnic University as a full professor, for the Mechanical Engineering Department, Quito-Ecuador (e-mail: ltoapanta@ups.edu.ec). ORCID number 0000-0002-0838-4702.

[2] Elizabeth Suquillo completed her master's degree in pedagogy with a mention in teaching and innovation at the Universidad Tecnológica Equinoccial, Quito-Ecuador (rsuquillo@est.ups.edu.ec). ORCID number 0000-0002-0507- 6042

[3] Carlos Cornejo completed his mechanical engineering and dedicated to practicing his profession. (ccomejoo@est.ups.edu.ec). ORCID number 0000-0001-8779-244X.

Manuscript Received: Sep 27, 2023
Revised: Nov 16, 2023
Accepted: Nov 22, 2023
DOI: https://doi.org/10.29019/enfoqueute.1006

Palabras Clave — **Ansys Fluent; Ebullición; Nanopartículas; Nanorefrigerantes; Simulación.**

I. INTRODUCTION

THE boiling process using nanoparticles is one of the most critical heat transfer mechanisms, which plays a significant role in industrial sectors, such as cooling systems, power plants, and chemical reactors [1]. The industrial sector continually seeks new ways to improve the heat transfer properties of working fluids in refrigeration systems.

Nanofluid boiling is considered an important research study that offers various opportunities to explore new frontiers. However, it also comes with great challenges. For several years, some studies have been based on nanofluids for the improvement of heat transfer during the boiling process, however, the data on the boiling heat transfer coefficient and the critical heat flux have been unpredictable [2], [3], [4].

Wang et al. [5] point out that the usefulness of nanofluids in refrigeration systems is considered a potential way to optimize the energy efficiency and reliability of heating, ventilation, air conditioning and refrigeration installations (HVAC & R) and to make the use of environmentally friendly refrigerants economical.

Yin et al. [6] established a nanofluid model consisting of suspended nanoparticles for the improvement of heat transfer of boiling flow. The results reveal that both flow rate and heating temperature have an effect on the heat transfer from boiling flow to lower heating temperature. On the other hand, they obtained that, with an increase in the heating temperature, the suspended nanoparticles have much more abrupt rotational and translational movements, which can significantly improve the heat transfer of the nanofluids.

Mukthiyar et al. [7] point out that the most used refrigerant is the R410A refrigerant. This is a mixture of difluoromethane *(CH2F2)* and pentafluoro methane *(CHF2CF3),* being successfully marketed in air conditioning. On the other hand, Heredia et al. [8] mention that the refrigerant R410A has a high global warming potential (GWP) of 2 088. However, Fannon et al. [9] suggest that R410A refrigerant has better performance and minimizes pressure drop, especially for high refrigerant flow rates. Which indicates that R410A would be a better option for the design of new cooling systems direct expansion (OX).

Shao et al. [10] carried out a numerical study on the heat transfer of R410A during the boiling flow. In this study thermal phase change model in fluent was used. The results of this research show that the heat transfer coefficient increased with the mass flow growth, while it decreased with the growth of vapor quality due to the interaction of nucleate boiling and fluid convection. However, the effect of heat flux was slight on the heat

transfer coefficient of boiling flux, indicating that boiling flux is mainly governed by fluid convection.

On the other hand, Nair et al. [11] in their study of nanorefrigerants: A Comprehensive Review of its Past, Present, and Future, point out that nanorefrigerants can greatly reduce the energy consumption of a cooling system. The show that improved thermal conductivity of a nano refrigerant is only partially responsible for a higher boiling heat transfer coefficient, also show the COP of the refrigeration system increases with the addition of nanoparticles in the refrigerant. Finally, the authors mention that for the R410A refrigerant nano lubricants based on polyol oils should be used ester (POE) due to its miscibility.

Low global warming potential (GWP) refrigerants, such as R600a, have become a very important topic of study. That because they significantly reduce the emission of greenhouse gases from industries dedicated to air conditioning [12]. One example of that is the research developed by Longo et al. [13] carried out the thermodynamic and heat transfer evaluation of low-GWP refrigerants such as R600a, R1234ze (Z), and R1233zd (E) as an alternative to traditional low-pressure HFC refrigerants, such as R245fa, for heat pump (HP) and organic Rankine cycle (ORC) applications.

Gobinath and Venugopal [14] claim that CuO nanoparticles of 0.1 % volume fraction in R600a established nearly 20 % enhancement in heat transfer coefficient of the refrigerant at higher heat flux. The optimum concentration of CuO nanoparticles in stable dispersion for a prolonged time and contribute for significant enhancement in the heat transfer coefficient of R600a refrigerant is experimentally found as 0.05 % by volume.

The incorporation of solid nanoparticles into common fluids results in the formation of a nanofluid which can be considered an interesting technique to improve the thermal characteristics of a working fluid [15]. Akhavan-Behabadi et al. [16] executed an experimental study on the effect of CuO nanoparticles on the boiling flux of the mixture (R600a/oil) inside a smooth horizontal tube. These experiments were carried out under parameters of mass velocities of 50 to 400 kg/m^2s, inlet vapor qualities of 0 to 0.9, heat fluxes of 3 to 8 kW/m^2 and mass fractions of CuO nanoparticles from 0 to 1.5 % by weight. The mixing of the nanoparticles with the base fluid was carried out by passing them through a system at high speed for approximately 3 hours. The results reveal that the addition of CuO nanoparticles significantly improves heat transfer by up to 63 % relative to the heat transfer coefficient of (R600a/oil) without nanoparticles.

In the research carried out by Rabiee and Atf [17], a numerical study was carried out using computational fluid dynamics (CFO), in which AZ2O3 and CuO nanoparticles were incorporated into the fluid, basis to achieve an increase in the heat transfer coefficient during the boiling process. For this study, the Reynolds-Averaged Navier-Stokes equations were used accompanied by a mechanistic model developed by the Rensselaer Polytechnic Institute (RPI) to simulate the boiling flow field with an Eulerian-Eulerian approach for each phase. They concluded that, copper oxide compared to alumina nanoparticles would lead to higher amounts of heat transfer coefficients along pipes.

Sharif et al. [18] developed a mechanism to improve the performance of the refrigeration system through the use of nanorefrigerants and nanolubricants. This study mention that, the use of nanorefrigerants and nanolubricants in the vapor compression refrigeration system (VCRS, for its acronym in English) increased heat transfer coefficients from 12 % to 101 % and improved thermal conductivity by up to 4 %. The solubility and miscibility of the coolant-oil mixture with nanoparticle additives was improved by up to 12 % and showed a 24 % COP improvement. On the other hand, Senthilkumar [19] in their prospective study of nanolubricants and nanorefrigerants on energy savings in the vapor compression refrigeration system point out that, in the R410A refrigeration system, COPs of 4 were obtained, likewise a 8 % with 0.1 % and 0.5 % and 7 % cooling capacity using diamond nanoparticles.

Flow patterns are considered to be the configurations of a fluid that are formed when transporting two or more phases together through a pipe. These have many applications in industry, such as nuclear power plants, heat exchangers and chemical reactors [20], [21].

Lee et al. [22] conducted an investigation on the boiling flow patterns and drying characteristics of R-1234ze (E) in a plate exchanger (PHE), classifying these patterns into three flow regimes which are: rough liquid film flow, pulsating annular and stable annular flow. The boiling flow pattern map of R- 1234ze (E) in the exchanger was carried out in terms of liquid and vapor surface moments. Transitions of flow regimes on the map were expressed in terms of dimensionless numbers. Furthermore, based on the relationship between heat transfer coefficient and flow patterns in the PHE, stable annular flow was recommended as a preferable pattern to achieve very high heat transfer coefficients.

Yang et al. [23] carried out an experimental study of the flow patterns of R600a in a smooth horizontal tube with an internal diameter of 6 mm using a high-speed camera, where four main flow regimes could be observed: piston flow, corrugated- stratified, slug and annular. The experiments were carried out under conditions of saturation pressure of 0.215 to 0.415 MPa, mass fluxes of 67 to 194 kg/m^2s and heat fluxes of 10.6 to 75.0 kW/m^2, respectively. Eight correlations were evaluated showing that the Liu and Winterton correlation provides the best fit to the experimental data with a mean absolute relative deviation of 11.5 %.

In another investigation, Copetti et al. [24] carried out an experimental study of the boiling flow of the refrigerant R600a in an aluminum tube of 1.47 mm hydraulic diameter. This study was carried out considering heat fluxes in the range of 5 to 30 kW/m^2, mass velocities adjusted to discrete values in the range of 50 to 200 kg/m^2s and a saturation temperature of 20 °C. In addition, they presented some images of flow patterns, in different conditions, the main patterns identified were slug, intermittent and annular. The results show that the heat coefficient increases with increasing heat flux, and when the mass velocity (G) is high the growth effect is even greater.

Abdollahi et al. [25] carried out a numerical investigation to study heat transfer characteristics of nanofluids flowing through heat sink having a V-type inlet and outlet arrangement. *SiO-2 — water, AI2O3 — water, ZnO — water,* and *CuO — water* nanofluids were used as working fluids in the investigation. The average diameter size of the nanoparticles used was 30 nm, 40 nm, and 60 nm and volumetric concentration varied from 1 % to 2 %.

The objective of this research is to know and understand how the flow patterns of two highly used refrigerants are affected when they are mixed with nanoparticles.

II. METHODS AND METHODOLOGY

Nanorefrigerants are mainly used in low temperature applications, such as air conditioning, refrigeration systems and vapor compression systems [26]. The addition of nanoparticles, especially metal oxides in the refrigerant, varies the properties and increases the heat transfer performance, improving the heat transfer performance of refrigeration systems [27].

A. Thermophysical Properties

Thermophysical properties represent important parameters that are obtained using the Engineering Equation Solver (EES) software.

Therefore, the corresponding properties of the R600a refrigerant in liquid and vapor states are observed in Table I.

TABLE I
THERMOPHYSICAL PROPERTIES OF R600A REFRIGERANT [28]

Property	Unit	Liquid	Vapor
Density	*kg/m³*	571	5.507
Specific heat	J/kg·K	2 345	1 690
Thermal conductivity	W/m·K	0.09535	0.01516
Viscosity	Pa·s	1.82E-04	7.21E-06
Enthalpy of vaporization	J/kg	347 149	347 149

The thermodynamic properties of R410A as a zeotropic refrigerant are shown in Table II, for both the liquid and vapor phases.

TABLE II
THERMOPHYSICAL PROPERTIES OF R410A REFRIGERANT [28]

PROPERTY	UNIT	LIQUID	VAPOR
Density	*kg/m³*	1137	39.4
Specific heat	J/kg·K	1 564	1 209
Thermal conductivity	W/m·K	0.09857	0.01336
Viscosity	Pa·s	1.50E-04	1.18E-05
Enthalpy of vaporization	J/kg	211 258	211 258

TABLE III
PHYSICAL AND THERMAL PROPERTIES OF COPPER OXIDE [29]

Property	Unit	Amount
Density	*kg/m³*	6 400
Specific heat	J/kg·K	550.5
Thermal conductivity	W/m·K	32.9

B. Analytical Model

To obtain the flow patterns, dimensionless variables proposed in the study carried out by Taitel-Dukler are used, which have been modified in the research by Kattan et al. [30], therefore it is necessary to define equations 1 to 6:

$$h_{LD} = \frac{h_L}{D} \tag{1}$$

$$P_{LD} = \frac{P_L}{D} \tag{2}$$

$$P_{VD} = \frac{P_V}{D} \tag{3}$$

$$P_{iD} = \frac{P_i}{D} \tag{4}$$

$$A_{VD} = \frac{A_V}{D^2} \tag{5}$$

$$A_{LD} = \frac{A_L}{D^2} \tag{6}$$

Where, h_L is the height of the liquid [m], D is the internal diameter of the tube [m], P_L is the wet part of the perimeter[m], while, P_v is the complementary part of the perimeter in contact with the vapor [m], A_L and A_v are the corresponding cross-sectional areas [m²]and P_i is the phase interface *[m]*.

On the other hand, for the calculation of the average local void fraction from the steam quality, derived from the work carried out by Rouhani and Axelsson [31] for horizontal pipes in a section void fraction transversal, e. Equation 7.

$$\varepsilon = \frac{x}{\rho_V}[(1+0.12(1-x))(\frac{x}{\rho_V}+\frac{1-x}{\rho_L}+\frac{1.18(1-x)[g\sigma(\rho_L-\rho_V]^{0.25}}{G\rho_L^{0.5}}]^{-1} \tag{7}$$

Where, x is the vapor quality, *Pv* and P_L are the density of the vapor and liquid respectively *[kg/m³],* g is the acceleration of gravity [m/s²], σ is the surface tension *[N/m]* and G is the total mass velocity of liquid and vapor *[kg/sm²].*

The average local void fraction model provides an explicit function of the total mass flux. Therefore, the surface section of tube A, the values of A_{LD} and A_{VD} are directly identifiable. Equations 8 and 9.

$$A_{VD} = \frac{A\varepsilon}{D^2} \tag{8}$$

$$A_{LD} = \frac{A-(1-\varepsilon)}{D^2} \tag{9}$$

On the other hand, the dimensions of the liquid height h_{LD} and the dimensionless length of the liquid-vapor interface P_{iD} can be expressed as a function of the stratified flow angle θ_{strat}. Where, $_{qstrat}$ is the stratified flow angle of the tube perimeter *[rad],* it can be determined from an approximate expression, evaluated by Biberg [32]. Equation 10.

$$\theta_{strat} = 2\pi - 2\{\pi(1-\varepsilon) + (\frac{3\pi}{2})^{1/3}[1-2(1-\varepsilon) + (1-\varepsilon)^{1/3} - \varepsilon^{1/3}] - \frac{1}{200}(1-\varepsilon)\varepsilon[1-2(1-\varepsilon)][1+4((1-\varepsilon)^2+\varepsilon^2)]\} \quad (10)$$

Consequently, since the void fraction e is a function of the mass velocity G, it influences the position of the transition curves in the flow maps, proposed by Klimenko-Fyodorov [33]. Equation 11.

$$G = \frac{[(\rho_L - \rho_V)]gD^{0.5}}{\{0.074(\frac{D}{(b_{La})^{0.67}}\frac{x^2}{\rho_V} + g[1-(\frac{\rho_V}{\rho_L})^{0.1}]^2\frac{(1-x)^2}{\rho_L}\}^{0.5}} \quad (11)$$

Where, b_{La} is the Laplace constant.

C. Stratified and Intermittent/annular Flow Pattern

This flow pattern occurs at very low G mass velocities when the Kelvin-Helmholtz instability criterion is counteracted by viscous forces. It is done using the equation 12 proposed by Kattan et al. [30].

$$G_{strat} = \left\{\frac{226.3^2 A_{LD}A_{VD}^2\rho_V(\rho_L-\rho_V)\mu_L g}{x^2(1-x)\pi^3}\right\}^{1/3} \quad (12)$$

Where, G_{strat} is the stratified flow transition mass velocity *[kg/m²s]*.

The annular flow pattern is obtained when the liquid wets the entire periphery of the tube with the vapor flowing in the center of the tube [34]. The annular flow pattern has been considered to be achieved when the movement of the liquid flowing at the top of the tube [35].

The intermittent flow pattern occurs at low temperature, therefore, between intermittent and annular flow is a function of the void fraction [35]. It is defined by a fixed Martinelli parameter *X*tt = 0.34

D. Stratified-Wavy and Drying-Fog Flow Pattern

It is characterized by a wavy interface of the liquid, where waves exist and these are of reduced magnitude and cannot reach the upper part of the tube [35].

It is calculated from the original expression of Kattan et al. [30]. Equation 13.

$$G_{wavy} = \left[\frac{16A_{VD}gD\rho_L\rho_V}{x^2\pi^2(1-(2h_{LD}-1)^2)^{0.5}}\right]^{0.5}\left[\frac{\pi^2}{25h_{LD}^2}\left(\frac{We}{Fr}\right)_L^{-1}+1\right]^{0.5}+50 \quad (13)$$

Where, *Gwavy* is the wave flow transition mass velocity *kg/m²s*. However, to obtain the Froude number the following expression is used. Equations 14 and 15:

$$Fr_L = \left[\frac{G^2}{\rho_L^2 gD}\right] \quad (14)$$

$$Fr_V = \left[\frac{G^2}{\rho_V^2 gD}\right] \quad (15)$$

Where, *FrL* and *FrV* is the Froude number for liquid and vapor, respectively.

Kattan et al. [36] used the following equations to find the transition limits of drying and fog flux. Equations 16 and 17.

$$G_{dryout} = \left[\frac{1}{0.235}\left(ln(\frac{0.58}{x})+0.52\right)\left(\frac{D}{\rho_v\sigma}\right)^{-0.17}\right]^{0.926}\left[\left(\frac{1}{gD\rho_V(\rho_L-\rho_V)}\right)^{-0.37}\left(\frac{\rho_V}{\rho_L}\right)^{-0.25}\left(\frac{q}{q_{crit}}\right)^{-0.70}\right]^{0.926} \quad (16)$$

$$G_{mist} = \left[\frac{1}{0.0058}\left(ln(\frac{0.61}{x})+0.57\right)\left(\frac{D}{\rho_v\sigma}\right)^{-0.38}\right]^{0.943}\left[\left(\frac{1}{gD\rho_V(\rho_L-\rho_V)}\right)^{-0.15}\left(\frac{\rho_V}{\rho_L}\right)^{-0.09}\left(\frac{q}{q_{crit}}\right)^{-0.27}\right]^{0.943} \quad (17)$$

Where, *Gdryout* is the drying transition mass velocity [*kg/m²s*], *G*mist is the fog flow transition mass velocity [*kg/m²s*] and q is the fog flux local heat [*W/m²*]. The approach of Mori et al. [37] includes the new drying limits in his research and they can be calculated from the equations 18 and 19:

$$X_{di} = 0.58e[0.52 - 0.23We_v^{-0.17}Fr_V^{0.37}\left(\frac{\rho_V}{\rho_L}\right)^{0.25}\left(\frac{q}{q_{crit}}\right)^{0.7}] \quad (18)$$

$$X_{de} = 0.61e[0.57 - 5.8x10^{-3}We_v^{0.38}Fr_V^{0.15}\left(\frac{\rho_V}{\rho_L}\right)^{-0.09}\left(\frac{q}{q_{crit}}\right)^{0.27}] \quad (19)$$

Therefore, to calculate the critical heat flux *q*crit [*kg/m²s*] the expression, given by Kutateladze [38] is used. Equations 20.

$$q_{crit} = 0.131\rho_V^{0.5}h_{LV}\left(g(\rho_L-\rho_V)\sigma\right)^{0.25} \quad (20)$$

E. Numerical Model

ANSYS CFD is a tool that offers higher accuracy quantitative forecasts of fluid interactions and connections [39].

The pipes are manufactured to transport fluids inside, so for this study a square horizontal pipe is used, whose design parameters are shown in Table IV.

For this purpose, within the Fluent setup, the materials and edge conditions are configured for correct operation. Below, Table V shows the simulation parameters.

The volume fractions for both liquid and vapor phases are defined by the equation 21:

$$V_q = \int_V \varphi_q dV \tag{21}$$

Where, the volume divisions refer to the space involved in each phase, and the laws of conservation of mass and moment are fulfilled in each stage exclusively [39].

TABLE IV
DESIGN PARAMETERS OF SQUARE PIPE

Parameter	Value	Unit
Hydraulic diameter (Dh)	0.01	m
Length (L)	2	m
Thickness (e)	0.5	mm
Material	Copper	

TABLE V
PARAMETERS USED IN THE SIMULATION

Parameter	Numeric value
Mass speed (kg/m^2s)	100 and 300
Heat flux (W/m^2)	10 000 and 20 000
Saturation temperature (°C)	8
CuO nanoparticle concentration (%)	3 and 5

Equation of conservation of mass or also called the equation of continuity, this defines the increase and decrease of mass that occurs in the phase change (liquid-vapor) taking into account the principle of conservation of mass. Equation 22.

$$\frac{\partial}{\partial_t}(\alpha_q \rho_q) + \nabla(\alpha_q \rho_q V_q) = \sum_{p=1}^{n}(m_{pq} m_{qp}) + S_q \tag{22}$$

Equation 23 for this balance shows the external forces acting within a phase change, which correspond to the movement of the mass, which are produced due to fluid turbulence. Equation 23.

$$\frac{\partial}{\partial_t}(\alpha_q \rho_q \overrightarrow{V_q}) + \nabla(\alpha_q \rho_q \overrightarrow{V_q}) = -\alpha_q \nabla_p + \nabla \overline{\overline{t_q}} + \alpha_q \rho_q \vec{g} \tag{23}$$

F. Mesh Generation

The geometry mesh is implemented for assigning the boundary conditions, using a body size of 1.5 mm, as can be seen in Figure 1.

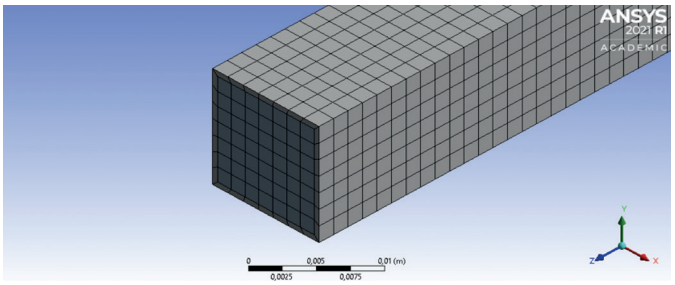

Fig. 1. Geometry meshing.

Obtaining its quality using the Skewnees tool within Fluent's metric meshing, the same as seen in Figure 2, this type of quality states that as long as the number of elements and nodes is located in a range of 0 to 0.5, the meshing will converge from successful way.

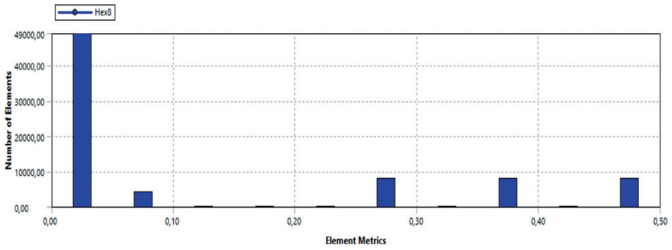

Fig. 2. Mesh quality.

III. RESULTS AND DISCUSSION

The flow maps of R600a refrigerant are compared with the research of Yang et al. [23] who studies pure flow maps. The flow maps for R600a/CuO upon adding 3 % and 5 % nanoparticles in concentration as shown in Figure 3 a) and b), the dimensions of diameter, mass velocity and heat flux are kept constant. Furthermore, it can be seen that the slug/stratified-wavy flow regime zone is more extensive, since the transition fine between slug and slug+SW has a higher mass velocity.

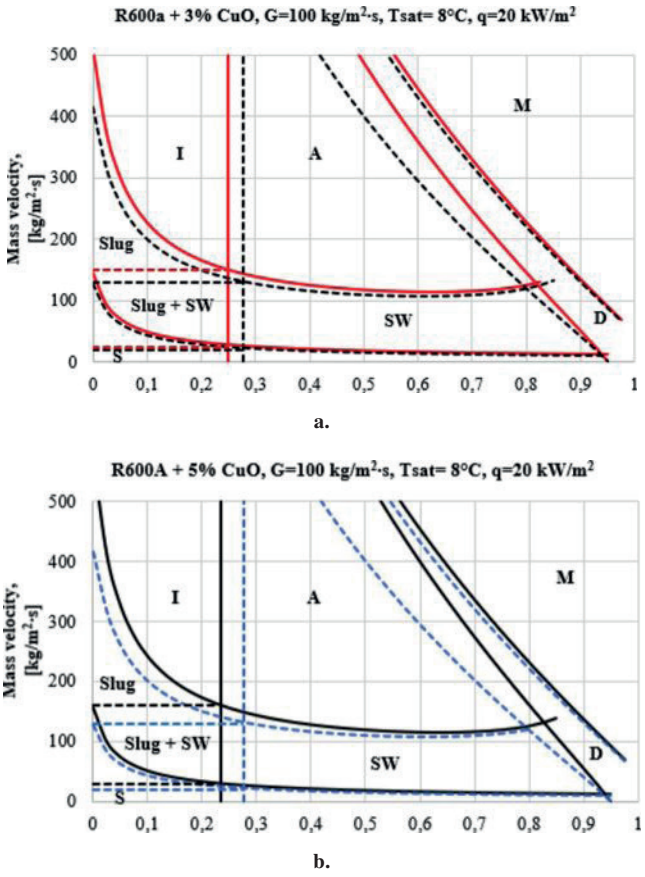

Fig. 3. a) Flow map for pure R600a refrigerant and R600a + 3 % CuO and **b)** Flow map for pure R600a refrigerant and R600a + 5 % CuO.

To check the accuracy of the flowchart, it is compared with the work of Hu et al. [40] who carried out a study of the flow diagrams of pure R410A refrigerant and R410A containing lubricating oil. In Figure 4 a) and b), the comparison of the flow maps for pure R410A and R410A with 3 % and 5 % nanoparticles, in which it is possible to see that the vapor quality is lower at the flow interface (I/A), however, this is directed to the left, thus accelerating the phase change process, because, when adding nanoparticles, the quality varies by 10 %, and reaching the drying regime is faster than for the pure refrigerant, in the same way as for the fog zone.

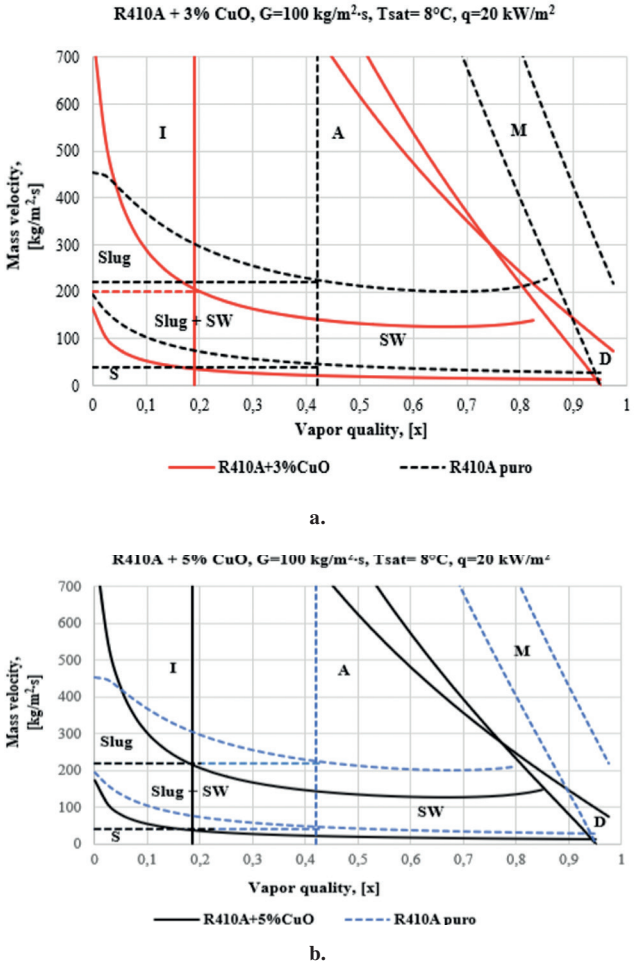

Fig. 4. a) Flow map for pure R410A refrigerant and R410A + 3 % CuO and **b)** Flow map for pure R410A refrigerant and R410A + 5 % CuO.

Figure 5 indicates that the flow maps for R600a/CuO with 3 % nanoparticles, the transition line between slug and slug+SW has a higher mass velocity. While, by adding 5 % of nanoparticles, a greater heat transfer occurs, causing an intersection between the zones of the annular intermittent flow.

Figure 6 shows the simulation results for the R410A refrigerant with a mixture of CuO nanoparticles, where the heat transfer is dominated by subcooled boiling and nucleated boiling, which is why the phase change when adding a 3 % and 5 % CuO nanoparticles are produced at lower vapor qualities, thus generating the transition limit (I/A) to develop early in the boiling process.

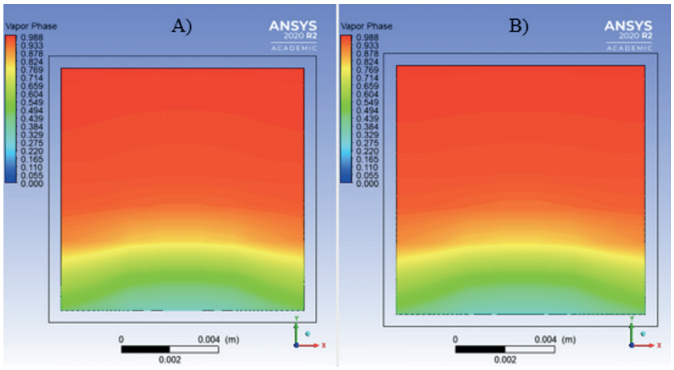

Fig. 5. Contour of the vapor volume fraction distribution for the R600a/CuO nanorefrigerant with G= 100 kg/m^2s and q= 20 kW/m^2 for A) R600a + 3 % CuO, B) R600a + 5 % CuO.

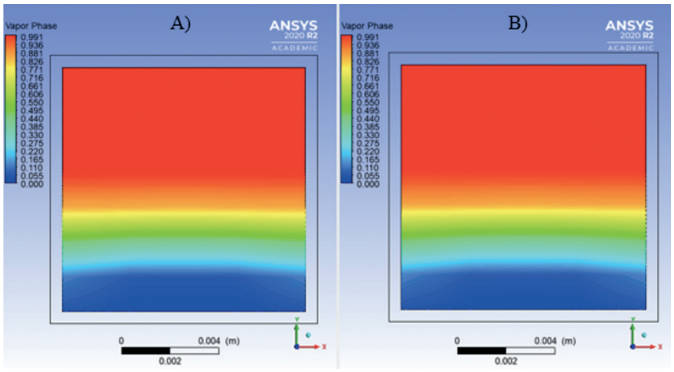

Fig. 6. Contour of the vapor volume fraction distribution for the R410A/CuO nanorefrigerant with G= 100 kg/m^2s and q= 20 kW/m^2 for A) R410A + 3 % CuO, B) R410A + 5 % CuO.

IV. CONCLUSIONS

The following conclusions are drawn by studying the flow patterns in R600a and R410A refrigerants in pure state and with nanoparticles:

- Through an analytical study, it was proven that by adding nanoparticles in concentrations of 3 % to 5 % to the R600a and R410A refrigerants, the transition between the flow regimes increases by 25 %, while the vapor quality is reduced. For this reason it is deduced that its heat transfer increases and the phase change process begins to occur at short lengths within the pipe.
- In the numerical study carried out it was concluded that in the R600a refrigerant the flow boiling heat transfer coefficient increased from 4500 to 5400 kg/m^2s using CuO nanoparticles. Also the heat transfer coefficient was improved in regimes such as slug and stratified-wavy (SW). That occur at vapor qualities between 0.1 to 0.5 and as its quality increased this coefficient decreased from 3600 to 2400 kg/m^2s. The result is drying (D) and fog (M) regimes occupying a vapor volume of less than 20 %.
- Through an analytical and numerical study, the flow boiling heat transfer performance of CuO nanoparticles in the refrigerants R600a and R410A was analyzed.

V. ACKNOWLEDGMENT

The authors thank the Salesian Polytechnic University and for the research group Research Group in Engineering, Productivity and Industrial Simulation (GUPSI) and the ASHRAE-UPS Branch group for the technical and administrative support provided to the development of this studio.

REFERENCES

[1] M. Goodarzi, I. Tlili, H. Moria, T. A. Alkanhal, R. Ellahi, A. E. Anqi, and M. R. Safaei, "Boiling heat transfer characteristics of graphene oxide nanoplatelets nano-suspensions of water-perfluorohexane (c6fl4) and water-n-pentane," *Alexandria Engineering Journal*, vol. 59, no. 6, pp. 4511-4521, 2020.

[2] A. Khan and H. M. Ali, "A comprehensive review on pool boiling heat transfer using nanofluids," *Thermal Science,* vol. 23, no. 5 Part B, pp. 3209-3237, 2019.

[3] S. Vafaei, "Nanofluid pool boiling heat transfer phenomenon," *Powder Technology,* vol. 277, pp. 181-192, 2015.

[4] A. Redhwan, W. Azmi, M. Sharif, and R. Mamat, "Development of nanorefrigerants for various types of refrigerant based: A comprehensive review on performance," *International Communications in Heat and Mass Transfer,* vol. 76, pp. 285-293, 2016.

[5] R. Wang, Q. Wu, and Y. Wu, "Use of nanoparticles to make mineral oil lubricants feasible for use in a residential air conditioner employing hydro-fluorocarbons refrigerants," *Energy and Buildings,* vol. 42, no. 11, pp. 2111-2117, 2010.

[6] X. Yin, C. Hu, M. Bai, and J. Lv, "An investigation on the heat transfer characteristics of nanofluids in flow boiling by molecular dynamics simulations," *International Journal of Heat and Mass Transfer,* vol. 162, p. 120338, 2020.

[7] S. Mukthiyar, D. R. Sarath, B. V. Kumar, and A. Madabhushi, "Design and cfd analysis of r410a refrigerant in convergent nozzle," *Materials Today: Proceedings,* vol. 5, no. 9, pp. 19463-19470, 2018.

[8] Y. Heredia-Aricapa, J. Behnan-Flores, A. Mota-Babiloni, J. Serrano-Arellano, and J. J. García-Pabón, "Overview of low gwp mixtures for the replacement of hfc refrigerants: R134a, r404a and r410a," *International Journal of Refrigeration,* vol. Ill, pp. 113-123, 2020.

[9] J.-L. C. Fannou, C. Rousseau, L. Lamarche, and S. Kajl, "A comparative performance study of a direct expansion geothermal evaporator using r410a and r407c as refrigerant alternatives to r22," *Applied Thermal Engineering,* vol. 82, pp. 306-317, 2015.

[10] Y. Shao, S. Deng, P. Lu, D. Zhao, L. Zhao, W. Su, and M. Ma, "A numerical study on heat transfer of r410a during flow boiling," *Energy Procedía,* vol. 158, pp. 5414-5420, 2019.

[11] V. Nair, P. Tailor, and A. Parekh, "Nanorefrigerants: A comprehensive review on its past, present and future," *International journal of refrigeration,* vol. 67, pp. 290-307, 2016.

[12] Y. Sun, J. Wang, and Y. Hu, "Effect of refrigerant/oil solubility on thermodynamic performance of the evaporator working with r600a and dme," *The Journal of Chemical Thermodynamics,* vol. 154, p. 106331, 2021.

[13] G. A. Longo, S. Mancin, G. Righetti, C. Zilio, and J. S. Brown, "Assessment of the low-gwp refrigerants r600a, rl234ze (z) and rl233zd (e) for heat pump and organic rankine cycle applications," *Applied Thermal Engineering,* vol. 167, p. 114804, 2020.

[14] N. Gobinath and T. Venugopal, "Nucleate pool boiling heat transfer characteristics of r600a with cuo nanoparticles," *Journal of Mechanical Science and Technology,* vol. 33, pp. 465-473, 2019.

[15] A. Shafee, B. Rezaeianjouybari, M. Sheikholeslami, M. Allahyari, and H. Babazadeh, "Boiling process with incorporating nanoparticles through a flattened channel using experimental approach," *Journal of Thermal Analysis and Calorimetry,* vol. 143, pp. 3569-3576, 2021.

[16] M. Akhavan-Behabadi, M. Nasr, and S. Baqeri, "Experimental investigation of flow boiling heat transfer of r-600a/oil/cuo in a plain horizontal tube," *Experimental Thermal and Fluid Science,* vol. 58, pp. 105-111, 2014.

[17] A. Rabiee and A. Atf, "A computational fluid dynamics investigation of various nanofluids in a boiling flow field," *Progress in Nuclear Energy,* vol. 95, pp. 61-69, 2017.

[18] M. Sharif, W. Azmi, R. Mamat, and A. Shaiful, "Mechanism for improvement in refrigeration system performance by using nanorefrigerants and nanolubricants-a review," *International Communications in Heat and Mass Transfer,* vol. 92, pp. 56-63, 2018.

[19] A. Senthilkumar, A. Anderson, and R. Braveen, "Prospective of nanolubricants and nano refrigerants on energy saving in vapour compression refrigeration system-a review," *Materials Today: Proceedings,* vol. 33, pp. 886-889, 2020.

[20] E. Costa-Patry and J. R. Thome, "Flow pattern-based flow boiling heat transfer model for microchannels," *International Journal of Refrigeration,* vol. 36, no. 2, pp. 414-420, 2013.

[21] S. Mimouni, S. Fleau, and S. Vincent, "Cfd calculations of flow pattern maps and les of multiphase flows," *Nuclear Engineering and Design,* vol. 321, pp. 118-131, 2017.

[22] D. Lee, C. Jo, B. Kim, and Y. Kim, "Boiling flow patterns and dry-out characteristics of r-1234ze (e) in a plate heat exchanger," *International Journal of Heat and Mass Transfer,* vol. 161, p. 120308, 2020.

[23] Z. Yang, M. Gong, G. Chen, X. Zou, and J. Shen, "Two-phase flow patterns, heat transfer and pressure drop characteristics of r600a during flow boiling inside a horizontal tube," *Applied Thermal Engineering,* vol. 120, pp. 654-671, 2017.

[24] J. B. Copetti, B. de Sá Bekerle, M. H. Macagnan, J. C. Passos, and J. D. Oliveira, "Flow boiling heat transfer characteristics of r600a in multiport minichannel," *Heat Transfer Engineering,* vol. 38, no. 3, pp. 323-331, 2017.

[25] A. Abdollahi, H. Mohammed, S. M. Vanaki, A. Osia, and M. G. Haghighi, "Fluid flow and heat transfer of nanofluids in microchannel heat sink with v-type inlet/outlet arrangement," *Alexandria Engineering Journal,* vol. 56, no. 1, pp. 161-170, 2017.

[26] S. Sanukrishna, M. Murukan, and P. M. Jose, "An overview of experimental studies on nanorefrigerants: Recent research, development and applications," *International Journal of refrigeration,* vol. 88, pp. 552-577, 2018.

[27] L. Cheng and L. Liu, "Boiling and two-phase flow phenomena of refrigerant-based nanofluids: fundamentals, applications and challenges," *International journal of refrigeration,* vol. 36, no. 2, pp. 421-446, 2013.

[28] F.-C. Software, "Engineering equation solver (ees)," 2015.

[29] Q. Peng, L. Jia, C. Dang, X. Zhang, and Q. Huang, "Experimental investigation on flow condensation of rl41b with cuo nanoparticles in a vertical circular tube," *Applied Thermal Engineering,* vol. 129, pp. 812-821,2018.

[30] N. Kattan, J. Thome, and D. Favrat, "Flow boiling in horizontal tubes: part 1—development of a diabatic two-phase flow pattern map," 1998.

[31] S. Z. Rouhani and E. Axelsson, "Calculation of void volume fraction in the subcooled and quality boiling regions," *International Journal of Heat and Mass Transfer,* vol. 13, no. 2, pp. 383-393, 1970.

[32] D. Biberg, "An explicit approximation for the wetted angle in two-phase stratified pipe flow," *The Canadian Journal of Chemical Engineering,* vol. 77, no. 6, pp. 1221-1224, 1999.

[33] V. Klimenko and M. Fyodorov, "Prediction of heat transfer for two-phase forced flow in channels of different orientation," in *International Heat Transfer Conference Digital Library.* Begel House Inc., 1990.

[34] C. Park and P. Hmjak, "Co2 and r410a flow boiling heat transfer, pressure drop, and flow pattern at low temperatures in a horizontal smooth tube," *International Journal of Refrigeration,* vol. 30, no. 1, pp. 166-178, 2007.

[35] O. Zürcher, D. Favrat, and J. Thome, "Development of a diabatic two-phase flow pattern map for horizontal flow boiling," *International Journal of Heat and Mass Transfer,* vol. 45, no. 2, pp. 291-301, 2002.

[36] N. Kattan, J. R. Thome, and D. Favrat, "Flow boiling in horizontal tubes: part 3—development of a new heat transfer model based on flow pattern," 1998.

[37] H. MORI, S. YOSHIDA, K. OHISHI, and Y. KAKIMOTO, "Dryout quality and post-dryout heat transfer coefficient in horizontal evaporator tubes," in *3rd European thermal sciences conference (Heidelberg, 10-13 September 2000),* 2000, pp. 839-844.

[38] S. Kutateladze, "On the transition to film boiling under natural convection," *Kotloturbostroenie,* vol. 3, p. 10, 1948.

[39] I. ANSYS, *ANSYS FLUENT User ' s Guide,* 2021.

[40] H. Hu, G. Ding, W. Wei, Z. Wang, and K. Wang, "Heat transfer characteristics of r410a-oil mixture flow boiling inside a 7 mm straight smooth tube," *Experimental Thermal and Fluid Science,* vol. 32, no. 3, pp. 857-869, 2008.

Powder Detergent Packaging Line Improvement by Lean Six Sigma DMAIC Methodology

Juan Pushug[1], Leonidas Ramírez[2], Isaac Simbaña[3], David Saquinga[4]

Abstract — **This investigation was a case of study in the powder detergent packaging line and aimed to reduce all those wastes that do not add value to the product, increasing the cost of production. Reducing or eliminating waste within the manufacturing industry becomes necessary for sustainable businesses over time and keeps generating development. To achieve it, the Lean Six Sigma DMAIC methodology was implemented in a detergent powder packaging line, to identify the problems that afflicted and made production more expensive. By using quality tools (such as Pareto and Ishikawa diagrams, 5S application, Poka-Yokes, SMED, training personnel, and standardizing processes) it was possible to reduce unproductive times. Energy consumption was reduced by up to 20 %, also efficiency and machine availability increased by 10.98 % and 7.32 %, respectively. The general performance of the line increased by 15.16 %, which translates into significant monthly savings of USD 71 442.05. By applying these improvement techniques, the most significant efficiency was registered in 1 kg packages, going from 47 % to 89 %, approximately. To maintain this productivity and even to perfect it, it is necessary to hire specialized personnel who know the production processes and industrial operations.**

Keywords — **Lean Six Sigma DMAIC; Productivity; Quality Tools; Poka-Yokes; SMED.**

Resumen — **Esta investigación fue un estudio de caso en una línea de empaque de detergente, con el objetivo de reducir todos los desperdicios que no añaden valor al producto y que aumentan el costo de producción. La disminución o eliminación de desperdicios de cualquier tipo dentro de la industria manufacturera se convierte en una necesidad para que los negocios continúen siendo sustentables en el tiempo y generan desarrollo. Para alcanzar este objetivo, se implementó la metodología *Lean Six Sigma* DMAIC en una línea de envasado de polvo detergente, permitiendo descubrir los problemas que agobiaban y encarecían la producción. Al utilizar herramientas de calidad (como Diagramas de Pareto e Ishikawa, la aplicación de la metodología 5S, Poka-Yokes, SMED, capacitando al personal, y estandarizando procesos) se logró reducir tiempos improductivos. El consumo de energía se redujo hasta en un 20 %, la eficiencia y la disponibilidad de la máquina aumentaron en 10.98 % y 7.32 %, respectivamente. También se incrementó el rendimiento general de la línea en 15.16 %, lo cual se tradujo en un ahorro significativo mensual de USD 71 442.05. Mediante la aplicación de estas técnicas de mejora, la eficiencia más significativa se registró en los empaques de 1 kg, pasando de 47 hasta 89 %, aproximadamente. Para mantener esta productividad y perfeccionarla, es necesario contratar personal especializado, que conozca los procesos productivos y operaciones industriales.**

Palabras Clave — **Lean Six Sigma DMAIC; Productividad; Herramientas de calidad; Poka-Yokes; SMED.**

I. INTRODUCTION

IN a competitive market, manufacturing companies look for habits to optimize their processes with the aim that the increase in the cost of production, due to various factors, does not affect the cost of the product to the final customer, nor does the quality of the product be affected. This would generate a loss of customers, who would opt for cheaper and better-quality products [1]. Reducing the cost of production is necessary after going through a pandemic that has increased the cost of imports and raw materials, leaving companies with a lower profit margin [2]. Hence, a continuous implementation of improvement methodologies becomes necessary in companies that want to persist, and be profitable and sustainable over time, to reduce production problems that result in efficient and profitable processes [3].

From the review of the literature, it is known that Lean Manufacturing and Six Sigma, with their quality tools, are better adapted to the manufacturing process. These methodologies seek excellence in processes, increasing production levels, and reducing waste [4]. To achieve it, Skalli et al. [5] utilized various quality tools and methodologies specific to each one. Lean Manufacturing grew out of the Toyota Production System, which seeks to use resources more efficiently and reduce waste. The Lean principle is to eliminate everything that does not generate value for the product or service. This is possible by eliminating overproduction, waiting times, defects, unnecessary movements, transportation, and reprocessing of products [6]. With the elimination of this waste, there are significant advantages, such as a reduction in production costs, an increase in productivity, and higher-quality produced products, as well as the time in which an order is manufactured [7].

Six Sigma is a methodology focused on quality and it uses statistics to find solutions to manufacturing problems based on data analysis. It aims to reduce the variability of the processes,

[1] Master's Degree in Productivity and Industrial Operations, Universidad Politécnica Salesiana, Quito, Ecuador. (e-mail: jpushug@est.ups.edu.ec). ORCID number 0009-0003-4038-5670

[2] Engineering, Productivity and Industrial Simulation Research Group (GIIPSI), Universidad Politécnica Salesiana, Quito, Ecuador. (e-mail: lramirezg@ups.edu.ec). ORCID number 0000-0003-2569-2974

[3] Electromechanical Career's Mechanical Engineering and Pedagogy Research Group (GIIMPCEM), Instituto Superior Universitario Sucre, Quito, Ecuador. (e-mail: isimbana@tecnologicosucre.edu.ec). ORCID number 0000-0002-3324-3071

[4] Electromechanical Career's Mechanical Engineering and Pedagogy Research Group (GIIMPCEM), Instituto Superior Universitario Sucre, Quito, Ecuador. (e-mail: dsaquinga@tecnologicosucre.edu.ec). ORCID number 0000-0001-8353-1621

Manuscript Received: Sep 06, 2023
Revised: Nov 08, 2023
Accepted: Nov 29, 2023
DOI: https://doi.org/10.29019/enfoqueute.996

which means, any product must be manufactured with the same specifications [8]. Depending on the Sigma level in which the process is located, there is a tolerable number of errors, excellence being a level of Six Sigma, where the maximum allowed is 3.4 defects per million opportunities. Therefore, there is no margin for errors within the manufacturing process, because as the Sigma level decreases, the acceptable errors increase.

Alternatively, Lean Six Sigma is a fusion of the two methodologies, taking the best of each one to correct any drawbacks that may result from implementing a separate methodology. This methodology combines the best and most efficient quality tools, therefore, companies can solve problems and increase productivity faster with a lower implementation cost [9]. The Define, Measure, Analyze, Improve, Control (DMAIC) methodology is a Six Sigma quality tool that helps detect problems and makes them visible. It consists of five stages that must be followed sequentially [10]. Figure 1 shows the five stages of the DMAIC cycle, where each stage must be followed in sequence, allowing solutions to problems to be developed in a structured and logical manner.

Fig. 1. DMAIC cycle.

Since its creation, Lean Six Sigma DMAIC has been implemented in several companies worldwide, developing notable benefits for the organization, regardless of the activity in which the company is engaged [11]. Among the main benefits of adopting this methodology are being more efficient in the use of resources, minimizing waste, and identifying inconveniences that generate low levels of production and cause high production costs [12]. Within these methodologies, there are very useful tools that are adapted to the production process and are very valuable after their implementation. Poka-Yoke devices are used in the context of manufacturing to prevent errors or defects in the processes. These can be mechanical or electronic and are intended to avoid human errors, which can save time, reduce costs, and improve product quality [13]. Single Minute Exchange Die (SMED) is a tool that seeks to reduce the time required to change molds or formats in a manufacturing line. To achieve this, the methodology focuses on identifying and eliminating all activities that do not add value during the change process. The successful implementation of SMED in the production line generates greater flexibility in orders, a reduction in changeover time, and a better-quality product [14].

Another widely utilized tool is the 5S methodology, which is a continuous improvement philosophy originating in Japan. It focuses on self-discipline, order, cleanliness, standardization, and customer interests. The methodology is part of Lean Manufacturing and allows classification of what is not necessary for the workplace, as well as generating discipline in the collaborators, therefore, they keep the workspace clean and orderly. A well-organized workspace generates an increase in competitiveness and decreases unproductive times, improving efficiency and safety, as well as motivating and generating well-being in employees to carry out their working activities [15].

Guleria et al. [16] implemented Lean Six Sigma in an automobile fuel filter manufacturing company that had a high rejection rate. The company was generating losses and could not supply the demand of its customers in the stipulated time. By applying DMAIC, Value Stream Mapping (VSM), and other Six Sigma tools, they detected the most significant problems affecting the process. After correcting the problems and implementing improvements, they managed to reduce the defects that generated non-conforming products by 8 %, and the delivery time was reduced from 12 to 11 days. According to Dinesh et al. [17], VSM is a visual technique that uses symbols and diagrams to facilitate the visualization and understanding of the flow of materials, information, and activities. It starts from the moment that the order is received until the final delivery of the product or service. Its main objective is to identify and eliminate waste and activities that do not add value to the process.

Kharub et al. [18] implemented the Lean Six Sigma DMAIC methodology in a company dedicated to the production of fruit juices. This study identified inefficiencies, and waste in the production process. With the application of DMAIC and the cause-and-effect diagram, the most significant problems were attacked and corrected, significantly. It increased the efficiency of the process, improving profits by 7 %, and reducing waste by almost 50 %. In addition, the return on investment is estimated to be recovered within three years.

Lean Six Sigma in conjunction with quality tools can improve any activity or process, one example of this is the study of Antosz et al. [19] which carried out in a floor covering company. They apply the DMAIC methodology and Total Productive Maintenance (TPM) to improve the efficiency and effectiveness of the maintenance process, as well as increase the operational availability of the machines. By running adequate maintenance and having effective management of the equipment, unexpected failures that produce production losses were eliminated. The correction of these failures had positive effects on the economy of the company since the cost of operation is minimized, also is more efficient in the use of energy, and the useful life of the equipment increases. The implemented actions to solve the problems were a training program for operators, planning of maintenance activities, and implementing autonomous maintenance. Therefore, it was possible to reduce the number of failures in the machines by 40 %, and the availability increased by 27 %.

Thakur et al. [20] affirm that the level of production without defects determines the continuity and growth of companies. They applied Lean Six Sigma to an agricultural equipment ma-

nufacturing company that had several quality defects in painted products. The information collected from the process was analyzed and then, through the application of a Pareto diagram, the most significant problems were known, complementing the information through a fishbone diagram to identify the root causes. After correcting the detected problems, the rejection range was reduced from 12 % to 5 %, and the Sigma level improved from 2.8 to 4.1. The process became more efficient, reducing defects and increasing the level of production.

Daniyan et al. [21] implemented the improvement of the performance and quality of the wagon assembly process by the Lean Six Sigma methodology and some of its tools. They seek to develop a profitable, sustainable organization that is competitive in the market, by decreasing manufacturing errors that generate additional costs without adding value to the manufacturing process, or that generate delays in delivery time. The applications of continuous improvement tools such as the Pareto Diagram, 5S, and standardizing the processes, achieved a 46.8 % improvement in process efficiency, delivery time improved by 27.9 %, and the time that does not generate value to the process was reduced by 71.9 %.

Within savings policies, another fundamental aspect of reducing the cost of production is keeping track of energy consumption. Erdil et al. [22] applied DMAIC to an energy project, where they showed that efficient energy management is a high priority for organizations. It has a significant impact on profits as long as the proposed improvements are achieved to be more efficient in consumption. Vásquez-Stanescu et al. [23] carried out an energy audit in the production and administrative areas intending to take control actions that allow for reducing consumption. The main taken actions were investing in more efficient machines, with lower energy consumption and a higher level of productivity. There was also personnel capacitation of those who are involved in the processes, to encourage rational consumption of resources. In addition, it is necessary to implement periodic energy audits to evaluate the actions that are being taken and generate an energy and environmental management plan. With these actions, it was possible to reduce electricity consumption by 30 % and production levels increased by 86 %.

Mercado and Peña [24] mention that to have operational reliability in the equipment and reduce energy consumption, the maintenance department and the production department must work together, Then, a management model can be implemented corrects the lack of planning, programming, and execution of maintenance activities. It is because if failures in the machines are not corrected, the useful life of the equipment is reduced, operational efficiency decreases, and electricity consumption can increase by 10 %.

According to the Latin American Energy Organization (OLADE), the consumption of industries represents one-third of the total electrical energy demand. This consumption is responsible for climate change, which causes droughts, floods, increases in temperatures, and rises in sea levels [25]. Therefore, environmental policies seek to reduce the consumption of electrical energy, which would reduce the impact on the environment by reducing greenhouse gases. Shah et al. [26] mention that greenhouse gas emissions can be reduced between 10 % and 30 % by implementing simple habits, such as using efficient electric motors and having a more rational consumption of energy.

In industries, energy savings vary depending on the activity, e.g. Stefanie et al. [27] analyzed industries dedicated to iron foundry. The analysis shows that by implementing efficient technology, such as solar panels or another type of green energy that provides an alternate energy supply, as well as using devices with higher electrical consumption in periods where demand is low, energy consumption can be reduced by 23 %. Using machines with the latest technology (which have lower energy consumption and can generate a higher level of production) also generates improvements in product quality as well as reducing reprocessing waste. The implementation of these technologies does not carry risks and, in addition, the required capital can be recovered in a couple of years [28].

Therefore, it was decided to implement the Lean Six Sigma DMAIC methodology in production line number 4 of detergent powder packaging in the Powder Tower area of an important company located in Quito, Ecuador. This line is chosen because is the only one with the oldest bottling machine, which generates the lowest efficiency compared to lines with the same characteristics. The line is made up of a Bosch SBV 2 510 packaging machine, a Yamato 14 balance dosing machine, and a Raumak Multi Baler 300 baling machine. The packaging machine makes products in presentations of 200, 480, and 1 000 g, in Floral and Lemon presentations. The wrapping machine makes bales of 36 sleeves for presentations of 200 g and 480 g, and 12 bags for the presentation of 1 000 g. To control the improvements that are achieved in the production line, values of indicators of availability, efficiency, quality, and Overall Equipment Effectiveness (OEE) will be taken. It is commonly used in the manufacturing industry and it also identifies where efforts can be focused to improve productivity [29].

In addition, since energy consumption is directly related to the cost of production, part of the project will be focused on reducing energy consumption. A WEM3080T energy meter was implemented to have a record of energy consumption, allowing to evaluate the behavior of the equipment and measure the impact of possible improvements. By making better use of natural, human, and economic resources, the company will be able to be more competitive in the market, and part of the generation of savings will be able to be invested in more efficient technology. By generating significant savings, it will become an environmentally responsible eco-efficient company [30].

This investigation aims to lower the cost of production by identifying and minimizing or even eliminating waste through the application of Lean Six Sigma DMAIC. Quality tools were utilized (such as the Pareto and the Ishikawa Diagram) to find out the root cause of the most significant problems. This document is distributed according to the following detail. Methodology details the current information on the company and the required tools for the implementation, following in an orderly phase, strictly complying with what the methodology recommends. The results show quantitatively the effectiveness of the implementation by contrasting a period before and after implementing the DMAIC methodology in the production line. Finally, conclusions debate the expectations of this investigation

to help new companies venture into implementing continuous improvement methodologies in their processes.

II. METHODOLOGY

This investigation collects information on the implementation carried out in production line No. 4 of the detergent powder packaging section of an important company located in Quito. For the study period, historical data from the second semester of 2021 was taken, and the study of the implementation of the DMAIC methodology began to be implemented from January 2022. Were defined three months to implement improvements, train personnel, and create instructions. Therefore, only from april began to record data for analysis, to evaluate the process before and after implementation.

The project started with a documentary investigation, analyzing information from publications that have implemented the methodology within their production processes, and the impact they had after implementation. As well as learning about the experiences of other projects to avoid making mistakes that cause the cost or implementation time to increase due to unexpected problems. The investigation was carried out through an experimental design since the conditions and variables that modified the efficiency, availability, and quality indices were corrected. This approach is quantitative type, data were analyzed from current production levels and after the implementation of the methodology. As the DMAIC methodology was implemented, it was followed in phases, and each phase had its tool or method to be developed.

The indicators are fundamental within the manufacturing processes to measure the performance of the process. The OEE was utilized, arising from the following equations:

Equation 1

$$A = \frac{Operative\ time}{Planned\ production\ time} \cdot 100\ \% \tag{1}$$

Equation 2

$$P = \frac{Processed\ quantity\ \cdot\ Cycle\ time}{Operative\ time} \cdot 100\ \% \tag{2}$$

Equation 3

$$Q = \frac{Number\ of\ useful\ products}{Total\ produced\ quantity} \cdot 100\ \% \tag{3}$$

Equation 4

$$OEE = A \cdot P \cdot Q \tag{4}$$

Where A is availability, P is performance, and Q is quality. Within the define phase, a project charter was carried out where the team members were established. A low level of efficiency and availability of the machine was defined as the main problem, currently finding efficiency of 76.71 %, availability of 81.40 %, and an OEE of 62.42 %. By taking the OEE values recommended worldwide as a reference, the minimum value was 72 %, which is within the acceptable range of production. With this purpose, it is intended to improve production levels and reach a cost-reduction of production.

In the measure phase, the data that the machine operators registered in the control sheet is digitalized and processed. Operators write the start time and end time of production, the failures that have occurred during the shift, as well as the duration time of each recorded failure. The amount of production that the machine has made in the shift is also written. As an additional indicator, the electrical consumption of the machine began to be recorded. By processing this data, the calculations of availability, performance, quality, and the global OEE indicator are made. All the contained data in the control sheet are recorded daily by the production assistant in a resource planning system (RPS) managed by the company. In this system, the information from the quality assurance department regarding returns or non-conforming product that affects the quality records is checked.

For the improve phase, an action plan was defined based on the failure analysis and the significant problems revealed by the Pareto Diagram and the Ishikawa Diagram of the previous phase. For this, the multidisciplinary work team, through brainstorming and consensus among all the areas involved, agreed to carry out a set of actions. Certain actions are of immediate priority and others are a little more complex to implement, a medium-term priority was given, defined as a period of three months. This period is given because it took three months to implement the DMAIC methodology. From the fourth month on, information is collected with which the level of the process improved was contrasted.

The analysis of the previous section and surveys of the operators allows to affirm that there are personnel operating the machines with a minimum of experience. It was concluded that one of the main shortcomings of low levels of production and availability of the machine is that operators have not been technically trained and they cannot carry out their work properly. Both the packaging machine and the dosing machine have several parameters that operators can access, nevertheless, sometimes is unclear because these parameters are related to others. In the training plan, they were taught the correct operation of the machine, and some parameters were established with minimum and maximum ranges that the operator could configure without the machine suffering any failure. To improve the levels of efficiency and availability of the machine, it was created instructions for the format and reel change, technically trained operators, and an operation guide for both the packaging machine and the dosing machine. A source of knowledge is generated for old operators and for new operators to have tools that allow them to learn the operation more easily.

The 5S methodology had been previously implemented in the area, but it did not continue. Since the staff already had notions, their knowledge was reinforced and it was resumed with more force and carrying out control by the quality department. In order not to burden and confuse the staff, this implementation was carried out from february 2022 and was divided as shown in Table I. This was mainly focused on the dosing machine since using it for a prolonged period without calibration and clea-

ning runs the risk of having weight failures, the dosing speed decreases, the feeding, and weighing hoppers are damaged, and the consumption of electrical energy increases. Based on the record of the failure, the maintenance department drew up a list of parts that must be kept in stock. On several occasions, there were cases in which a lack of spare parts caused the machine to be out of order until the part was ordered to be manufactured.

TABLE I
5S METHODOLOGY IMPLEMENTATION

S	Definition	Implementation
Seiri	Only what is necessary	Week 1
Seiton	Order	Week 2
Seiso	Cleaning	Week 2
Seiketsu	Standardize-Security	Week 3
Shitsuke	Discipline	Week 4

With the headquarters, it was decided to make a significant investment to carry out a complete reconditioning of the machine. This is to prolong its useful life and reduce the frequency of failures that occur due to wear and tear in the operation. Even more when the machine has not been deeply intervened since it was acquired in 2016.

Finally, in the control phase was implemented a dashboard to show the availability, performance, quality, and OEE of the machine. This information is uploaded daily, allowing operators to know if they are doing a good job or need to work on improving. On this board, there is a checklist that evaluates the cleanliness of the area and cleanliness of the machine, the second one considers that there are no strange objects in the area and that the 5S are complied. With the objective that the improvements last over time, it was defined to hold monthly reunions to evaluate the impact of the implemented improvements and to provide training every six months to the operators to refresh their knowledge.

III. RESULTS

To know the situation of the company before the implementation of improvements, a review of the production records for the second half of 2021 was developed. Fig. 2 shows historical data of production indicators corresponding to the second half of 2021. It is possible to see how due to the low efficiency and availability of the machine the *OEE* is directly affected.

A device was installed to measures electricity consumption in the machine in real time and records it in a spreadsheet for later analysis. Machine energy consumption is a new indicator that was implemented in december and began acquiring data in january 2022. In this stage of the methodology, an analysis of the historical data of failures was carried out to find out the root cause of the problems that cause low efficiency and availability of the machine.

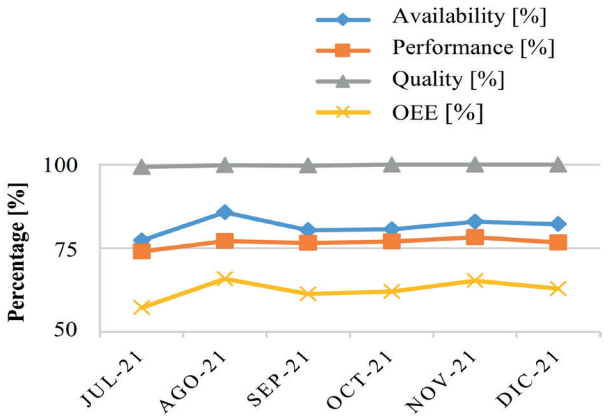

Fig. 2. Indicator trend between July and December 2021.

Figure 3 shows energy consumption data that was collected after cleaning and calibrating the dosing machine. It can be seen that energy consumption increases as the weeks go by. This is because when a mattress of product is generated stuck to the vibrating plate, the vibration level must be increased and the product continues to fall in the same amount.

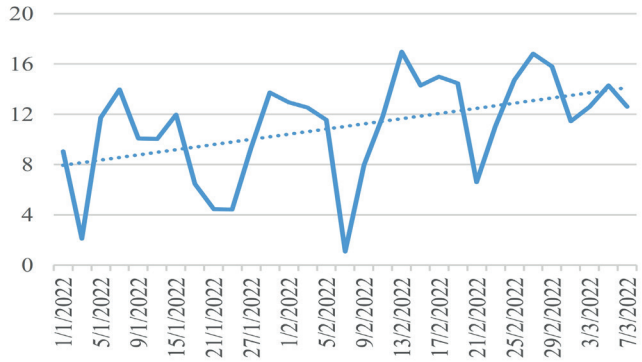

Fig. 3. Analysis of energy consumption of the production line.

As regards the analysis of energy consumption, it was concluded that the machine in normal operation consumes an average of 14.6 kW·h in a 24-hour shift. It was determined that due to a lack of cleaning and maintenance of the vibrator plate of the dosing machine, energy consumption can increase by up to 20 %. This is because detergent dust accumulates on the walls of the vibrator plate, making it necessary to increase the level of vibration intensity, thus increasing energy consumption.

To determine the most significant problems, a Pareto Diagram was designed, which identified 20 % of problems that occur 80 % of the time within the process. It seeks to focus efforts on the problems that have the most incidence and with what best results obtained when correcting them. Figure 3 presented the main problems that the operators register in the roadmap. Through the Pareto Diagram, it was identified that four failures are the most recurring, and they are the ones on which the efforts will be focused.

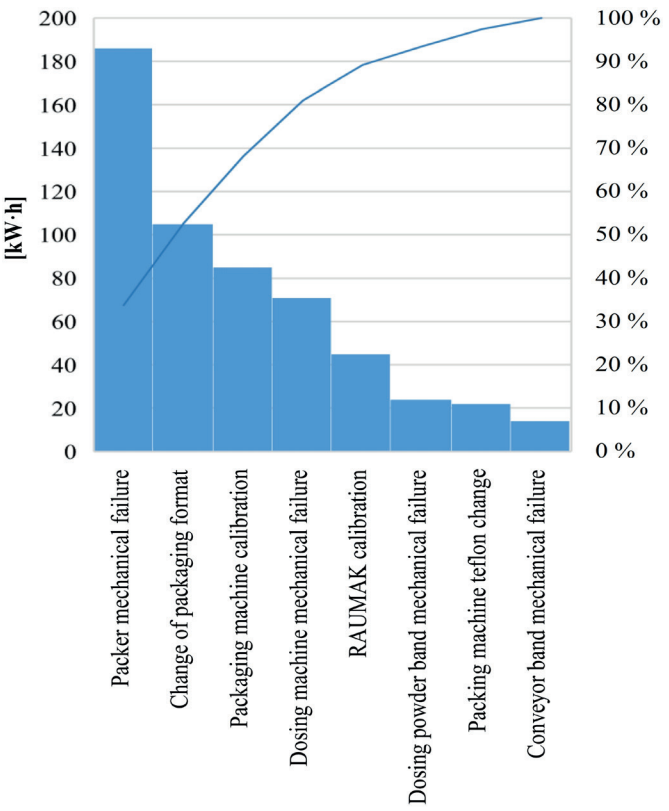

Fig. 4. Pareto Diagram of recorded failures.

Table II shows the 4 most significant problems and their recurrence in a 24-hour shift. After analyzing the Pareto Diagram, the analysis defined that the main cause of a low level of availability and efficiency in the machine is due to operators who have not been trained to properly operate the product packaging and dosing machine. Therefore, it is observed that their lack of knowledge causes breakdowns in the machine, in addition to the lack of standardization and lack of spare parts.

TABLE II
SIGNIFICANT PROBLEMS

Problems	Frequency [min]
Packer mechanical failure	186
Change of packaging format	105
Packaging machine calibration (parameterization)	85
Dosing machine mechanical/electrical failure	71

The objective of implementing Poka-Yoke was to reduce the time that takes operators to change formats and put the machine into production. A Poka-Yoke was placed to center the former with the clamp, one to center the coil, one for the entry of the blade angle, one for the location of the coding, and one for the centering of the bag cut. This training consisted of teaching the operators an efficient change of product or format, leveraged with the instructions. By implementing Poka-Yoke in the machine, it was possible to considerably reduce the time of format change, which was lost the most of the time was lost. Table III shows the improvements in terms of format change.

TABLE III
FORMAT CHANGEOVER EFFICIENCY

Presentation [g]	Format change [min]	Standard [min]	Efficiency [%]	
			Before	Now
200	45	25	55.56	83.3
480	68	30	44.12	81.0
1 000	85	40	47.06	88.8

Increasing production levels and reducing waste are directly related to reducing the cost of production. The methodology focused on decreasing everything that generated waste, that did not allow the machine to be operational, and that energy consumption increases. From the analysis of energy consumption, it was determined that, due to a lack of cleaning of the components of the dosing machine, especially the vibrator plate, energy consumption can increase by 20 %. It requires that a cleaning period of a maximum of three weeks be established. Energy savings could also be obtained by disconnecting the heating resistances of the horizontal and vertical seals, which are some of the elements that consume the most energy when the machine is not operating. Table IV shows the average consumption of the machine when it is not producing, and the hours that pass until the machine returns to production on Mondays. With this action, an average of 10.4 kW could be saved each weekend.

After implementing Poka-Yoke, SMED, and standardization of operating parameters, the format change became around 34 minutes, when before the implementation it was bordering on 55 minutes. It represents a decrease of 21 minutes in each format change, with which availability is 7.32 %. In addition to the significant reduction in time, there was also a reduction in laminate of around 2.5 kg for each format change. It was obtained by calibrating faster and together with all the mechanical and operating parameters of the machine, the operator sets up the machine faster and does not waste laminate.

TABLE IV
FORMAT CHANGEOVER EFFICIENCY

Average hourly consumption without production [kW]	Weekend free hours	Weekend consumption [kW]
0.26	40	10.4

With the implemented improvements in the first three months of 2022, favorable changes began to be noticed. It was compared with data collected from april to august 2022 to verify to what extent the implementation of improvements contributed to the levels of availability, performance, quality, and therefore the OEE. Table V shows the significant improvement in the availability and performance after the methodology implementation in the production line.

TABLE V
PRODUCTIVITY INDICATORS
AFTER IMPLEMENTING IMPROVEMENTS

Month	Availability [%]	Performance [%]	Quality [%]	OEE [%]
Apr-22	87.20	86.06	100.00	75.04
May-22	88.61	88.21	99.82	78.02
Jun-22	88.49	87.52	100.00	77.45
Jul-22	89.76	87.03	99.23	77.52
Aug-22	90.15	89.08	99.48	79.89

Figure 5 presents the productivity indicators of the improving implementations in the process, such as operator training, 5S methodology, creation of operating instructions, implementation of Poka-Yoke, and training in SMED. It is important to mention that the purpose was to achieve an OEE of at least 72 %.

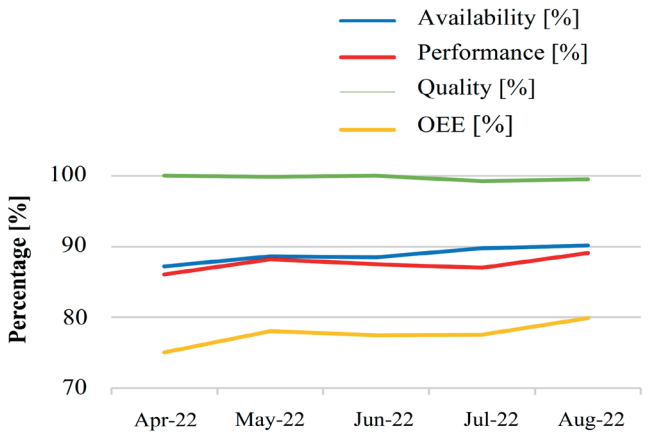

Fig. 5. Analysis of energy consumption of the production line.

Figure 6 shows all the efforts made by the implementation team to improve the levels of availability, performance, and quality. The OEE increased 5 % more than the planned objective, reaching 77.58 %.

Due to internal confidentiality policies, the production cost value cannot be disclosed exactly. However, an approximation is that producing a 480g bag of detergent powder costs USD 0.425 in which is included working hours, machine hours, materials, and other items. Regarding production costs, it is evident that due to the low efficiency and availability of the machine, the production cost was around USD 0.524 for each detergent bag, leaving the company with a small profit margin. After the implementation of the DMAIC methodology, the cost dropped to USD 0.478, representing a saving of USD 0.046 compared to the cost before implementation. With the actual machine availability and performance rates, a monthly savings of USD 71 442.05 was achieved.

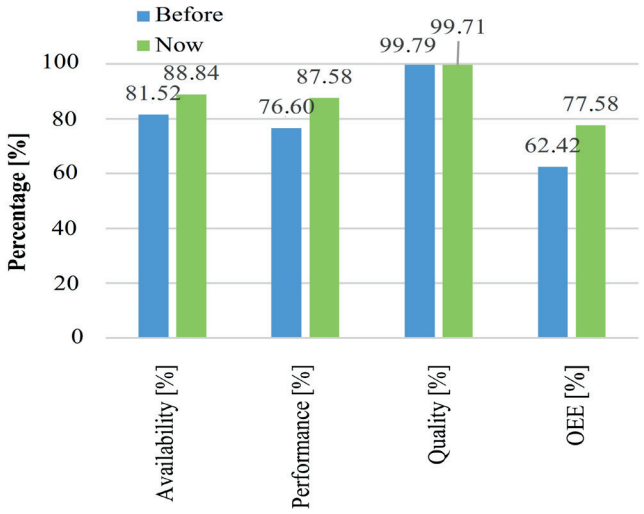

Fig. 6. Analysis of energy consumption of the production line

IV. CONCLUSIONS

After the literature review, where the implementation of the DMAIC methodology had favorable results, the implementation in production line No. 4 of the powder detergent packaging area was as effective as expected. An energy consumption indicator was implemented that allowed the creation of maintenance and cleaning plans to reduce energy consumption. This indicator identified that a lack of cleaning of the vibrating plates of the dosing machine due to an accumulation of product on its walls, increases the vibration intensity, generating an additional 20 % electrical energy consumption.

Within the improvement phase, several quality tools were implemented, such as 5S, Poka-Yoke, SMED, standardization of operating parameters, instructions, and training for operators. All of this together contributed to improving the production process and minimizing or eliminating the problems detected in the production line. Thus, the availability went from 81.52 % to 88.84 %, the performance increased from 76.60 to 87.58 %, the quality was maintained, and the OEE that was 62.42 % reached 77.58 %. The OEE was 5 % above the objective that was set before starting the implementation.

With the increase of the performance in the operation of the machine, as well as having greater availability when correcting the problems that afflicted the line, the main objective was achieved. The implementation of the DMAIC methodology decreased the cost of production, reducing USD 0.046 for each produced bag and it resulted in savings USD 71 442.05. To continue with the philosophy of continuous improvement, to solve those problems that need deeper analysis, operators with specialized technical training must be hired. An alternative is also to hire a supervisor who is specialized in the proper handling and operation of the machines, since current operators, despite having been trained, have a lack of technical instruction.

Statistical information on the production processes was collected and it is important to mention that, despite the

pandemic, the packaging line did not stop, but it reduce the operational capacity. For this reason, obtained information until 2023 will be considered to analyze the preliminary improvement results. In this manner, this production line must be continuous analyzed, to define whether the techniques applied are appropriate or whether they should be updated. Therefore, future investigations may emphasize the search for the latest information and the comparison of results with similar cases of study.

REFERENCES

[1] S. Krishna Priya, V. Jayakumar, and S. Suresh Kumar. "Defect Analysis and Lean Six Sigma Implementation Experience in an Automotive Assembly Line," *Materials Today: Proceedings*, vol. 22, pp. 948-958, 2020. Available: 10.1016/j.matpr.2019.11.139.

[2] C. Castro, Z. Castañeda, K. R. Ruiz, G. González, and G. Poveda. "El sector florícola ecuatoriano y su afectación en el mercado internacional producto de la pandemia causada por el Covid-19," in *Congreso Internacional Virtual Sobre Covid-19. Consecuencias Psicológicas, Sociales, Políticas Y Económicas*, 2020, pp. 53-65.

[3] L. Villar-Zamora. "Uso de sistemas expertos en el ciclo de carguío y acarreo y su influencia en el proceso de mejora continua y gestión de costos operativos," 2020.

[4] O. M. Ikumapayi, E. T. Akinlabi, F. M. Mwema, and O. S. Ogbonna. "Six Sigma Versus Lean Manufacturing – An Overview," *Materials Today: Proceedings*, vol. 26, pp. 3275-3281, 2020. Available: 10.1016/j.matpr.2020.02.986.

[5] D. Skalli, A. Charkaoui, and A. Cherrafi. "Assessing Interactions Between Lean Six-Sigma, Circular Economy and Industry 4.0: Toward an Integrated Perspective," *IFAC-Papers OnLine*, vol. 55, no. 10, pp. 3112-3117, 2022. Available: 10.1016/j.ifacol.2022.10.207.

[6] A. U. Abhijit and S. Pillai, "Sustainable Practises in Lean Manufacturing: A Critical Review," *International Journal of Management Studies*, vol. 5, no. 1-2, pp. 1-12, 2018.

[7] A. Jamwal, S. Nayim, R. K. Shukla, R. Agrawal, and S. Gupta. "Assessment of Barriers in Lead Time Improvement: An Exploratory Study of Electronics Manufacturing Companies in Himachal Pradesh (India)," *International Journal of Business and Systems Research*, vol. 15, no. 2, pp. 182-199, 2021.

[8] D. H. Stamatis. *Six Sigma and Beyond: Design for Six Sigma, Volume VI*. CRC Press, 2002.

[9] P. Guleria, A. Pathania, R. K. Shukla, and S. Sharma. "Lean Six-Sigma: Panacea to Reduce Rejection in Gear Manufacturing Industry," *Materials Today: Proceedings*, vol. 46, pp. 4040-4046, 2021. Available: 10.1016/j.matpr.2021.02.559.

[10] M. Smętkowska and B. Mrugalska. "Using Six Sigma DMAIC to Improve the Quality of the Production Process: A Case Study," *Procedia - Social and Behavioral Sciences*, vol. 238, pp. 590–596, 2018. Available: 10.1016/j.sbspro.2018.04.039.

[11] R. Edwin-Joseph, N. Kanya, K. Bhaska, J.Francis Xavier, S. Sendilvelan, M. Prabhahar, N. Kanimozhi, S. Geetha. "Analysis on Productivity Improvement, Using Lean Manufacturing Concept," *Materials Today: Proceedings*, vol. 45, pp. 7176-7182, Jan. 2021. Available: 10.1016/J.MATPR.2021.02.412.

[12] N. Nandakumar, P. G. Saleeshya, and P. Harikumar. "Bottleneck Identification and Process Improvement by Lean Six Sigma DMAIC Methodology," *Materials Today: Proceedings*, vol. 24, pp. 1217-1224, 2020. Available: 10.1016/j.matpr.2020.04.436.

[13] T. A. Saurin, J. L. D. Ribeiro, and G. Vidor, "A Framework for Assessing Poka-Yoke Devices," *Journal of Manufacturing Systems*, vol. 31, no. 3, pp. 358-366, 2012. Available: 10.1016/j.jmsy.2012.04.001.

[14] G. Toki, T. Ahmed, M. Hossain, R. Khan-Alave, M. Omar-Faruk, R. Mia, S. Rashedul-Islam. "Single Minute Exchange Die (SMED): A Sustainable and Well-Timed Approach for Bangladeshi Garments Industry," *Cleaner Engineering and Technology*, vol. 12, p. 100592, 2023. Available: 10.1016/j.clet.2022.100592.

[15] K. M. Senthil Kumar, K. Akila, K. K. Arun, S. Prabhu, and C. Selvakumar. "Implementation of 5S Practices in a Small Scale Manufacturing Industries," *Materials Today: Proceedings*, vol. 62, pp. 1913-1916, 2022. Available: 10.1016/j.matpr.2022.01.402.

[16] P. Guleria, A. Pathania, H. Bhatti, K. Rojhe, and D. Mahto. "Leveraging Lean Six Sigma: Reducing Defects and Rejections in Filter Manufacturing Industry," *Materials Today: Proceedings*, vol. 46, pp. 8532-8539, 2021. Available: 10.1016/j.matpr.2021.03.535.

[17] S. N. Dinesh, M. Shalini, M. Vijay, R. C. Vijey Mohan, R. Saminathan, and R. Subbiah. "Improving the Productivity in Carton Manufacturing Industry Using Value Stream Mapping (VSM)," *Materials Today: Proceedings*, vol. 66, pp. 1221-1227, 2022. Available: 10.1016/j.matpr.2022.05.015.

[18] M. Kharub, B. Ruchitha, S. Hariharan, and N. Shanmukha Vamsi, "Profit enhancement for small, medium scale enterprises using Lean Six Sigma," *Mater Today Proc*, vol. 56, pp. 2591-2595, 2022, doi: 10.1016/j.matpr.2021.09.159.

[19] K. Antosz, M. Jasiulewicz-Kaczmarek, R. Waszkowski, and J. Machado. "Application of Lean Six Sigma for Sustainable Maintenance: Case Study," *IFAC-PapersOnLine*, vol. 55, no. 19, pp. 181-186, 2022. Available: 10.1016/j.ifacol.2022.09.204.

[20] P. Thakur, R. Kumar, S. Kumar, A. Pathania, and B. Goel. "Analysis and Optimization of Properties of Paint Materials for Reduction of Paint Defects in Agro Products," *Materials Today: Proceedings*, vol. 45, pp. 5617–5623, 2021. Available: 10.1016/j.matpr.2021.02.349.

[21] I. Daniyan, A. Adeodu, K. Mpofu, R. Maladzhi, and M. G. Kana-Kana Katumba, "Application of Lean Six Sigma Methodology Using DMAIC Approach for the Improvement of Bogie Assembly Process in the Railcar Industry," *Heliyon*, vol. 8, no. 3, p. e09043, 2022. Available: 10.1016/j.heliyon.2022.e09043.

[22] N. O. Erdil, C. B. Aktas, and O. M. Arani. "Embedding Sustainability in Lean Six Sigma Efforts," *Journal of Cleaner Production*, vol. 198, pp. 520–529, 2018. Available: 10.1016/j.jclepro.2018.07.048.

[23] C. L. Vásquez Stanescu, A. G. Carillo Ozal, M. E. Tona Castillo, M. V. Galíndez Jimenez, K. A. Macias Camacaro, and C. Esposito de Díaz. "Sistema de gestión energética y ambiental de productos Alimex CA," *Suma de Negocios*, vol. 8, no. 18, pp. 115-121, 2017. Available: 10.1016/j.sumneg.2017.11.003.

[24] V. Mercado and J. B. Peña. "Modelo de gestión de mantenimiento enfocado en la eficiencia y optimización de la energía eléctrica," *Saber*, vol. 28. scielo, pp. 99-105, 2016.

[25] E. Guitérrez and I. Trejo. "Efecto del cambio climático en la distribución potencial de cinco especies arbóreas de bosque templado en México," *Revista Mexicana de Biodiversidad*, vol. 85, no. 1, pp. 179-188, 2014. Available: 10.7550/rmb.37737.

[26] S. A. R. Shah, Q. Zhang, J. Abbas, H. Tang, and K. I. Al-Sulaiti. "Waste Management, Quality of Life and Natural Resources Utilization Matter for Renewable Electricity Generation: The Main and Moderate Role of Environmental Policy," *Utilities Policy*, vol. 82, p. 101584, Jun. 2023. Available: 10.1016/J.JUP.2023.101584.

[27] S. Stefanie, S. Christoph, and S. Michael. "Identifying Energy Flexible Manufacturing Layouts in a Light Metal Foundry," *Procedia CIRP*, vol. 104, pp. 1589-1594, 2021, Available: 10.1016/J.PROCIR.2021.11.268.

[28] A. Aranda-Usón, G. Ferreira, M. D. Mainar-Toledo, S. Scarpellini, and E. Llera Sastresa. "Energy Consumption Analysis of Spanish Food and Drink, Textile, Chemical and Non-Metallic Mineral Products Sectors," *Energy*, vol. 42, no. 1, pp. 477-485, 2012. Available: 10.1016/j.energy.2012.03.021.

[29] T. Dunn. "8 - OEE Effectiveness," in *Flexible Packaging*. Oxford: William Andrew Publishing, 2015, pp. 77-85. Available: 10.1016/B978-0-323-26436-5.00008-4.

[30] P. J. López Abad. *Cambia la energía, cambia el clima. Cambio climático y su impacto en el sector energético.* 2016. Available: 10.13140/RG.2.2.10284.62085.

Containers-Based Network Services Deployment: A Practical Approach

Andrés Yazán[1], Christian Tipantuña[1], and Jorge Carvajal-Rodriguez[1]

Abstract — **In recent years, virtualizing network services and functions has enabled optimizing hardware resources on resource-constrained devices, such as CPU, memory, and storage. Traditional virtualization is achieved through virtual machines using a layer known as a hypervisor. While this form of virtualization offers advantages such as scalability and portability, it has disadvantages in terms of performance compared to nonvirtualized deployments. In this context, alternative virtualization technologies (like containers) allow virtualization on the same physical infrastructure, improving overall performance, portability, and service scalability. This paper implements the deployment of network services on the Raspberry Pi development platform, which has limited resources. This is achieved through a multi-container virtualization solution using the Docker Compose tool, based on Docker containerization technology. Finally, a performance analysis of the implemented virtualization solution is conducted in terms of resource utilization by each service.**

Keywords — **Virtualization; Virtual Machines; Container Raspberry Pi; Docker; Docker Compose; Performance.**

Resumen — **En los últimos años, la virtualization de servicios y funciones de red ha permitido optimizar los recursos de hardware, como CPU, memoria y almacenamiento, en equipos con limitaciones de recursos. La virtualization tradicional se lleva a cabo mediante máquinas virtuales, utilizando una capa conocida como hipervisor. A pesar de que esta forma de virtualization ofrece ventajas como escalabilidad y portabilidad, presenta desventajas en términos de rendimiento en comparación con un despliegue no virtualizado. En este contexto, han surgido tecnologías alternativas de virtualization (como los contenedores) que permiten la virtualization en la misma infraestructura física, mejorando el rendimiento general, la portabilidad y la escalabilidad de los servicios. En este artículo se implementa el despliegue de servicios de red en la plataforma de desarrollo Raspberry Pi que cuenta con recursos limitados. Esto se logra mediante una solución de virtualization multicontenedor utilizando la herramienta Docker Compose, basada en la tecnología de contenerización Docker. Finalmente se lleva a cabo un análisis del rendimiento de la solución de virtualization implementada en términos de la utilization de recursos por parte de cada uno de los servicios.**

Palabras Clave — **Virtualization; Máquinas Virtuales; Contenedor; Raspberry Pi; Docker; Docker Compose; Rendimiento.**

I. INTRODUCTION

THE growing demand for network services, applications, and resources from end-users has created limitations in the capacity of service providers to meet these needs due to a shortage of necessary hardware resources to scale proportionally to the demands. Service providers have had to adopt new technologies to meet current demands, maximize resource efficiency, and offer end-users high-quality service (QoS). In this context, virtualization technologies plays a fundamental role in the information technology industry. While virtualization technologies such as Virtual Machines (VMs) provide virtualized services, they present significant performance and resource efficiency problems. For this reason, container-based virtualization technologies have become the preferred choice, as they offer highly efficient virtualized services by operating directly on a device's native software infrastructure, leveraging the features of an operating system kernel to create virtualization. These features include 'namespaces' and 'cgroups', which provide an isolated and independent environment within the native infrastructure in which they run [1].

This paper aims to describe, implement, and analyze a solution for network services based on Docker containers. Is analyzed the performance of containerized services in environments with limited CPU, memory, and storage resources, such as Raspberry Pi development boards. To achieve this, the work is structured as follows:

Section II: A brief description of concepts and related work on virtualization technologies, virtual machines, Docker containers, network services, and microservices is provided.

Section III: Describes the methodology, test environment, software tools, and hardware used for designing and implementing network services using Docker containers.

Section IV: are presented the results obtained in the implementation, and evaluated the performance of the implemented containerization system based on CPU usage, memory usage, and load.

Section V: Provides concluding remarks about the work developed.

Authors acknowledge the support provided by Escuela Politécnica National in the project PIIF-21-04. Corresponding author: christian.tipantuna@epn. edu.ec.

[1] Andrés Yazán is in the Department of Electronics, Telecommunications and Information Networks of the National Polytechnic School, Quito 170517, Ecuador, (e-mail: andres.yazan@epn.edu.ec). ORCID number 0009-0001-7811-1275.

[2] Christian Tipantuña is in the Department of Electronics, Telecommunications and Information Networks of the National Polytechnic School, Quito 170517, Ecuador, (e-mail: christian.tipantuna@epn.edu.ec). ORCID number 0000-0002-8655-325X.

[3] Jorge Carvajal-Rodriguez is in the Department of Electronics, Telecommunications and Information Networks of the National Polytechnic School, Quito 170517, Ecuador, (e-mail: jorge.carvajal@epn.edu.ec). ORCID number 0000-0003-0369-9964.

Manuscript Received: Sep 22, 2023
Revised: Nov 08, 2023
Accepted: Nov 27, 2023
DOI: https://doi.org/10.29019/enfoqueute.1005

II. BACKGROUND AND RELATED WORK

This section presents the fundamental concepts of virtualization architectures based on Virtual Machines (VMs), followed by container-based virtualization, emphasizing Docker technology. Additionally, we will provide a brief description of microservices infrastructure.

Virtualization is a process or technology that allows the segmentation of software and hardware resources from a physical architecture to deploy multiple dedicated resources in virtual environments for processes or applications. The main virtualization technologies include those based on hypervisors and container-based technologies. Hypervisor-based technology adds a layer of software to the conventional computational architecture, specifically to the underlying operating system, also known as the hypervisor. This layer virtualizes and manages the system's physical resources, such as CPU, RAM, and storage, distributing them optimally for each Virtual Machine (VM). Thus, the hypervisor creates an isolated environment for each VM with its complete operating system, allowing independent execution from the main operating system [2], However, this hypervisor-based approach may decrease overall performance, especially in environments with high resource demand. It is important to note that this hypervisor layer is present in all traditional virtualization technologies, meaning its negative impact on performance is constant in any implementation case, as mentioned [3].

On the other hand, containerization technologies are software that represents a virtualization operating at the kernel level of the operating system. They enable the execution of applications and services in isolated and portable environments within the same physical system, called containers [2], Additionally, using namespaces and cgroups, this technology allows the isolation and resource management for each container [4].

In practice, container processes outperform hypervisorbased solutions by eliminating the virtualization layer and operating directly on the host system's kernel, as shown in Figure 1 [2], In addition to this advantage, containers have inherent characteristics derived from underlying technologies, such as autonomy and independence between containers in resource usage and deployment. Portability is also noteworthy, as containers use lightweight application images, usually in the order of MBs, compared to the GBs images of VMs that include a complete operating system. These features enable services to achieve high scalability and easy migration. Furthermore, they ensure high service availability by allowing the execution of multiple instances of the same application to maintain uninterrupted service, even if one or more containers of the same image stop working [1], [3], [5]. These advantages are enhanced when combined with a microservices-based architecture, which defines a software design model with functions of a service distributed through autonomous and independent modules (Figure 2b), unlike the traditional architecture of monolithic applications, where functions are integrated into a single structure and are interdependent (Figure 2a) [6]. Container characteristics allow leveraging this type of model to optimize service deployment, unlike those based on VMs.

On the other hand, containers also have disadvantages compared to VMs. For example, although containers are independent and isolated entities, they do not provide complete isolation with the operating system where they share kernel resources, as in the case of VMs. This, in turn, poses a security issue, as any impact at the operating system level can affect containers, as indicated in previous lines [7], [8], [9].

In environments with limited hardware resources, such as the one in this study, a container-based approach leverages these characteristics for optimal and scalable service deployment. In this case, security is not a parameter of study, this work focuses exclusively on measuring resource usage.

Docker is an open-source containerization technology that creates, runs, and manages fightweight, portable, and self- sufficient containers. These features have established Docker as a leader in the containerization technology market [10]. Docker implements its architecture on the operating system kernel to achieve container deployment with these characteristics, utilizing namespaces and cgroups to isolate and manage container resources. Docker also uses a file system known as the 'Advanced Union File System' (AUFS) for layer based image construction, contributing to storage resource optimization during Docker image creation [11].

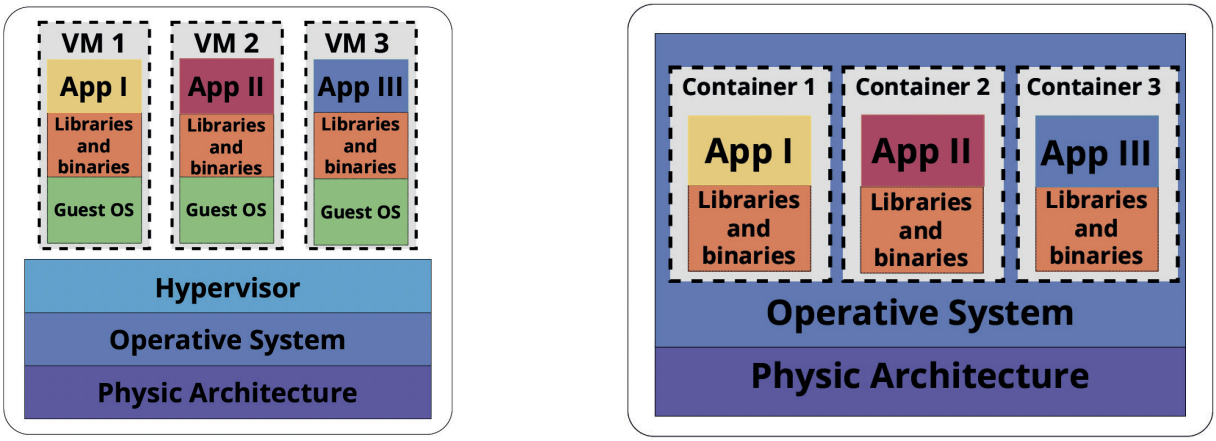

(a) Virtualization Architecture based on Hypervisor

(b) Virtualization Architecture based on Containers

Fig. 1. Virtualization Architectures Comparison, based on [2], [4].

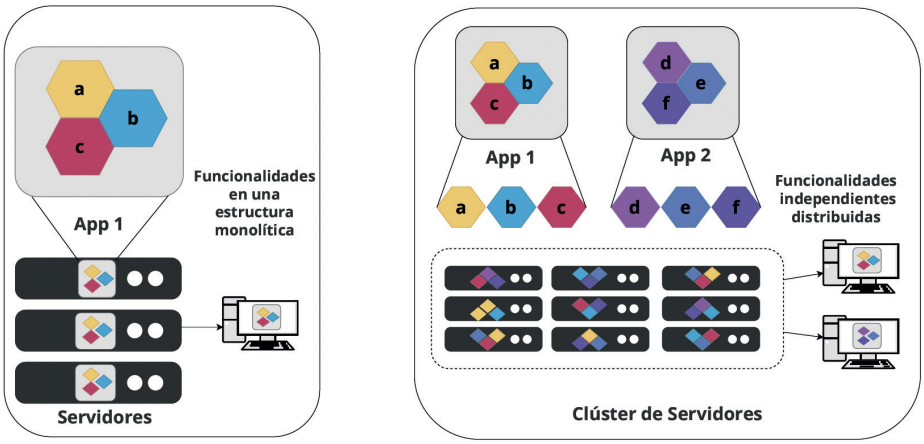

(a) Monolithic Architecture.

(b) Microservices-based Architecture.

Fig. 2. Comparison of service architectures, based on [6].

Above the underlying technologies, there is Docker's architecture known as 'Docker engine', which is the specific name for the containerization technology developed by Docker. This architecture comprises 'Docker objects', representing functionalities within the Docker environment. These functionalities relate to storage, networking, container images, and containers. These elements can have different types depending on their utility and characteristics. Docker objects related to storage functionality are called 'Docker volumes'. These are storage mechanisms created from directories or files stored on the host. Once created, directories are mounted into the container to access a file system outside the isolated environment, as shown in Figure 3a [12].

On the other hand, storage mechanisms are similar to volumes known as 'bind mounts'. Unlike volumes, these are not managed by Docker. They allow data to be mounted to a specific folder on the host into a container, and the stored data persists beyond the container's lifecycle, as illustrated in Figure 3b [13]. 'Volumes' and 'bind mounts' can be used by multiple containers to share the same storage space. Additionally, these mechanisms can be employed for migrating data from containerized services, considering their functionality and ability to maintain data persistence between containers and over time.

Regarding network functionalities, Docker offers what are known as 'Docker networks', entities responsible for providing basic network functionalities through 'network drivers', which share the same name as the network they manage [14]. Docker provides three default networks:

- None: This Docker network has no network interface outside the container. It only has a connection between the container and the loopback interface, and it is commonly used for offline testing, as illustrated in Figure 4a [15].
- Bridge: The 'bridge' network is Docker's default network and uses Linux's bridge functionality to allow communication between containers. Docker creates virtual connections between containers and the virtual network interface called 'dockerO', as shown in Figure 4b. An internal network is created when this connection is established, and IP addresses are automatically assigned to each container, enabling communication within this network. However, initially, they cannot communicate outside of this network. Nevertheless, using iptables and Docker's Network Address Translation (NAT), it is possible to configure the port mapping to allow communication from the container network to the external network [16].

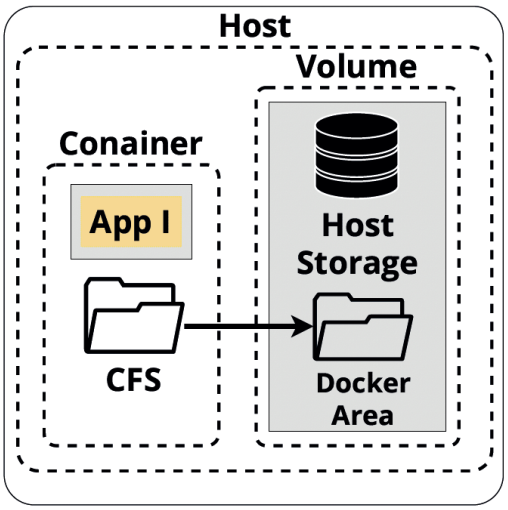

(a) Volumes

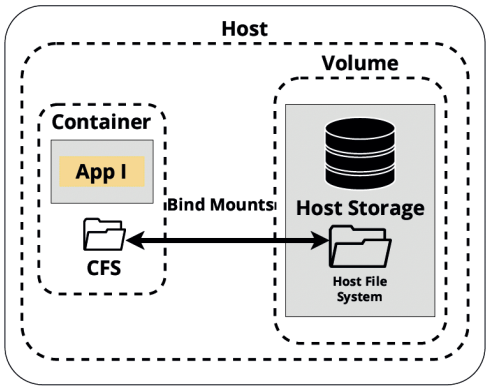

(b) Bind Mount

Fig. 3. Docker storage mechanisms: Volumes, Bind Mounts, Tmpfs Mounts, based on [12], [13].

- Host: The ‘host’ network allows the container to share the same network namespace as the host. In other words, the container shares all network interfaces of the host without any level of abstraction between them, as shown in Figure 4c. Due to this configuration, this network offers better performance than other networks, as it does not require addressing, port mapping, or NAT for container connections to an external network since the container network is identical to the host network. However, it is important to mention that if two or more containers attempt to use the same port under a host network, conflicts may arise [17].

It is worth mentioning that, according to [18], [19], [20], ‘bridge’ type networks tend to have lower performance than other types of networks. On the other hand, ‘host’ type networks, due to their network characteristics, do not have an abstraction level that limits their performance, as is the case with ‘Bridge’ type networks.

III. METHODOLOGY

This section describes the process and methodology for implementing network services in Docker containers. All files used for deploying the services, such as ‘dockerfiles’ and ‘Docker compose’, along with the employed procedure, are available in [21]. The images corresponding to the implemented services are also hosted in the Docker Hub repository in [22].

A. Scenario

The implemented solution is based on Docker Compose and utilizes two Raspberry Pi boards to carry out a multi-container deployment of services. These services constitute a traditional Internet architecture, including DHCP, DNS, FTP, Web, VoIP, and Routing. All of this is achieved through a YAML file. In this approach, one of the Raspberry Pi boards serves as the main host for the containerized services, while the second one is used for remote client connections through the containerized DHCP and Routing services.

In this work, the performance of containerized services is examined in a wired connection, taking into account the delays that a wireless network may introduce. This approach is essential for delay-sensitive services, such as VoIP services, which require delays below 150 ms. A more detailed exploration of this approach is reserved for future work.

B. Physical and logical configurations

Each Raspberry Pi board uses USB-Ethernet adapters from the Realtek brand, model RTL8152, with up to l00baseT/Full-Duplex capacity. This is done to expand the number of physical ports available for the routing service. There are 4 Ethernet interfaces, 1 WLAN interface, and five virtual WLAN interfaces. These interfaces are associated with both an IPv4 address of a containerized service and a monitoring application, as shown in Figure 5, representing the logical distribution of the implementation on the Raspberry Pi board. Figure 6, illustrates the topology for the joint implementation through Docker Compose. The Access Point function is also used on one of the Raspberry Pi boards using Hostap software. This is done to establish a wireless connection for network monitoring. The SSH remote access service installs the board’s dependencies, access, and configuration. This enables wireless access to the equipment’s configuration or through any available Ethernet cable.

C. Base images for docker containers

The base images for Docker containers are based on Alpine Linux, the recommended choice for conserving storage resources in both the resulting images and container instances, as shown in [23]. As for service images, Nginx, Asterisk, and FRRouting are already available as dedicated images in the ARM32v7 architecture. Therefore, instead of building these services completely, files based on these images are generated to leverage their functionality.

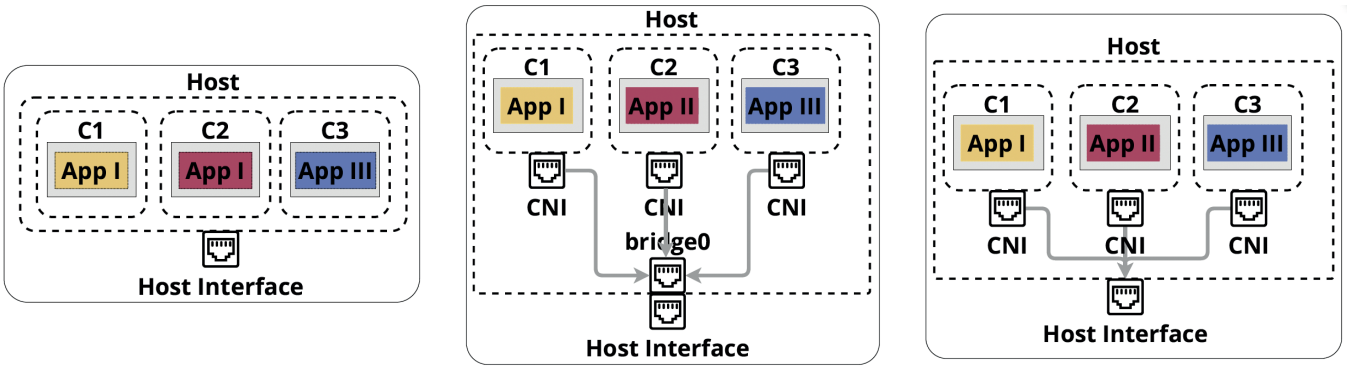

(a) None Networks (b) Bridge Networks (c) Host Networks

Fig. 4. Docker networks: None, Bridge, and Host Networks, based on [18].

D. Storage

Two types of volumes are used for storage: Named Volumes and Bind Mounts. Named Volumes are used to maintain the persistence of logs from containerized services and to share them with other containers. On the other hand, bind mounts are used to configure container files directly from the host.

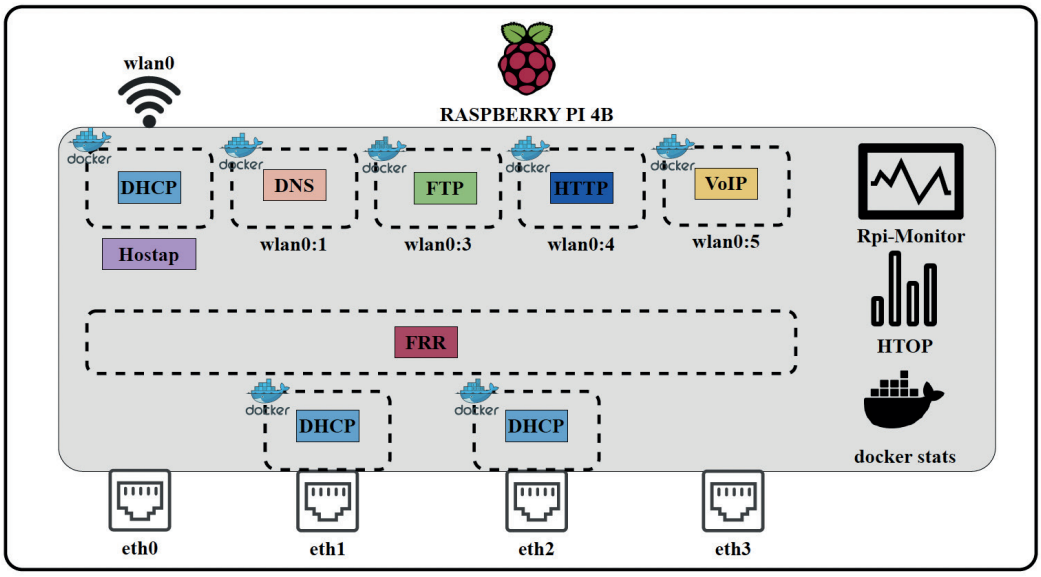

Fig. 5. Design: Logical distribution of Docker Containers on the Raspberry Pi board.

E. Docker networks

Regarding Docker networks, the 'host' type network is used exclusively. This choice is based on previous considerations about Docker network performance and aims to optimize the implementation's performance.

F. Measurement tools, metrics ant testing setup

For the performance analysis of containerized services, various general performance parameters are considered, such as CPU usage, memory usage, CPU load average, network traffic in and out, and a physical parameter, CPU temperature, for each containerized service. To perform this task, two computing devices are used to test the services: i) One to evaluate the service's operation and ii) A second to monitor the host's performance. Detailed descriptions of these devices can be found in Table I.

Client 2, acting as a monitoring device in the topology shown in Figure 6, connects wirelessly via SSH to collect these metrics using various software tools. Among them is the 'docker stats' command from Docker, which measures CPU and memory usage performance, and 'Htop' as a tool for visualizing CPU and RAM system resources and processes. Additionally, the RPI-Monitor tool, a monitoring software based on a web interface, is employed for system usage statistics visualization on Raspberry Pi devices. This allows access to performance metric data such as CPU load average, memory usage, and additional parameters like temperature.

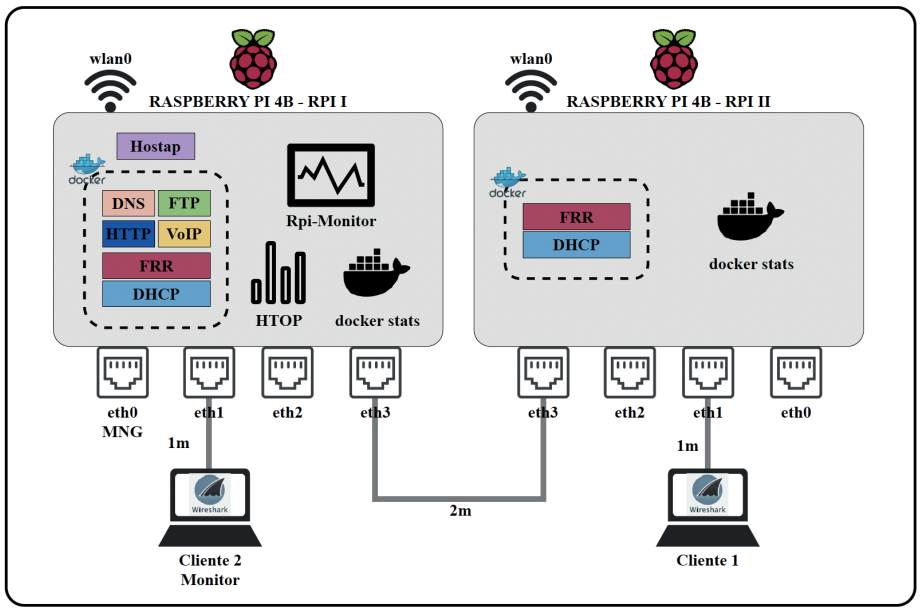

Fig. 6. Design: Container-Based Service Deployment Topology using Docker Compose.

TABLE I
HARDWARE USED FOR THE TEST SCENARIO.

Model	Processor	Ram Memory	Operative System
LENOVO IdeaPad S410p	Intel(R) Core(TM) i5-4200 de 64bits CPU@1.6GHz	8 GB	Windows 10 Pro
HP 15-ef1xxx	AMD Ryzen 5 4500U de 64bits CPU@2.38GHz	8GB	Windows 11 Home
Raspberry Pi 4B	Broadcom BCM2711 Cortex-A72 (ARM v8) de 64bit @1.8GHz	4GB	Debian 11 (Bullseye)

Furthermore, it is essential to consider the analysis of services such as VoIP and assess Quality of Service (QoS) parameters like delay and jitter [24], For this purpose, Wireshark software is used on each device in Figure 6, allowing the capture and analysis of data packets based on SIP and RTP protocols. This provides a deeper insight into the quality of real-time communication. For the measurement process, measurements are taken during specific periods for each containerized service, and then the data is tabulated according to the respective measurement period. The data from each service's test period is used and averaged in the case of results obtained through the RPI-Monitor tool. For data obtained through HTOP and Docker stats, the maximum values for each metric are taken, as visualized in the open SSH terminals during the test period.

G. Service software

The network services implemented in Docker containers are based on Linux servers following a client-server architecture. In this context, each service incorporates a daemon that runs and manages the services according to predefined configuration parameters. Below are the details of each software, its configuration, and the type of implementation in containers:

- Domain name resolution service: It uses a server based on the Internet Systems Consortium's Berkeley Internet Name Domain (Bind9), one of the most popular DNS servers in Linux distributions. This server acts as a master server, locally hosting primary DNS zone records and responding to pre-configured name resolution requests for each containerized service and the monitoring service.
- Addressing service: It is based on the Internet Systems Consortium DHCP (ISC DHCP) server, widely used for IP address assignment and network configuration. The implementation follows a basic configuration of IPv4 address assignment to DHCP clients, providing the addresses of the containerized DNS server and the gateway address configured for each of the Raspberry Pi's Ethernet ports.
- File transfer service: It uses the Very Secure File Transfer Protocol (VSFTP) server, which allows secure and efficient file or directory transfers. The implementation uses active mode and supports custom file transfers for configured local users. These users are within a chroot environment containing a 64KB file and 70KB of storage space for file transfers with the FTP client.
- Web service: It uses a server based on Nginx, known for its high performance, scalability, and low resource consumption [25]. The web service implements a default web server along with two virtual web servers based on Nginx virtual blocks, allowing the hosting of multiple web pages. These pages are accessed along with the aforementioned containerized DNS service.
- VoIP service: It is based on the Sangoma Asterisk server, an open-source framework under the GPL license that enables the development of real-time multiprotocol communication applications, such as high-quality voice and video applications. This service implements a PBX server to configure and manage VoIP extensions. Four IP phone station extensions are configured, of which two are used for functional tests between two clients connected to the Raspberry Pi's Ethernet ports to evaluate the containerized VoIP service without the limitations of wireless connections.
- Routing service: It is based on the open-source FRRouting software, providing traditional router functionality. For the current implementation, the OSPF protocol is one of the most widely used routing protocols today. This protocol is the routing system between the Raspberry Pi boards, enabling connection to the services.

IV. RESULTS

A. CPU and Memory Performance Analysis

In this section, are presented the results obtained from the implementation using Docker Compose. As initial indicators of the results, data collected through the 'Rpi-Monitor' tool are obtained, which display CPU utilization statistics in Figure 7a, memory usage in Figure 7b, and CPU temperature in Figure 7c, over an entire testing interval for each of the containerized services. For the deployment using Docker Compose, the CPU load average indicator starts with an initial value of 1.88 (47.08 %) at the host's startup. Subsequently, this load decreases to 0.37 (9.25 %). From this point onwards, the network service tests are initiated and divided into sections as detailed below.

- Section I (11:30 am - 11:40 am) - Routing: During the connection between the RPI devices, a maximum load value of approximately 1.0 (25 %) can be observed. This value corresponds to the initial OSPF routing process between the devices.
- Section II (11:45 am - 11:50 am) - End-to-end Connection: When starting the end-to-end connection tests between the clients. During this period, the maximum load value reached is 0.518 (12.95 %).
- Section III (11:52 am - 11:53 am) - Connection to servers: The maximum load reached during the tests for connections to the containerized servers is 0.5 (12.5 %).
- Section IV (11:53 am - 11:54 am) - DNS: In this section, the load reaches values of 0.44 (11 %).

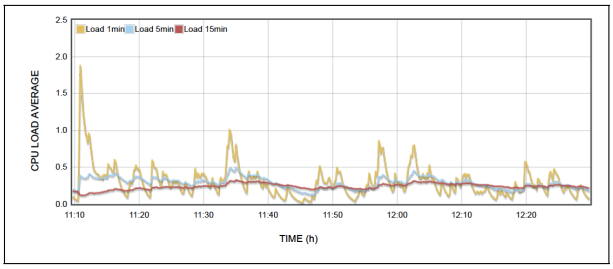

(a) Resource Usage: CPU Load Average.

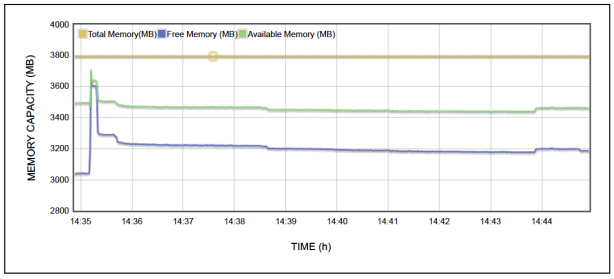

(b) Resource Usage: Memory Usage.

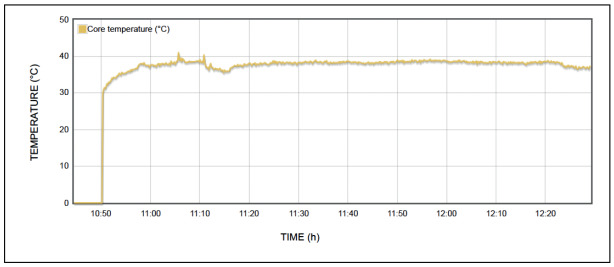

(c) Resource Usage: Temperature.

Fig. 7. Resource Usage Using RPI-MONTTOR for Docker Compose.

- Section V (11:59 am - 12:00 pm) - HTTP: The load reached during the access to the HTTP pages obtains a maximum value of 0.863 (21.575 %). Additionally, according to the DNS traffic I/O graphs analysis, the traffic increases considerably during the HTTP testing period and remains elevated after this test.
- Section VI (12:00 pm - 12:04 pm) - FTP: During the tests of the 2 FTP connections, maximum load values of 0.801 (20.025 %) are recorded for client 1.
- Section VII (12:04 pm - 12:22 pm) - VoIP: During the VoIP tests, it is observed that during the call from extension 2001 to extension 2002, the CPU load reaches its peak, reaching 0.413 (0.33 %). The load remains low for the rest of the calls at an average of 0.180 (4.5 %).

Figure 7b shows the system memory usage, which remains constant as the tests run. The available free memory starts at 3 280 MB during the host's startup and remains close to 3 176.5 MB. This reflects a constant memory usage of approximately 617.8 MB, concerning a total of 3 794.32 MB of available memory.

In Figure 7c the CPU temperature can be observed, which goes from 35.95°C at startup and increases to maintain an average temperature of 38.6°C, with a maximum of 39.2°C during the HTTP tests. After the VoIP tests, it drops to 36.7°C.

The second performance indicator obtained through the 'docker stats' and 'htop' tools is detailed in Table II. The DNS service stands out with a maximum CPU usage of 15.02 %, followed by the FTP service with usage of up to 11.89 %, and the VoIP service with 5.18 %. The other containerized services show relatively low values, all below 1 %.

Regarding memory usage, the DNS service also has the highest value, with 1.1 %, followed by the VoIP service, with 0.8 %. It is important to note that these memory values are constant for all services during the Docker Compose implementation.

B. Quality of Service Analysis

The analysis of RTP traffic provides information about the QoS of the VoIP service, as detailed in Figure 8. The results for VoIP calls are similar to those implemented previously, including:

- Payload codec: g711U vocoder.
- Packet loss: 0 % packet loss for all calls.
- Delays: Minimal delays are recorded, with slightly higher values for client 1 than for client 2. The averages of these values are 18.39 ms for client 1 and 7.63 ms for client 2. The average delay is 19.99 ms for both clients, with maximum delays of 21.74 ms for client 1 and 32.87 ms for client 2.
- Jitter: Regarding jitter, values vary significantly for client 2, where they can reach up to 7, while client 1 experiences jitters of up to 1.46.

V. CONCLUTIONS

- Implementing network services through containers allows for effective deployment on systems with limited CPU, memory, and storage resources, such as Raspberry Pi boards. As demonstrated in services like HTTP and VoIP, these instances achieved a final product, a web page, or a voice call without significant degradation in service quality and with optimal resource usage. For example, three web pages were loaded without errors in the implementation using Docker CLI for HTTP, with CPU usage as low as 0.47 % and memory consumption as 0.1 %. Regarding the VoIP service, calls were made without distortions, delays, or audio loss, maintaining CPU usage at 5.18 % and memory consumption at 0.8 %.
- The implementation of network services through containers has shown minimal resource usage in most cases. Services like DHCP, HTTP, and Routing show zero CPU and memory consumption. In contrast, services like DNS, FTP, and VoIP show high consumption. This can be partly explained by factors such as the volume of request traffic, which, in the case of DNS, was considerably higher than other services. It can also be due to the transfer of information, as in the case of FTP. Additionally, their position in the network architecture should be considered. This is because their location may imply implicit involvement in other services, which, in turn, can increase resource consumption. This is evident in the case of the DNS service when used implicitly to support web services when making domain name resolutions to access a web page.

TABLE II
RESOURCE USAGE: CPU USAGE VIA DOCKER STATS AND ETOP

Server	Docker Stats - Max. CPU Usage (%)	HTOP - Max CPU Usage (%)	HTOP - Max. RAM Memory Usage (%)
DHCP WlanO	0.11	0.0	0.2
DHCP Ethl	0.11	0.0	0.2
DHCP Eth2	0.11	0.0	0.2
DNS	15.02	7.3	1.1
FTP	11.89	8.5	0.0
HTTP (www, web 1, web2)	0.47	0.7	0.1
VoIP	5.18	5.3	0.8
Routing	0.12	0.10	0.1

Source Address	Source Port	Destination Address	Destination Port	SSRC	Start Time	Duración	Payload	Paquetes	Lost	Min Delta (ms)	Mean Delta (ms)	Max Delta (ms)	Min Jitter	Mean Jitter	Max Jitter	Estado
192.168.5.10	50451	192.168.0.6	10076	0x1b6efc54	2023-08-16 12:18:25.110	19.84	g711U	993	0 (0.0%)	18.385000	19.999764	21.690000	0.002938	0.385861	0.581178	
192.168.5.10	60524	192.168.0.6	10048	0x40b37d24	2023-08-16 12:16:25.884	20.86	g711U	1044	0 (0.0%)	17.743000	19.999598	22.879000	0.000562	0.499972	0.931110	
192.168.5.10	52930	192.168.0.6	10050	0x9a9f8eac	2023-08-16 12:15:32.634	20.72	g711U	1037	0 (0.0%)	17.342000	19.999571	22.819000	0.040146	0.805904	1.467908	
192.168.5.10	56019	192.168.0.6	10010	0xffb25126	2023-08-16 12:14:09.019	20.34	g711U	1018	0 (0.0%)	18.604000	20.000493	21.655000	0.002625	0.415269	0.597000	
192.168.5.10	62923	192.168.0.6	10066	0xb3d2565e	2023-08-16 12:13:09.791	21.16	g711U	1059	0 (0.0%)	18.578000	19.998974	21.740000	0.002000	0.364309	0.554573	
192.168.5.10	59881	192.168.0.6	10048	0x8cbcc209	2023-08-16 12:12:52.297	0.26	g711U	14	0 (0.0%)	19.032000	19.940923	20.249000	0.001875	0.040590	0.115222	
192.168.5.10	50420	192.168.0.6	10080	0xbdac85a1	2023-08-16 12:11:37.273	20.46	g711U	1024	0 (0.0%)	13.803000	19.999960	26.110000	0.029500	0.891532	1.422795	

(a) VoIP Service: RTP Details of Calls for Client 1

Source Address	Source Port	Destination Address	Destination Port	SSRC	Start Time	Duración	Payload	Paquetes	Lost	Min Delta (ms)	Mean Delta (ms)	Max Delta (ms)	Min Jitter	Mean Jitter	Max Jitter	Estado
192.168.2.10	60568	192.168.0.6	10012	0x505bdcb0	2023-08-16 12:18:27.916	20.00	g711U	1001	0 (0.0%)	6.581000	19.999271	33.191000	0.698750	4.465511	7.288791	
192.168.2.10	57875	192.168.0.6	10054	0x37974df9	2023-08-16 12:16:29.002	20.64	g711U	1033	0 (0.0%)	8.617000	19.997191	29.940000	0.164649	1.112223	3.607699	
192.168.2.10	62222	192.168.0.6	10004	0x4db8d0e0	2023-08-16 12:15:35.454	20.86	g711U	1044	0 (0.0%)	7.820000	20.002165	33.089000	0.088750	1.071696	2.909141	
192.168.2.10	58833	192.168.0.6	10042	0x77ee67f	2023-08-16 12:14:12.193	20.04	g711U	1003	0 (0.0%)	6.958000	20.002512	32.637000	0.026938	4.760490	7.429664	
192.168.2.10	53212	192.168.0.6	10052	0x1c2d110f	2023-08-16 12:13:12.568	21.30	g711U	1066	0 (0.0%)	16.325000	20.004633	24.366000	0.123213	0.706344	1.245788	
192.168.2.10	58674	192.168.0.6	10062	0xd04f3acd	2023-08-16 12:11:40.761	19.85	g711U	994	0 (0.0%)	7.431000	19.992930	33.104000	0.209277	1.957921	4.742771	

(b) VoIP Service: RTP Details of Calls for Client 2
Fig. 8. VoIP Service: SIP Call Details for VoIP Calls.

- The architecture of containerized services also significantly influences their performance. This is because the underlying software has a variety of architectures to offer the service. Some services, like DHCP, DNS, and FTP, adopt a simple client-server architecture based on daemons and configuration files. Others, like HTTP, VoIP, and Routing, have more complex architectures with dedicated modules to provide the service. For example, the HTTP service, based on NGINX, which allows for efficient deployment without containerization, highlights the importance of decentralization, even when dealing with a single application. Its structure consists of modules with internal management that favors efficiency. In contrast, services like VoIP and Routing have architectures that can be more challenging regarding management and performance.
- Containerizing services provide a high level of scalability, allowing the deployment of multiple containers to provide versatile, flexible, and efficient services. An example is the DHCP service, where multiple containers based on the same image are deployed. This provides a highly flexible addressing service with multiple configurations available for deployment. This achievement is partly due to using environment variables, which allow modifying a containerized service without directly modifying it. This creates a scalable, dynamic, and adaptable service that can be efficiently offered to users, as determined by CPU usage and memory consumption.
- Docker is a highly versatile tool that brings significant benefits to the deployment of network services. Its diverse ecosystem encompasses essential plugins, such as storage through volumes and bind mounts. In this context, it has been observed that these mechanisms allow interaction with a container's file system, making it easier to modify and configure a service without the need to directly access the containerized environment or altogether remove the isolated environment to make changes. Additionally, it has been found that rebuilding containers using volumes is a valuable mechanism for migrating services. An example of this is the use of containers to store configuration logs, as in the case of routing services with 'daemon' and 'zebra.config' files or in the case of the DHCP service with lease records in 'dhcpd.lease'. These records allow replicating the same configurations in other containers, ensuring the continuity of the service. However, it is important to note that logs stored via volumes can be prone to corruption. This is because, over time, these files

can begin to record incomprehensible strings of characters, affecting the service's operation.

- Another highly versatile tool for service deployment is network controllers through network objects. These networks enable the configuration and modification of service management and communication, providing essential features such as network isolation, traffic control, access, and scalability. This flexibility is evident when implementing services with 'bridge'-type networks. In this configuration, services were mapped to specific ports to allow external access through the container. As observed, using ports different from the default value for Network Address Translation (NAT) between the container and the external network provided greater isolation and security for the service. It also allowed the incorporation of multiple containers offering the same service but mapped to different ports to receive the service. This is especially useful in services like HTTP, where high scalability is achieved using a different port for each container. However, in services like passive FTP and VoIP, port mapping involves maintaining constant NAT over a range of ports (FTP: for transfer, random port >1 048, and VoIP: audio transmission via RTP, random port between 10 000 and 20 000). In these cases, considering a NAT that covers the entire port range to obtain service connection on a non-specific port was impractical as it affects performance, as mentioned in [19], [20]. For this reason, using 'host'-type networks, which remove the isolation level between containers and share the network with the host, allowed for services with low resource usage but limited scalability.
- Regarding the containerized VoIP service, significantly high performance and QoS are observed when using Ethernet cable transmission. This is confirmed through RTP parameters captured with Wireshark, where the average delay of calls is 20 ms, compared to the maximum allowable delay of 150 ms, and maximum Jitter values of 7 ms between both implementations, staying below the maximum allowable of 50 ms. In summary, containerizing VoIP services for end-to-end calls through wired connections does not affect this QoS.

REFERENCES

[1] A. Khan. Key Characteristics of a Container Orchestration Platform to Enable a Modem Application. Vol. 4. 2017, pp. 42-48. Available: doi: 10.1109/MCC.2017. 4250933.

[2] T. Salah, M. J. Zemerly, C. Y. Yeun, M. Al-Qutayri, and Y. Al-Hammadi. Performance Comparison Between Container-Based and Vm-Based Services. Institute of Electrical and Electronics Engineers Inc., 2017, pp. 185-190. isbn: 9781509036721. Available: doi: 10.1109/ICIN.2017.7899408.

[3] Z. Kozhirbayev and R. O. Sinnott. A Performance Comparison of Container-Based Technologies for the Cloud. Vol. 68. North-Holland, 2017, pp. 175-182. Available: doi: 10.1016/J.FUTURE.2016.08.025.

[4] A. Bhardwaj and C. R. Krishna. Virtualization in Cloud Computing: Moving from Hypervisor to Containerization — A Survey. Vol. 46. Springer Science and Business Media Deutschland GmbH, 2021, pp. 8585-8601. Available: doi: 10.1007/s13369-021-05553-3.

[5] V. G. da Silva, M. Kirikova, and G. Alksnis. Containers for Virtualization: An Overview. Vol. 23. Walter de Gruyter GmbH, 2018, pp. 21-27. Available: doi: 10. 2478/acss-2018-0003.

[6] V. Singh and S. K. Peddoju. Container-based Microservice Architecture for Cloud Applications. 2017. ISBN: 9781509064717. Available:

[7] S. Sultan, I. Ahmad, and T. Dimitriou. Container Security: Issues, Challenges, and the Road Ahead. Vol. 7. Institute of Electrical and Electronics Engineers Inc., 2019, pp. 52976-52996. Available: doi: 10.1109/ ACCESS.2019.2911732.

[8] E. Casalicchio and S. Iannucci. The State-of-the-Art in Container Technologies: Application, Orchestration and Security. Vol. 32. John Wiley and Sons Ltd, 2020. Available: doi: 10.1002/cpe.5668.

[9] J. Chelladhurai, P. R. Chelliah, and S. A. Kumar. Securing Docker Containers from Denial of Service (DoS) Attacks. Institute of Electrical and Electronics Engineers Inc., 2016, pp. 856-859. isbn: 9781509026289. Available: doi: 10.1109/SCC.2016.123.

[10] C. C. Chen, M. H. Hung, K. C. Lai, and Y. C. Lin. Docker and Kubemetes. In *Industry 4.1: Intelligent Manufacturing with Zero Defects*. 2022. Vol. 1, pp. 169- 213. Available: doi: 10.1002/9781119739920.ch5.

[11] K. Kumar and M. Kurhekar. Economically Efficient Virtualization Over Cloud Using Docker Containers. Institute of Electrical and Electronics Engineers Inc., 2016, pp. 95-100. isbn: 9781509045730. Available: doi: 10.1109/CCEM.2016.24.

[12] S. Bhat. Understanding Docker Volumes. In *Practical Docker with Python: Build, Release, and Distribute Your Python App with Docker*. Berkeley, CA: Apress, 2022, pp. 105-132. isbn: 978-1-4842-7815-4. Available: doi: 10.1007/978-1-4842-7815-4_5.

[13] N. G. Bachiega, P. D. Souza, S. M. Bruschi, and S. D. Souza. Performance Evaluation of Container's Shared Volumes. Institute of Electrical and Electronics Engineers Inc., 2020, pp. 114-123. isbn: 9781728110752. Available: doi: 10.1109/ICSTW50294.2020.00031.

[14] Dockerinc. Networks Overview - Docker Documentation. Available: [Online]. Available: https://docs.docker. com/network/.

[15] Dockerinc. Disable Networking for a Container - Docker Documentation. Available: [Online]. Available: https://docs.docker.com/network/none/.

[16] Dockerinc. Use Bridge Networks - Docker Documentation. Available: [Online]. Available: https://docs.docker. com/network/bridge/.

[17] Dockerinc. Use Host Networking - Docker Documentation. Available: [Online]. Available: https://docs.docker. com/network/host/.

[18] R. Dua, S. K. Konduri, and V. Kohli. *Learning Docker Networking: Become a Proficient Linux Administrator by Learning the Art of Container Networking with Elevated Efficiency Using Docker*. 1st ed. Packt Publishing Ltd., 2016. Vol. 1, pp. 2-11. isbn: 9781785280955. Available:

[19] S. Kun, Z. Yong, C. Wei, and R. Jia. An Analysis and Empirical Study of Container Networks. Institute of Electrical and Electronics Engineers Inc., 2018, pp. 189-197. isbn: 9781538641286. Available: doi: 10.1109/INFOCOM.2018.8485865.

[20] L. L. Mentz, W. J. Loch, and G. P. Koslovski. Comparative Experimental Analysis of Docker Container Networking Drivers. Institute of Electrical and Electronics Engineers Inc., 2020, pp. 1-7. ISBN: 9781728194868. Available: doi: 10. 1109 / CloudNet51028 . 2020 . 9335811.

[21] A. Endara. Network Service on Containers. 2023. Available: [Online]. Available: https://github.com/AndresYE/Network_Service_on_Containers_a_Practical-Approach.

[22] A. Endara. Network Service on Containers - Docker Hub. 2023. Available: [Online]. Available: https://hub.docker.eom/u/andresye.

[23] J. Islam, E. Harjula, T. Kumar, P. Karhula, and M. Ylianttila. Docker Enabled Virtualized Nanoservices for LocalIoT Edge Networks. 2019. ISBN: 9781728108643. Available:

[24] M. Mejia, C. Ortiz, W. Ramos, and L. Moscoso. Network Traffic Management in the Quality of Service 'QoS' WAN in Tambopata-Peru 2021. Vol. 28. 2022, pp. 300-318. Available:

[25] W. Kithulwatta, K. Jayasena, B. Kumara, and R. Rathnayaka. Performance Evaluation of Docker-based Apache and Nginx Web Server. In *2022 3rd International Conference for Emerging Technology (INCET)*. 2022, pp. 1-6. Available: doi: 10.1109/INCET54531. 2022.9824303.